STUDIES IN REACTIVE PRECIPITATION: MORPHOLOGY OF AMMONIUM DIURANATE

By

SUBHANKAR MANNA

ENGG01200904022

Bhabha Atomic Research Centre, Mumbai, India

A thesis submitted to the

Board of Studies in Engineering Sciences

In partial fulfillment of requirements

for the Degree of

DOCTOR OF PHILOSOPHY

Of

HOMI BHABHA NATIONAL INSTITUTE, MUMBAI

September, 2016

Homi Bhabha National Institute

Recommendations of the Viva Voce Committee

As members of the Viva Voce Committee, we certify that we have read the dissertation prepared by **Subhankar Manna** entitled "**Studies in Reactive Precipitation: Morphology of Ammonium Diuranate"** and recommend that it may be accepted as fulfilling the thesis requirement for the award of Degree of Doctor of Philosophy.

Chairman - Prof. S. B. Roy	**Date:**
Guide / Convener - Prof. J. B. Joshi	**Date:**
Co-guide - Prof. S. B. Roy	**Date:**
Member 1 - Prof. D. Srivastava	**Date:**
Member 2 - Prof. (Smt.) S. Mukhopadhyay	**Date:**
Member 3 - Prof. R. Kapoor	**Date:**

Final approval and acceptance of this thesis is contingent upon the candidate's submission of the final copies of the thesis to HBNI.

I/We hereby certify that I/we have read this thesis prepared under my/our direction and recommend that it may be accepted as fulfilling the thesis requirement.

Date:

Place:

Co-guide	**Guide**
Prof. S .B. Roy	Prof. J. B. Joshi

STATEMENT BY AUTHOR

This dissertation has been submitted in partial fulfilment of requirements for an advanced degree at Homi Bhabha National Institute (HBNI) and is deposited in the Library to be made available to borrowers under rules of the HBNI.

Brief quotations from this dissertation are allowable without special permission, provided that accurate acknowledgement of source is made. Requests for permission for extended quotation from or reproduction of this manuscript in whole or in part may be granted by the Competent Authority of HBNI when in his or her judgment the proposed use of the material is in the interests of scholarship. In all other instances, however, permission must be obtained from the author.

Subhankar Manna

DECLARATION

I, hereby declare that the investigation presented in the thesis has been carried out by me. The work is original and has not been submitted earlier as a whole or in part for a degree / diploma at this or any other Institution / University.

Subhankar Manna

List of Publications

Journal

[1] "Study of crystallization and morphology of ammonium diuranate and uranium oxide", **Subhankar Manna**, Saswati B. Roy, and Jyeshtharaj B. Joshi, Journal of Nuclear Materials, 2012, 424, 94-100.

[2] "Study of calcinations of ammonium diuranate at different temperatures", **Subhankar Manna**, Phani Karthik, Abhishek Mukherjee, Joydipta Banerjee, Saswati B. Roy, and Jyeshtharaj B. Joshi, Journal of Nuclear Materials, 2012, 426,229-232.

[3] "Study of crystal growth and effect of temperature and mixing on properties of sodium di-uranate", **Subhankar Manna**, Umesh R. Thakkar, Santosh K. Satpati, Saswati B. Roy, Jyeshtharaj B. Joshi and Jayanta K. Chakravartty. Progress in Nuclear Energy, 2016, 91, 132-139.

[4] "Study on effect of process parameters and mixing on morphology of ammonium diuranate", **Subhankar Manna**, Chandrabhanu Basak, Umesh R. Thakkar, Shital Thakur, Saswati B. Roy and Jyeshtharaj B. Joshi. Journal of Radioanalytical and Nuclear Chemistry, 2016, 310, 287-299.

[5] "Study on changes of composition of ammonium diuranate with progress of precipitation and study on properties of ammonium diuranate and its subsequent products produced from both uranyl nitrate and uranyl fluoride solution", **Subhankar Manna,** Raj kumar, Santosh K. Satpati, Saswati B. Roy, and Jyeshtharaj B. Joshi, accepted in Nuclear Engineering and Technology

Conferences

[1] "Microstructural investigation on the effect of calcination temperature on UO_3", J. Banerjee, **S. Manna**, Phani Karthik, T.R.G. Kutty, Arun Kumar, S.B. Roy, Second International Conference on Advances in Nuclear Materials (ANM 2011), BARC Mumbai, 9-11 February 2011.

[2] "Study of Microstructure of Ammonium Di Uranate and Uranium Oxide Produced from Differently Sourced Ore", **S. Manna,** K. N. Hareendran, J. Banerjee, T.R.G. Kutty, S. B. Roy & J. B. Joshi, The International Conference GLOBAL 2011 organized by Atomic Energy Society of Japan and Japan Atomic Energy Agency, Makuhari Messe, Chiba, Japan 11-16 December, 2011.

[3] "Study on particle morphology during ammonium diuranate precipitation", S. Manna, P. U. Sastry, S. V. Kadam, S. K. Satpati, S. B. Roy and J. B. Joshi, DAE-BRNS 4th Interdisciplinary Symposium on Materials Chemistry 2012, BARC, Mumbai. December 11-15, 2012

Others

1. Crystal growth and morphological study of ADU and its calcined product, **Subhankar Manna**, Saswati B. Roy and Jyeshtharaj B. Joshi, BARC News Letter, Founder's Day Special, 162-166, October 2013.

Subhankar Manna

Dedicated to my dear Parents,
Spouse and Shreyan

ACKNOWLEDGEMENTS

It is my pleasant duty to place a deep sense of indebtedness and gratitude to the authorities of Bhabha Atomic Research Centre, in particular to Prof. A. K. Suri, former Director, Materials Group and Prof. (Smt.) S. B. Roy, Director, Chemical Engineering Group and Head, UED for their kind permission to carry out this research work and their strong support and encouragement.

It gives me immense pleasure to express my deep gratitude and thankfulness to my Guide Padma Bhushan Emeritus Prof. J. B. Joshi, Homi Bhabha National Institute, Mumbai and Prof. (Smt.) S. B. Roy, Director, Chemical Engineering Group and Head, UED for their valuable guidance in hours of need, constant encouragement, keen interest, good wishes and valuable suggestions throughout my entire research tenure. Their constant inspiration throughout the work, even on temporary setback during the course of this work, has kept my spirits high and resurgent.

I would like to express my gratitude to all the members of my doctoral committee namely Prof. D. Sathiyamoorthy, Outstanding Scientist, Head Powder Metallurgy Division and Ex-Chairman, Doctoral Committee, Prof. P. K. Tiwari, Distinguish Scientist, former Associate Director, Chemical Engineering Group and Ex- Chairman, Doctoral Committee and Prof. (Smt.) S. B. Roy, Director, Chemical Engineering Group and Head, UED and present Chairman, Doctoral Committee for their suggestions, critical evaluation and continuous encouragement. It gives me immense pleasure to acknowledge other members of my doctoral committee namely Prof. R C Hubli, former Head, MPD, Prof. D. Srivastava, Outstanding Scientist, MSD, Prof. S. Mukhopadhyay, SO/G, ChED and Prof. R. Kapoor, SO/G, MMD for their constant support and for critically evaluating my research activities time to time.

I thankfully acknowledge the generous support, motivation and help given by Shri. S. K. Satpati, Head HPS, UED. I wish to express my sincere thanks to my colleague Shri U. R. Thakkar and Shri R. Kumar for their diversified help especially during experiments. My special thanks go to my senior colleagues Shri M. L. Sahu, Shri S. Chowdhury and Shri K. N. Harindran for their moral support, diversified help. I would like to thank to Mrs. K. Mitra, Mrs. Mousumi Sinha, Shri S. K. Gupta, Dr. S. Biswas, Shri N. Singh, Dr. C. Rane, Dr. Ekambara, Dr. H. Joshi, Shri N. Minocha, Ms. Isita, Shri Ankur and Shri V. Bhushare for their diversified help, and several funs which will always be remembered. My sincere thanks to Dr. B. Mandal of ChD, Dr. R. Chowdhury of BOD and Shri A. Sharma of UED for their help in writing the Thesis. I take this opportunity to thank all the staff members of UED for their kind cooperation.

I would like to express my gratitude to Prof. G. K. Dey, Distinguish Scientist, Director, Materials Group and Shri S. Neogy, MSD for their cooperation in TEM. I would like to express my gratitude to Dr. C. B. Basak of G&AMD, Dr. K. V. Mani Krishna of MSD and Dr. B. Pal of MPD for SEM. My sincere thanks to Smt. S. Thakur of UED for their kind help in carrying out XRD of the samples and to Quality Control Section of UED for carrying out chemical analysis.

I want to thank my friends who have supported and helped me to overcome setbacks and to stay focused on my work, without which all this work would not have been possible. I owe a special distinction to my parents Shri. G. C. Manna and Smt. R. R. Manna for their continuous encouragement during course of my research work. I am also infinitely thankful to my wife Smt. Sangeeta Manna for her unconditional love, advice, care and emotional support in the entire endeavor. My son Shreyan has always been a source of happiness and joy throughout the period of research work.

(Subhankar Manna)

CONTENTS

Homi Bhabha National Institute

SYNOPSIS OF Ph. D. THESIS

1.	**Name of the Student:**	**Subhankar Manna**
2.	**Name of the Constituent Institution:**	**BARC/ UED (ChEG)**
3.	**Enrolment No. and Date of Enrolment:**	**ENGG01200904022**
4.	**Title of the Thesis:**	**Studies in Reactive Precipitation:** **Morphology of Ammonium Diuranate**
5.	**Board of Studies:**	**Engineering Science**

SYNOPSIS

1. Introduction:

Ammonium diuranate (ADU) is one of the most important intermediate products in nuclear industries. ADU is thermally decomposed to UO_3 or U_3O_8 by calcination. The oxide is then reduced to UO_2. The UO_2 is either used as a fuel or is converted to U metal ingot or powder via metallothermic reduction route, depending on requirements. ADU is generally produced either via uranyl nitrate route or via uranyl fluoride route. In both the production process, uranyl solution (either nitrate or fluoride) reacts with ammonia (either gaseous or aqueous form) and precipitation occurs when concentration of product (ADU) exceeding the solubility. The process is called reactive precipitation or crystallization. Reaction, nucleation, growth, agglomeration and breakage are the kinetics of reactive precipitation. Nucleation is the first formation of the solid phase. Crystal growth is a diffusion and integration process, modified by the effect of the solid surfaces on which it occurs [1]. Agglomeration is a particle size enlargement process by which fine particles, rather than ions or molecules, are joined in an assembly. Agglomeration of Ammonium diuranate (ADU) like materials also depends on zeta potential barrier [2] and particle-particle interaction. Existing particles are broken down into a larger number of smaller fragments depending upon the interaction of particles with surrounding particles, impeller, wall and also on the fluid shear. Both nucleation and crystal growth rates are function of super-saturations. Higher the supersaturation, higher is the both. The mean crystal size and morphology is determined by the competition between nucleation and growth, both of which depend on supersaturation. In general, very high supersaturation favors nucleation over growth, resulting in a large number of smaller crystals. This is especially true above the critical value of supersaturation (above metastable zone) at which homogeneous nucleation starts to predominate over heterogeneous nucleation [3]. This causes formation of very small size crystallites. Whereas in metastable zone crystal growth occurs and bigger size crystallites are formed [4]. Because of the high level of supersaturation due to very fast reaction kinetics and low solubility of ADU, the involved mechanisms of primary nucleation, crystal growth, aggregation and breakage occur simultaneously and control the morphology.

Motivation for the research work: Production process and properties of uranium oxide, which is used as fuel in power reactor and uranium metal, which is used as fuel in research reactor, largely depend on ADU characteristics, as morphology of ADU is retained by its subsequent products [5]. Thus ADU precipitation process is very much important in nuclear industry. The performance of precipitator is assessed not only by the yield of product but also by the quality of product such as powder morphology, specific surface area, particle size distribution and percentage recovery of uranium. Morphology of ADU powders controls their flow-ability required for further material movement through different equipment, surface area required for chemical reactivity of powder, carryover losses occurred during gas solid counter current reaction and tap density required for effective capacity determination. Very small particles may give very high surface area, but very high surface area or reactivity also damages product because of sintering due to high heat of reaction. Small particles also cause carryover losses during gas solid counter current flow. Over all rounded shape is also helpful to increase flow-ability. Morphology of the ADU particles largely depends on process parameters like temperature, pH of solution, uranium concentration, feed free acidity, NH_3 feed rate and mixing mechanism. An understanding of effect of different process parameters on morphology of ADU is very much desired. Though, morphology of ADU is maintained in its calcined product uranium oxide (UO_3), surface area of uranium oxide is largely depends on temperature of calcination. Commercial pure uranium metal in massive form is produced in nuclear industries by Magnesio-Thermic Reduction (MTR) of uranium tetra fluoride (UF_4) [6]. Performance of metallothermic reaction and recovery of uranium largely depends on properties of UF_4 [7]. The properties of UF_4 are inherited from its precursors UO_2, UO_3 and ADU.

The scope of this doctoral program is divided into the following specific areas of study: (a) changes in pH, uranium concentration in solution and composition of ADU with progress of precipitation reaction, (b) effect of uranium concentration in feed, initial temperature of feed and mixing on reaction time of ADU precipitation, morphology, crystal structure and other physical properties of ADU produced from uranyl nitrate solution, (c) effect of calcination temperature on morphology and physical properties of calcined product of ADU produced from uranyl nitrate route and (d) effect of the properties of ADU produced from uranyl nitrate and uranyl fluoride on the properties of subsequent products.

2. Experimental:

ADU was produced by reaction of gaseous NH_3 with both uranyl nitrate solution (UNS) and uranyl fluoride solution (UFS) in an agitated 3 l (liquid volume) glass reactor fitted with 4 number equally spaced 15 mm width baffles. The reactor was provided with sparger, muffle electrical heater, pH electrode, RTD. To study change in uranium concentration and pH with time, samples (aliquot) were withdrawn after regular intervals. The samples collected were filtered using Büchner funnel and 542 grade Whatman filter paper. The pH and uranium concentration in the filtrate were measured.

Study on effect of process parameters (uranium concentration in feed and feed temperature) and mixing (type of impeller and rotational speed of impellers) has been carried out based on

ADU precipitation from UNS only. To generate UNS of different uranium concentration, UNS containing 50 g/l uranium was either evaporated (to increase uranium concentration) or diluted with required DM water (to reduce uranium concentration). UNS was heated up to preset temperature to study the effect of initial temperature of UNS. To reduce the temperature below the room temperature, ice blocks were used. To study the effect of impeller types, three impeller designs were used: (a) six bladed disc turbine (DT), (b) six bladed 45° pitched blade (PBT) and (c) three bladed hydrofoil (HF). In all the three cases the impeller sweep diameter was 0.4 times the tank diameter (150 mm). The impeller speed was varied using variable frequency drive (VFD). For all the experiments ammonia was added until pH of the solution reached to 7.5. After pH 7.5, the addition of ammonia was stopped. The final slurry was then filtered under vacuum using the Büchner funnel and 542 grade Whatman filter paper. The pH and uranium concentration in the filtrate were measured. The cake after washing with distilled water was dried.

The dry ADU was calcined in muffle furnace at different preset temperature to study effect of calcination temperature on its calcined product. ADU produced from both UNS and UFS were calcined to UO_3, further reduced to UO_2 and subsequently hydroflorinated to UF_4 at similar conditions to study the effect of two different process routes of ADU precipitation process on the characteristics of ADU, UO_3, UO_2 and UF_4.

Results and discussion:

2.1. Variation of uranium concentration and pH with time:

Changes in uranium concentration and pH of the filtrates with time during the course of ADU precipitation reaction via UNS route have shown in Fig 1. It was observed that initially there was slow increase of pH and then there was sudden small reduction in pH, followed by almost flat zone and then there was a sharp increase in pH followed by slow increase in pH. The first precipitation point was detected by inception of permanent turbidity which was found to coincide with the reduction of pH. To get clarity in reduction of pH at the starting of precipitation a selected portion (in between point A at time 13 min to D at time 22 min) of Fig. 1a has been enlarged in Fig. 1b. pH was increased very fast in between A to B from 2.95 to 3.19. No reaction took place in this zone as no change in uranium concentration was observed. Reduction in both the uranium concentration and pH was observed after point B. pH was reduced from 3.19 to 3.18 and uranium concentration was reduced from 62 g/l to 56.22 g/l from point B to C. With further addition of NH_3, pH and uranium concentration were further reduced to 3.15 and 40.08 g/l respectively at point D. No reduction in pH was observed after point D, but reduction in uranium concentration was continued.

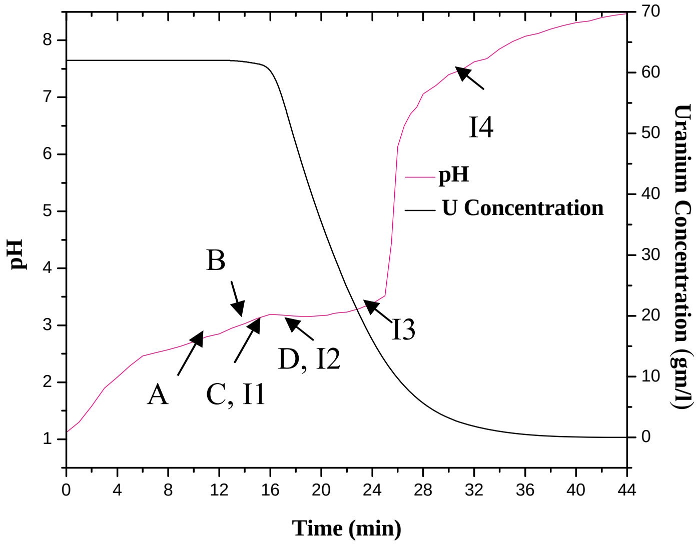

a)

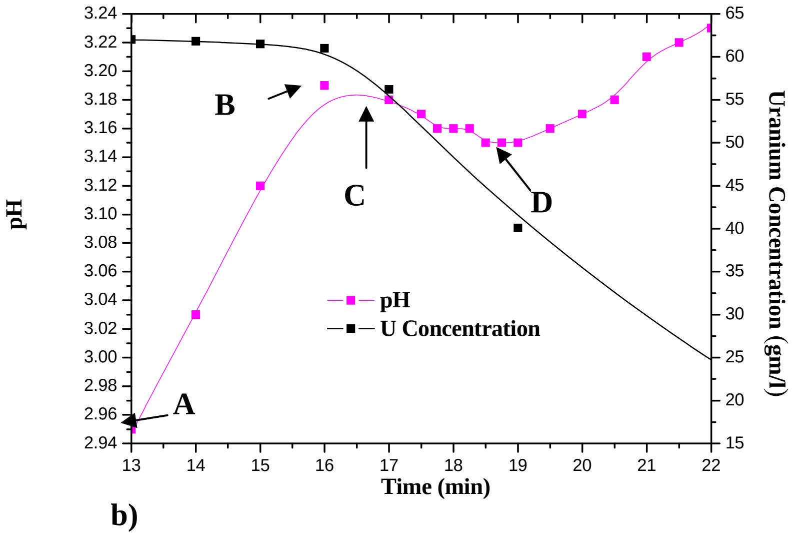

Fig. 1: Changes in pH and uranium concentration with time a) across the total duration of precipitation b) across the selected duration (13 min to 22 min) of the precipitation.

Initial increase in pH can be explained due to neutralization of free acid present in UNS. Small reduction of pH was occurred due to generation of H^+ ion at the inception of precipitation [79]. It was further notices from uranium concentration vs time plot that precipitation started only after reaching certain pH. It was also observed that around 90% recovery of uranium was took place at the end of flat zone. Recovery was further increased to 99.98 % when pH reached to 7.5. Almost no improvement in recovery was observed when pH was further increased to 8.5. Depending on the process parameters, point of inception, end of flat zone, length of flat zone and slope of lines may change but overall nature of the curve remains same. It was further observed that ADU obtained at inception via UNS route was consisted of orthorhombic $3UO_{3.}\ NH_{3.}\ 5H_2O$. Another hexagonal phase ($2UO_{3.}\ NH_{3.}\ 3H_2O$) was appeared in ADU with further addition of NH_3.

Unlike UNS route, pH of the solution was increased continuously and no flat zone was observed during course of precipitation via UFS route (Fig. 2). However, precipitation was started only after reaching certain pH as earlier, but at higher pH compare to the precipitation from UNS. The recovery of uranium at any pH in UFS route was lower than that in case of UNS route. It was also studied that ADU produced at inception via UFS route was consisted of $(NH_4)_3UO_2F_5$ (orthorhombic). Composition of ADU was changed with further addition of ammonia and it became mixture of $(NH_4)_3UO_2F_5$ (orthorhombic), $2UO_3.NH_3.3H_2O$ (hexagonal) and $(NH_4)(UO_2)_2F_5.4H_2O$ (hexagonal).

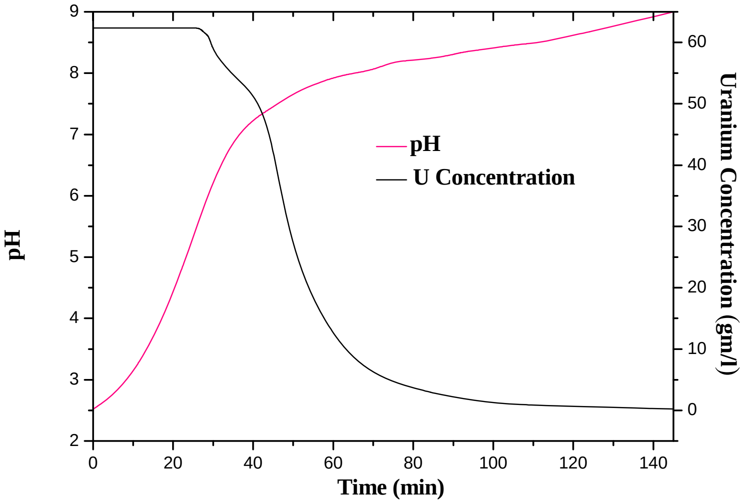

Fig. 2: Variation of pH and uranium concentration with time during ADU precipitation reaction from uranyl fluoride solution (UFS).

2.2. Effect of Uranium concentration:

To study the effect of uranium concentration in UNS, experiments were carried out with six different uranium concentration: 20 g/l, 40 g/l, 60 g/l, 80 g/l, 100 g/l and 120 g/l at room temperature. Similar nature of pH vs time curve as shown in Fig. 1 was observed in all the cases.

Filterability of ADU slurry was very poor when uranium concentration was 20 g/l, but filterability was improved with an increase in uranium concentration and became good (filtration rate 700 ml/min) when uranium concentration was 60 g/l and above.

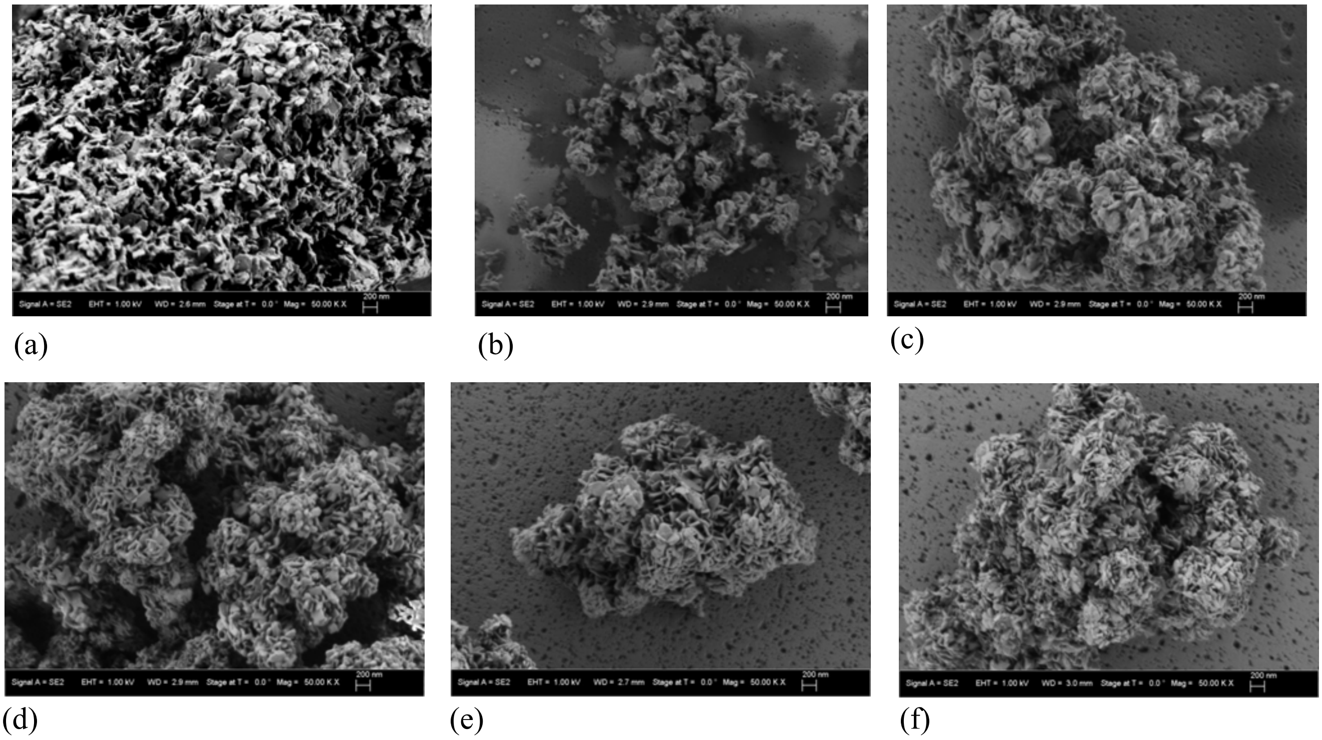
(a) (b) (c)

(d) (e) (f)

Fig 3: Effect of uranium concentration in feed on morphology of ADU (a) 20 g/l, b) 40 g/l, (c) 60 g/l, (d) 80 g/l, (e) 100 g/l and (f) 120 g/l

Fig. 3 shows morphology of ADU produced from UNS of different uranium concentrations. As ADU is sparingly soluble, very high level of super saturation occurs during precipitation. It causes primary nucleation. But crystals are not able to grow at very low uranium concentration. This is why platelet like structure was not observed in case of ADU obtained from UNS containing 20 g/l uranium (Fig. 3a). With an increase of uranium concentration crystals grow due to increase in diffusion flux and platelet like structure becomes prominent. Agglomeration has also been increased due to reduction of zeta potential barrier with increase of uranium concentration [3]. As a result, both mean particle size (mean agglomeration size) and specific surface area (SSA) of ADU were increased with an increase of uranium concentration. It was also observed that the conversion of uranium during precipitation was more than 99% in all the cases.

2.3. Effect of temperature of feed:

To study the effect of UNS temperature, experiments were carried out at four different temperatures: 10 ˚C, 28 ˚C (room temperature), 50 ˚C and 70 ˚C. It can be observed in all the four experiments that variation of the pH was similar to that shown in Fig. 1. Filtration rate of ADU slurry produced at 10 ˚C was very poor and cake was very sticky in nature. Filtration rate of ADU slurry improved with an increase of UNS temperature and filtration rate was good when temperature of UNS was 50 ˚C or above. It was observed that there was no effect of temperature on recovery of uranium during ADU precipitation.

Prominent platelet like structure was not visible in ADU produced at 10 ˚C and 28 ˚C (Fig. 4 a and b) due to lack of crystal growth of ADU platelets. Visible growth of ADU platelets was observed due to the increase in rate of diffusion at higher temperature and concomitantly size of platelet was increased with an increase of temperature. As a result, SSA of ADU particles was increased with an increase of temperature. However, overall morphology of ADUs obtained both at 50 ˚C and 70 ˚C are almost similar (Fig. 4 c and d). It has been observed that the SSA increases by about 38.5% with an increase of temperature from 28 ˚C (RT) to 50 ˚C and by only 10% with further increase of temperature from 50 ˚C to 70 ˚C. Whereas, energy required to increase temperature to 70 ˚C is twice than increase temperature to 50 ˚C. So, it has been optimized to operate ADU precipitation process at 50 ˚C.

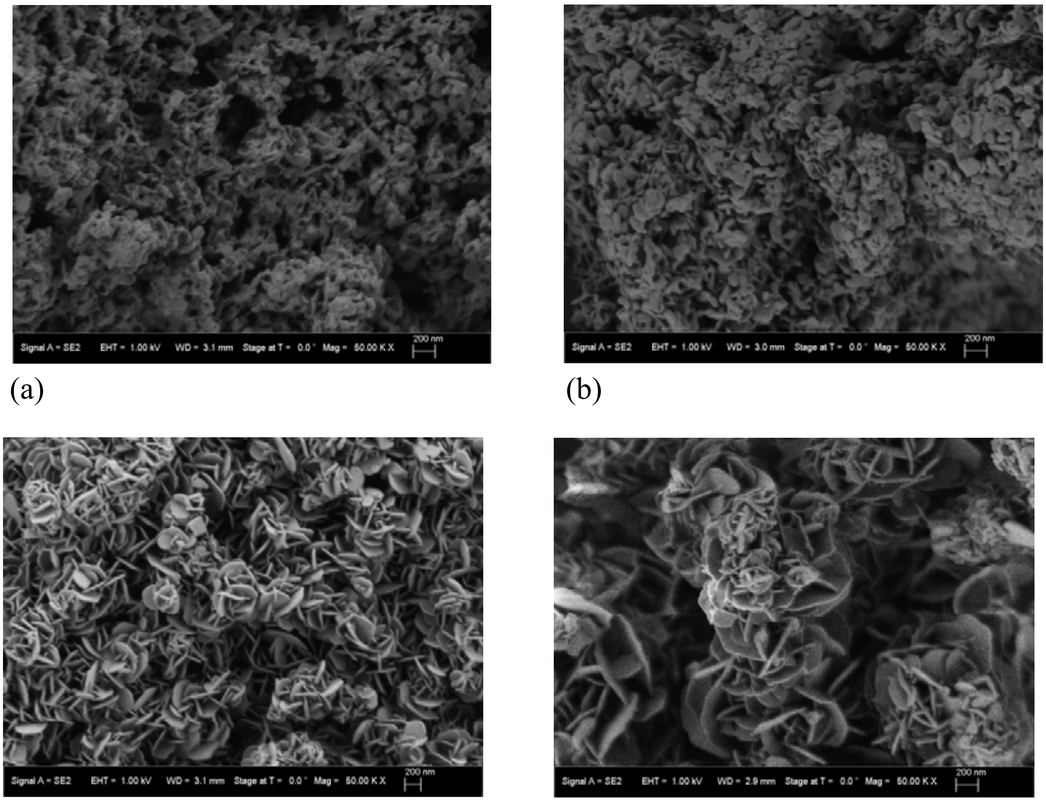

(a) (b)

(c) (d)

Fig 4: Effect of temperature in feed on morphology of ADU (a) 10 ˚C, b) 28 ˚C (RT), (c) 50 ˚C and (d) 70 ˚C

2.4. Effect of type of impeller:

Three types of impellers were used to study the effect of impeller design. Power number (N_P) of the HF, PBT and DT are 0.27 [8], 1.73 and 5.18 [9] respectively. It was seen that the pH variation was similar to that shown in Fig. 1 in all the cases. Though filtration rate was good in all the cases, the filtration rate was improved with an increase N_P. Power input per unit volume increases with an increase of N_P. With an increase of power input per unit volume, mixing inside the reactor is also increased and concomitantly, bulk convection inside the reactor is increased. As ADU reaction kinetics is very fast and ADU is sparingly soluble in solution, very high level of local super saturation occurs near the NH_3 feeding zone. It causes primary nucleation. But supersaturation level reduced to metastable zone due to mixing, as a results crystal growth dominates. Simultaneously agglomeration occurs due to particle-particle interaction and breakage also occurs due to interaction of particle with particles, reactor hardware and fluid shear. In this way mixing plays role in determination of morphology, particle size distribution and other physical properties.

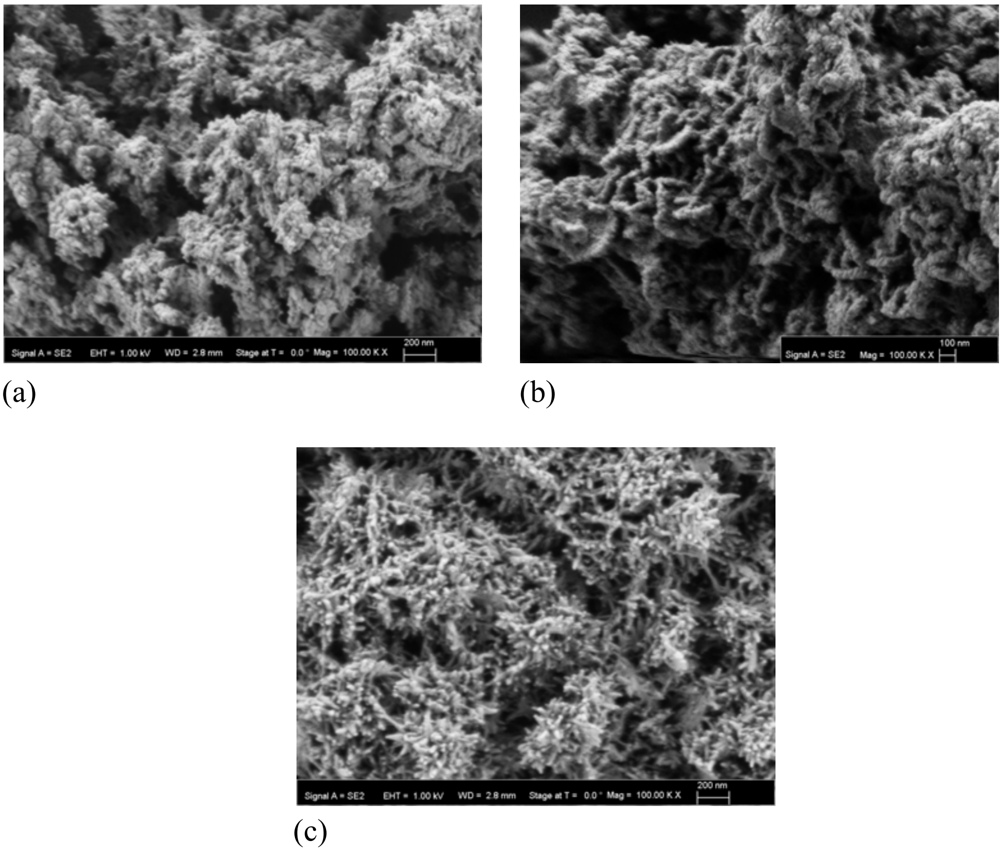

(a) (b)

(c)

Fig 5: Effect of impeller design on morphology of ADU (a) Hydrofoil, (b) Pitched Blade Turbine and (c) Disc Turbine.

Fig. 5 shows SEM images of ADU produced using HF, PBT and DT type of impeller respectively. It has been observed that numbers of platelets were more and sizes of platelets were very small due to lack of crystal growth in case of HF type impeller (Fig. 5 a). In the case of PBT

(Fig. 5 b), the size of individual platelets can be seen to be increased due to increase of crystal growth and numbers of platelets were reduced. It increased porosity in ADU particles. Morphology of ADU produced using DT has been shown in Fig. 5 c. The platelets size was smaller than that produced by PBT but larger than HF. More breakage of agglomerates was observed in case of DT. This is why mean particle size (mean agglomerate size) was decreased with an increase of N_P. SSA of ADU was substantially increased with an increase of N_P from HF to PBT but then slightly decreased for DT. It was observed that conversion of UNS was more than 99% and irrespective of the impeller design.

2.5. Effect of impeller speed:

To study the effect of impeller speed, experiments were carried out with four different impeller speeds (5, 6.66, 8.33 and 10 r/s). It was observed that the pH variation was similar to that shown in Fig 1 in all the cases. Though filtration rate was found to be good in all the cases, the filtration rate improved with an increase of RPM. SEM images of ADU produced with different impeller speed have been shown in Fig. 6. At lower RPM (5 and 6.66 r/s) bulk convection was lesser, so nucleation was more and crystal growth was lesser. This is why platelet size was relatively small. SEM images (Fig. 6 c and d) show growth of platelets in ADU produced at 8.33 and 10 r/s. However, breakage of agglomerates and platelets also occur with an increase in impeller speed. It was clearly seen from Fig 5 d. Further, it was observed that decrease in particle size and an increase of specific surface area with an increase in impeller speed. Power per unit volume increases 73% times with an increases in impeller speed from 8.33 to 10 r/s, whereas increase in SSA is only 4.1% and SSA obtained at 8.33 r/s is of good quality ADU. So, impeller speed has been optimized at 8.33 r/s. It may be pointed out that the overall conversion was more than 99% irrespective of impeller speed.

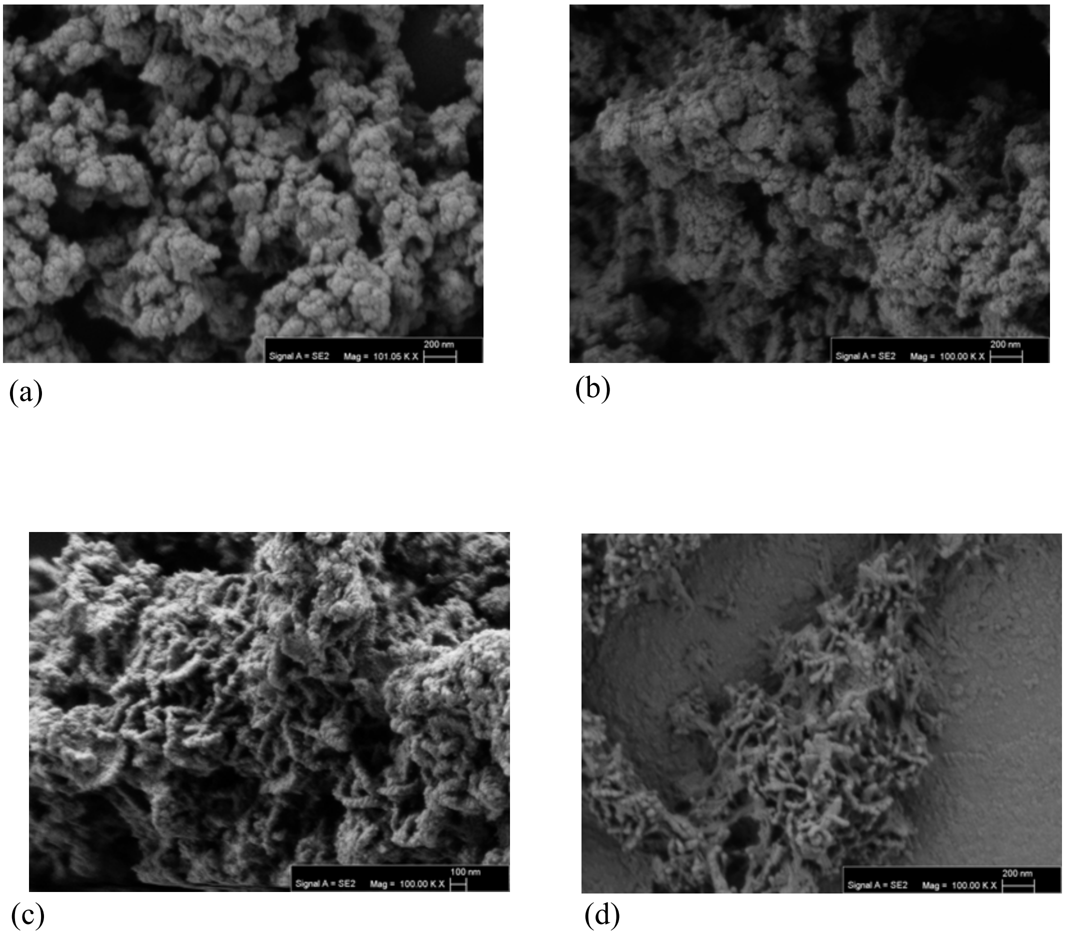

Fig 6: Effect of impeller speed on morphology of ADU a) 5 r/s, b) 6.67 r/s, c) 8.33 r/s and d) 10 r/s

2.6. Effect of ADU calcination temperature on properties of its calcined product:

Uranium oxide was produced by thermal decomposition or calcination of ADU produced from UNS. Effect of calcination temperature on O/U ratio, bulk density, tap density, surface area and morphology of the uranium oxide has been studied here. Morphology of uranium oxides produced by calcination of ADU at different temperatures has been shown in Fig 7. The SEM micrograph at 50,000X, shows pores on the primary platelet of uranium oxide calcined at 550 $^{\circ}$C and at higher temperatures, but no pores has been observed in uranium oxide produced at 450 $^{\circ}$C.

These pores were generated due to release of gaseous NH_3 and water vapors during calcination. The micrographs clearly indicate that sintering of UO_3 powder took place at 650 °C onwards. Specific surface area of uranium oxide, produced by the calcination of ammonium di urinates is generally a function of two competing processes: generation of surface area due to generation of pores and the loss of surfaces due to sintering. This is why surface area of uranium oxide was first increased with an increase of temperature and then was decreased.

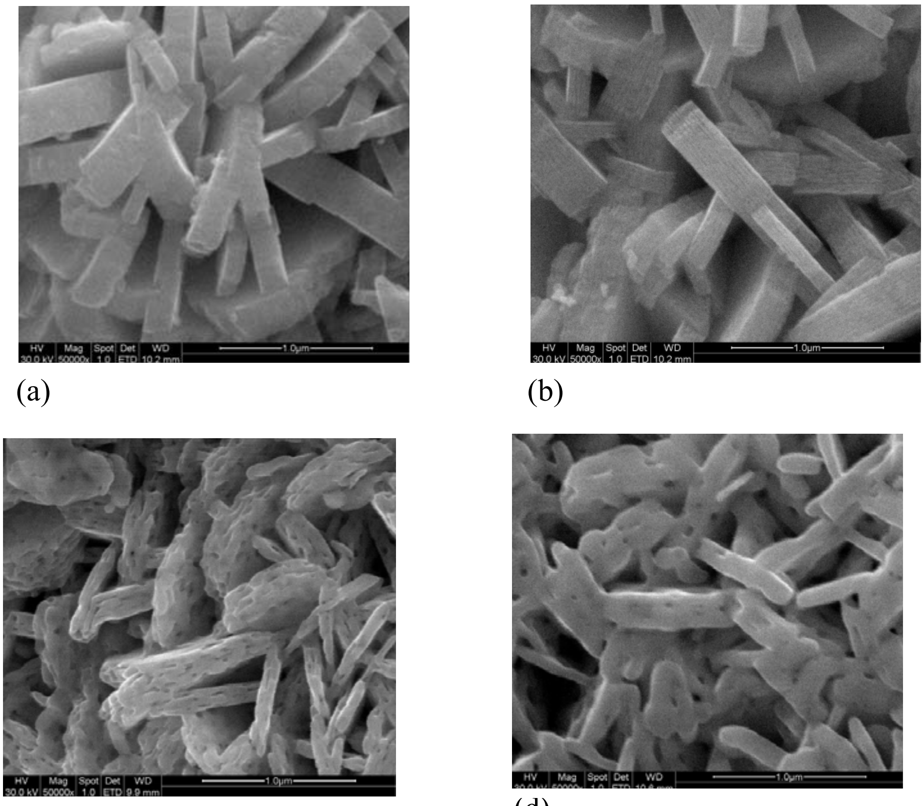

(a) (b)

(c) (d)

Fig 7: morphology of uranium oxide produced by calcination of ADU at different temperatures (a) 450 °C, b) 550 °C, c) 650 °C and d) 750 °C

It was also observed that the O/U ratio of the uranium oxide was reduced with an increase in the calcination temperature. However, the temperature was not found to have significant effect on tap density, bulk density and mean particle size.

2.7. Effect of properties of ADU produced from uranyl nitrate and uranyl fluoride on properties of subsequent products:

ADU produced from both UNS and UFS (containing 65 g/l uranium) by addition of gaseous NH_3 were calcined to UO_3, then further reduced to UO_2 and hydroflorinated to UF_4 at similar conditions. Effect of two different process routes of ADU precipitation on the characteristics of ADU, UO_3, UO_2 and UF_4 were studied here. Uranium recovery during ADU precipitation via UNS route was found more than that of via UFS route. Reduction of UO_3 to UO_2 was lesser in UFS route than UNS route due to presence of fluoride in ADU and subsequent UO_3.This caused more presence of UO_2F_2 in UF_4 produced via UFS route. SSA of UO_2 obtained from UFS is lesser than that of UNS route. This is why UF_4 produced via UFS route content more unconverted uranium oxide (generally indicated as AOI content in UF_4) than UF_4 produced via UNS route. ADU produced from UNS was consisted of orthorhombic $3UO_3.NH_3.5H_2O$ [10] and hexagonal $2UO_3$. NH_3. $3H_2O$ [10] and ADU produced from UFS was consisted of orthorhombic $(NH_4)_3UO_2F_5$ [11], hexagonal $(NH_4).(UO_2)_2F_5.4H_2O$ [12] and hexagonal $2UO_3.NH_3.3H_2O$. Calcined products of ADU produced from these two routes were basically mixture of UO_3 and U_3O_8. Further it was observed that crystal structure of UO_2 and UF_4 produced by two different routes were similar.

3. Summary:

ADU is first intermediate product in solid powder form in flow sheet of uranium metal or uranium oxide fuel production. Its morphology and other properties are important as subsequent products are also retaining the morphology of ADU. Morphology of ADU powders controls their flow-ability required for further material movement through different equipment, surface area required for chemical reactivity of powder, carryover losses occurred during gas solid counter current reaction and tap density required for effective capacity determination. Very small particles may give very high surface area, but very high surface area or reactivity also damages product due to sintering and small particles cause carryover losses occurred during gas solid counter current reaction. Over all rounded shape is also helpful to increase flow-ability. Effect of uranium concentration of feed, temperature of feed, impeller type and impeller speed on the morphology, particle size, specific surface area and crystal structure has been systematically studied. Though growth of platelets increases with an increase of uranium concentration, temperature, power number and rotational speed, effect of temperature has been found to be more dominant. UNS temperature, type of impeller and impeller speed are chosen as 50 $^{\circ}$C, PBT and 8.33 r/s respectively considering required morphology and properties. High resolution SEM has revealed that pores were generated during calcination and at higher temperature sintering of powder took place. As a results surface area was increased with temperature and then was reduced after passing through a maxima. Further, UF_4 was produced from the ADU obtained from both UNS route and UFS route. It has been observed that UF_4 produced via UFS route content more UO_2F_2 and AOI than UF_4 produced via UNS route. Crystal phase analysis shows that inspite of different composition of ADU produced by two routes, crystal structure of UO_2 and UF_4 produced by two different routes were similar.

References:

[1] J. W. Mullin, Crystallization (2001), Butterworth-Heinemann, Oxford.

[2] R. C. Hoyt (1978), Precipitation kinetics of a continuous precipitator, with application to the precipitation of ammonium polyuranate, Retrospective Theses and Dissertations. Paper 6459.

[3] A. G. Jones (2002), Crystallization process systems. Butterworth-Heinemann, Oxford.

[4] H. H.Tung (2013), Industrial Perspectives of pharmaceutical crystallization, Org. Process Res. Dev., 17, 445−454.

[5] J. L. Woolfrey (1978), The precipitation of UO2 powder: effect of ammonium uranate properties, J. Nucl. Mater., 74, 123-131.

[6] C. K. Gupta (2001), Chemical Metallurgy: Principles and Practice, Wiley-VCH, Springer, Germany.

[7] S. Manna, S. Chowdhury, S.K. Satpati and S.B. Roy (2007), Prediction of firing time of magnesio thermic reduction (MTR) reaction and study of relative importance of the dependent parameters using artificial neural network, Indian Chem. Engg., 49 (3), 221-232.

[8] B. N. Murthy and J. B. Joshi (2008), Assessment of standard k–ε, RSM and LES turbulence models in a baffled stirred vessel agitated by various impeller designs, Chem. Eng. Sci., 63, 5468-5495.

[9] V. B. Rewatkar, K. S. M. S. R. Rao and J. B. Joshi (1990), Power consumption in mechanically agitated contactors using pitched bladed turbine impellers, Chem. Eng. Comm., 88, 69-90.

[10] P. C. Debets and B. O. Loopstra (1963), On the Uranates of Ammonium-II X-Ray investigation of the compounds in the system NH_3-UO_2-H_2O, J. Inog. Nucl. Chem., 25, 945-953.

[11] Nguyen-Quy-Dao (1968), On the formation of Alkali Uranates in aqueous solutions: A General Review, Bull. Soc. Chim. Fr, 6, 2403-2407.

[12] V. Seleznev (1971), Russ. J. Inorg. Chem.(Eng Transl.) 16, 1174.

LIST OF FIGURES

LIST OF TABLES

LIST OF ABBREVIATIONS

ADU	Ammonium diuranate
AOI	Ammonium Oxalate Insoluble
ASTM	American Society for Testing and Materials
BET	Brunner-Emmet-Teller
CSD	Crystal size distribution
D	Impeller diameter (m)
DT	Disc Turbine
EDXRF	Energy Dispersive X-Ray Fluorescence
HF	Hydrofoil
ISE	Ion Selective Electrode
JCPDS ICD	Joint Committee on Powder Diffraction, International Centre for Diffraction
LEU	Low enriched uranium
MDU	Magnesium diuranate
MTR	Magnesio thermic reduction
N	Impeller speed (r/s)
NRV	Non return valve
N_P	Power number
P	Power consumption (w)
PBT	Pitched blade turbine
PDF	Powder diffraction file
PVD	physical vapor deposition

PSD	Particle size distribution
RTD	Resistance temperature detector
SDU	Sodium diuranate
SAD	The selected area diffraction
SEM	scanning electron microscope
SSA	Specific Surface Area
TD	Tap density
TEM	Transmission electron microscope
UF_4	Uranium tetra fluoride
UFS	Uranyl fluoride solution
UNS	Uranyl nitrate solution
UO_3	Uranium tri oxide
UO_2	Uranium di oxide
UO_2F_2	Uranyl fluoride
$UO_2(NO_3)_2$	Uranyl nitrate
VFD	Variable frequency drive
XRD	X Ray diffraction
ρ	Liquid density (kg/m^3)

CHAPTER 1

CHAPTER 1

INTRODUCTION

1.1. Introduction

Precipitation or crystallization is one of the oldest unit operations known to mankind. It is a phase transition process of one or more substances from an amorphous solid, liquid or gaseous state to a crystalline state [1]. The processes are used across the chemical, petrochemical, pharmaceutical, speciality industries and nuclear industries to produce bulk chemicals. The rise of the modern chemical industry and the increasing requirements for the quality and quantity of crystalline products were the triggers for the development of industrial precipitators or crystallizers [2].

A high purity products are produced from a supersaturated solution by crystallization process at low energy cost [3]. The non-equilibrium supersaturated condition can be induced in a variety of ways such as removal of solvent by evaporation, addition of another solvent, changes of temperature or pressure, addition of other solutes, chemical reactions, or even combinations of these. The first step in industrial application of crystallization is often to examine equilibrium data and select appropriate mode of crystallization. A typical solubility curve which determines the mode of crystallization to be employed, in order to crystallize a particular substance is shown in Fig. 1.1 [1]. There are three zones: 1. undersaturated: crystals present will dissolve; 2. Metastable: a supersaturated region in which crystals will grow and 3. Labile: a region in which a solution will nucleate spontaneously. The curve also correlates the degree of solution concentration (i.e. supersaturation) to the type of secondary phase (i.e. amorphous solid, or crystalline solid), thus providing a practical guide for the development of crystallization. The condition of supersaturation alone is not sufficient cause for a system to begin to crystallize. The formation of a crystal in a homogeneous fluid requires that an energy barrier be scaled. The total excess free energy between a solute particle and the solute in solution is the sum of the surface excess free energy and the volume excess free energy. The excess free energy tends to be minimized, and this is accomplished through crystal growth or dissolution. The energy necessary to form a new crystal is called the critical free energy, which is a maximum one free energy diagram. If the number of molecules which come together in solution is less than the number required to reach the critical free energy, then the cluster will redissolve. The molecules also have to orientate into a fixed lattice. [4]. At present, there are no theoretical models available which can quantitatively estimate the solution concentration corresponding to the type of secondary phase with industrial significance. Supersaturation can be obtained by many methods such as cooling, evaporation, vacuum, pressure, and reaction, or a combination of these processes.

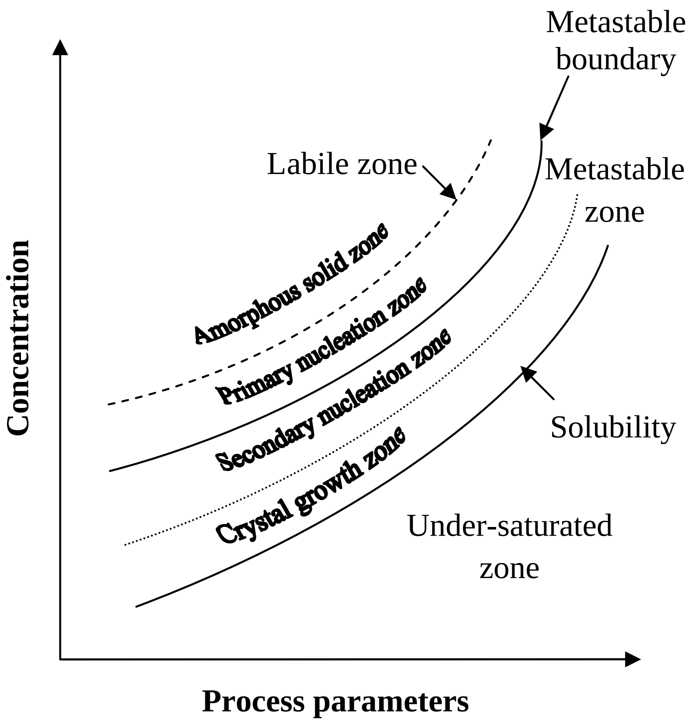

Fig. 1.1: Solubility map showing the relationship between solution concentration and physical characters of the secondary phase [1]

This solubility curve is also useful to determine the method of crystallization to be employed, in order to crystallize a particular substance. If the curve is steep, i.e., the substance exhibits a strong temperature dependence of solubility (e.g., many salts like $NaNO_3$, NH_4CO_3, $NaClO_3$, KNO_3 etc. and organic substances), then a cooling crystallization might be suitable. But if the metastable zone is wide (e.g., sucrose solutions), addition of seed crystal might be necessary. Nucleation occurs at a lower degree of supersaturation as seeding causes secondary nucleation. This may be desirable, particularly if a uniformly sized product is required. If on the other hand, the equilibrium line is relatively flat (e.g., for aqueous common salt solutions), then an evaporative process might become necessary. Pressure crystallization is a process used when the solubility increases with temperature until it reaches a maximum, after which the solubility decreases as the temperature increases (e.g. Na_2SO_4 and Na_2SO_3). If the yield from either of the processes is low, then non-solvent or drowning out processes are used. In non-solvent processes, supersaturation is achieved through the addition of a solvent designed to reduce the solubility of the solute. For example, a significant decrease in solubility of potash-alum in aqueous solutions was seen upon the addition of acetone [5]. The addition of other solutes (other crystallisable species; species not considered as solvents) designed to reduce solubility is known as drowning-out crystallization. If the solute occurs as a consequence of chemical reaction or addition of a common ion, and is relatively insoluble, then precipitation or 'fast crystallization' occurs. The choice of method for generation of supersaturation to crystallize a substance also depends on the product properties desired and economic aspects [6]. The distinction between precipitation and crystallization is quite often based on the speed of the process and the size of the solid particles produced. The term precipitation commonly refers to a process which results in rapid solid formation that can give small crystals that may not appear crystalline to the eye, but still may give very distinct X-Ray diffraction peaks. Amorphous solids (at least as indicated by x-ray diffraction) may also be produced. In nuclear industries, ammonium diuranate (ADU), sodium diuranate (SDU), magnesium diuranate (MDU), uranium peroxide are produced by reactive precipitation or crystallization process.

In reactive precipitation, a solution of one reactant often is mixed with a solution of the other, and the product is formed in concentrations exceeding the solubility. Frequently, the reaction is fast or very fast, and the process parameters influence the product size distribution significantly [7]. In a batch process, the entire volumes of the two reactant solutions are mixed instantaneously in a stirred vessel. In a continuous process, both solutions are fed to the vessel, and there is a continuous or semi-continuous withdrawal of product suspension. In a semi batch process, there is no outlet. An often used technique is to feed a solution of one of the reactants to a stirred solution of the other. One or more reactants react with one or more components in the liquid phase for homogeneous reaction crystallization, and a reactant is often added in the gas or vapour form for heterogeneous reaction crystallization [8]. Chemical reaction, nucleation, growth, agglomeration and breakage are the key process parameters for reactive crystallization. Supersaturation of product is generated by chemical reaction. The primary particle formation process occurring during crystallization and precipitation is firstly nucleation, which determines the initial formation of crystals, and secondly crystal growth, which determines their subsequent size. Important secondary processes can also occur. Particle disruption can occur by which existing particles are broken down into a larger number of smaller fragments. The latter process is also related to secondary nucleation, an additional mode of nucleation particularly prevalent in industrial crystallizers. Agglomeration is a particle size enlargement process by which fine particles, rather than ions or molecules, are joined in an assembly [1]. Both physical and chemical interaction among solute, solvent and solid are involved in reactive precipitation from aqueous solution as suggested in Fig. 1.2 [9].

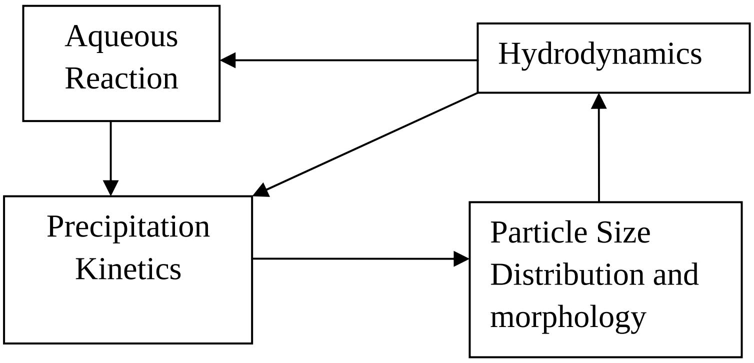

Fig. 1.2: Physical and chemical interactions in liquid solid reactive crystallization or precipitation process

These kinetic parameters (reaction, nucleation, growth, agglomeration and breakage) in turn have an effect on the morphology, size distribution and other properties. The most significant factors affecting the kinetic parameters are the flow field pattern, mixing, residence time, temperature, concentration, degree of supersaturation, and suspension density [10]. Producing a material with the desired quality often requires a sound knowledge of the elementary steps involved in the process: creation of supersaturation, nucleation, crystal growth, aggregation and other secondary processes [6]. Morphology and particle size distribution (PSD) control is important physical attribute because of its potential impact on product quality, purity and downstream filtration, drying, and formulation [11]. One of the main challenges in industrial precipitator is to control the morphology and PSD and to predict the influence of vessel geometry, configuration, operating conditions, and the effect of scale on the process behaviour. A complex variety of different processes occur in precipitators, such as reaction, nucleation, crystal growth, attrition and agglomeration of crystals, fluid dynamics, and heat and mass transfer [12]. Some of these processes are not yet well understood in spite of their need for design and operation of large-scale crystallizers. Process time scale, reactor opacity and the inconvenience and intrusive nature of in-situ experimental assessments are some of the formidable obstacles that prevent full understanding of the process dynamics within the precipitator. The geometrical complexity of crystallizers has rendered theoretical flow field study impractical. Experimental study, on the other hand, is difficult, expensive, and time consuming.

1.2. Motivation for the research work

ADU is first intermediate product in solid powder form in flow sheet of uranium metal or uranium oxide fuel production. Production process and properties of uranium oxide, which is used as fuel in power reactor and uranium metal, which is used as fuel in research reactor, largely depend on ADU characteristics, as morphology of ADU is retained by its subsequent products [13]. Thus ADU precipitation process is very much important in nuclear industry. ADU is generally produced from uranyl nitrate ($UO_2(NO_3)_2$) for natural uranium fuel production and from uranyl fluoride (UO_2F_2) for low enriched uranium fuel production. In the first route, ADU is generated by a reaction between uranyl nitrate and ammonia. In the second route, ADU is produced by reaction between UO_2F_2 and ammonium.

$$UO_2(NO_3)_2 + NH_3 + H_2O \longrightarrow ADU\downarrow + NH_4NO_3 + H_2O \qquad \text{……….. (1)}$$

$$UO_2F_2 + NH_3 + H_2O \longrightarrow ADU\downarrow + NH_4F + H_2O \qquad \text{……….. (2)}$$

The performance of precipitator is assessed not only by the yield of product but also by the quality of product such as powder morphology, specific surface area, particle size distribution and percentage recovery of uranium. Morphology of ADU powders controls their flow-ability required for further material movement through different equipment, surface area required for chemical reactivity of powder, carryover losses occurred during gas solid counter current reaction and tap density required for effective capacity determination. Very small particles may give very high surface area, but very high surface area or reactivity also damages product because of sintering due to high heat of reaction. Small particles also cause carryover losses during gas solid counter current flow. ADU particles of larger platelets and high surface area due to porosity are favourable. Over all rounded shape is also helpful to increase flow-ability. Morphology of the ADU particles largely depends on process parameters like temperature, pH of solution, uranium concentration, feed free acidity, NH_3 feed rate and mixing mechanism. Very high level of supersaturation occurs during precipitation. This is why seeding of ADU particle does not need to facilitate nucleation. As shape and size of ADU particle is basically determined by shape and size of agglomerate, effect of seeding may not be significant. An understanding of effect of different process parameters on morphology of ADU is very much desired. Commercial pure uranium metal in massive form is produced in nuclear industries by Magnesio-Thermic Reduction (MTR) of uranium tetra fluoride (UF_4) [14]. ADU is calcined to UO_3. The UO_3 is then reduced to UO_2 followed by hydrofluorination of UO_2 to UF_4. Performance of metallothermic reaction and recovery of uranium largely depends on properties of UF_4 [15].

1.3. Scope

The scope of this doctoral programme is divided into the following specific areas of study: (a) changes in pH, uranium concentration in solution and composition of ADU with progress of precipitation reaction, (b) effect of uranium concentration in feed, initial temperature of feed and mixing on reaction time of ADU precipitation, morphology, crystal structure and other physical properties of ADU produced from uranyl nitrate solution, (c) effect of calcination temperature on morphology and physical properties of calcined product of ADU produced from uranyl nitrate route and (d) effect of properties of ADU produced from uranyl nitrate and uranyl fluoride on properties of subsequent products.

CHAPTER 2

CHAPTER 2

LITERATURE SURVEY

2.1. Introduction

Ammonium diuranate (ADU) is one of the most important intermediate products in nuclear industries. ADU is thermally decomposed to UO_3 or U_3O_8 by calcination. The oxide is then reduced to UO_2. The UO_2 is either directly used for fuel or converted to uranium metal which is also used for fuel. Uranium metal in form of ingot as well as powder is used for fuel fabrication. UO_2 is hydrofluorinated to UF_4 and then UF_4 is further reduced to uranium metal ingot by Magnesio Thermic Reduction (MTR). Uranium metal powder is produced by direct reduction of UO_2 with calcium. Intermetallic compounds like UAl_3, U_3Si_2, U-Mo etc are generally produced from uranium metal powder. As ADU is first intermediate product in powder form in the flow sheet, production process and properties of uranium oxide, which is used as fuel in power reactor and uranium metal, which is used as fuel in research reactor, largely depend on ADU characteristics, as morphology of ADU is retained by its subsequent products [13, 16]. Thus ADU precipitation process is very much important in nuclear industry. The performance of precipitator is assessed not only by the yield of product but also by the quality of product such as specific surface area, powder morphology, particle size distribution and the purity. These are required for its flow ability, further processing and quality and recovery of the final product.

ADU is generally produced from uranyl nitrate ($UO_2(NO_3)_2$) for natural uranium fuel production and from uranyl fluoride (UO_2F_2) for low enriched uranium fuel production. In the first route, ADU is generated by a reaction between uranyl nitrate and ammonia. In the second route, ADU is produced by reaction between UO_2F_2 and ammonium.

$$UO_2(NO_3)_2 + NH_3 + H_2O \longrightarrow ADU\downarrow + NH_4NO_3 + H_2O \qquad \ldots\ldots\ldots\ldots (1)$$

$$UO_2F_2 + NH_3 + H_2O \longrightarrow ADU\downarrow + NH_4F + H_2O \qquad \ldots\ldots\ldots\ldots (2)$$

In both the production process uranyl solution (either nitrate or fluoride) react with ammonia and precipitation occurs when concentration of product (ADU) exceeding the solubility. The process is called reactive precipitation or crystallization. ADU Chemistry and precipitation kinetics are the key parameter for reactive precipitation process. Products are produced by chemical reaction as per process chemistry and very high level supersaturation occurs due to chemical reaction. Precipitation kinetics control particle morphology, slurry filterability, particle size distribution, surface area and other physical properties. This kinetics depend on process parameters like temperature, pH of solution, uranium concentration, feed free acidity, NH_3 feed rate, hydrodynamics and mixing mechanism.

An effort has been taken in the present research work to understand mechanism of both reaction and precipitation as well as effect of process parameters on the properties of ADU. Research work has been further extended to study effect of ADU calcination temperature on properties of calcined product and effect of ADU properties on its subsequent products.

This chapter systematically describes related available literatures on

(a) Ammonium diuranate chemistry, (b) precipitation kinetics, (c) effect of process parameters on properties of ADU (d) thermal decomposition of ADU and (e) **e**ffect of properties of ADU on properties of its subsequent products.

2.2. ADU Chemistry

The name ammonium diuranate (ADU) has been given to the insoluble product of reaction between either gaseous or aqueous ammonia and solutions containing uranyl ions despite the fact that the molecular composition of the precipitates can be a variable. A number of investigators have studied the crystal structure and chemistry of ammonium diuranate. Addition of ammonia to uranyl nitrate yields a product that originally was believed to be ammonium diuranates: $(NH_4)_2U_2O_7$. Tridot [17] reported some evidence of formation of

$(NH_4)_2U_2O_7$. Bourns and Watson [18] reported that the yellow precipitate (ADU) had NH_3 : U ratio varying from 0.3-0.5, depending on the pH of the supernatant liquid and the amount of washing the precipitate receives. Deane [19] studied ammonium diuranate composition using infra-red spectra and reported that NH_3: U ratio varies from 0.19 to 0.57. He assigned general formula of $UO_2\ (OH)_2$. x NH_3.y H_2O. Deptula [20] observed that NH_3:U ratio varied from about 0.2-0.5.

Garner [21] indexed ammonium diuranate crystals as face centered orthorhombic. He further reported that, under the conditions of rapid precipitation, the products tend to be poorly crystalline, giving X-ray diffraction patterns consisting of relatively few, somewhat diffuse reflections. However, by adding a quantity of ammonia just insufficient to produce a permanent precipitate, and allowing the solution to stand, a highly crystalline product was obtained.

Cordfunke [22] produced ADU of four different solid phases in the range of NH_3-UO_3-H_2O ratios by a reaction between UO_3, NH_3 and water at 40^OC. They produced ADU by mixing of UO_3, water and ammonia of variable concentration for various periods of time (1-4 weeks). After that, the solids were filtered off, washed with water free acetone until free of ammonium ions and dried in air and finally over concentrated H_2SO_4; it was checked that the products do not change composition by this treatment. The crystallinity (XRD) of the four samples was studied by Debets and Loopstra [23]. Compositions and their structures are given in Table 2.1.

Hermans and Markkestein [24] reported that different compositions are possible depending on the method of preparation. He assigned a general formula UO_3 xNH_3 (2-x) H_2O (UO_3-hydrates-ammoniates). The reaction of gaseous or dissolved ammonia with a 0.15 to 0.60 molar uranyl nitrate solution at room temperature yielded (below pH = 9.5) three products, with distinctly different XRD, indicating closely related orthorhombic lattices. The products were designated α, *β* and *γ*, with transition points at a pH around 3 and 9 respectively. The strong resemblance of the XRD of the α, *β* and *γ* forms and that of $UO_3.2H_2O$ suggested that ammonia replaced H_2O in the lattice as NH_3, instead of being present in the form of NH_4^+.

Table 2.1: Chemical composition and crystal structure of ammonium diuranates [22, 23]

Type	Formula	PH	NH_3: U	Crystal structure
I	$UO_3.2H_2O$	3.5	-	Orthorhombic
II	$3UO_3.NH_3.5H_2O$	4-7	1:3	Orthorhombic
III	$2UO_3.NH_3.3H_2O$	>7	1:2	Hexagonal
IV	$3UO_3.2NH_3.4H_2O$	Not mentioned	2:3	Hexagonal

For further experiments, Hermans and Markkestein washed a reactive $UO_3.2H_2O$ several times with dry, liquid ammonia and then dried to make free from adsorbed liquid. A compound with a hexagonal structure (ε) was obtained with lattice parameters a = 4.03 Å and c = 7.12 Å. Whereas washing with water resulted in another hexagonal ADU compound δ with a = 4.09 Å and c = 7.50 Å. In another set of experiments Hermans and Markkestein passed dry gaseous NH_3 over $UO_3.2H_2O$ (prepared as mentioned earlier) powder at room temperature. Dry nitrogen with different percentage of NH_3 gas was conducted across a well stirred sample of UO_3. $2H_2O$ powder. With NH_3 contents of the solid approximately between 1.0 and 1.7 percent by weight, a new orthorhombic compound (ζ) was obtained. At 1.7% NH_3 a trifling but definite shift of the lines was observed (diagram η) which did not change until well above 3 percent NH_3. Then, a hexagonal compound somewhere between δ and ε was obtained. Further action of dry NH_3 gas gave a hexagonal compound with an even smaller c parameter than ε: a = 4.03 Å and c = 7.07 Å. The NH_3 content was at that moment 4.2 percent corresponding to a composition: $(UO_3).(1.2H_2O).(0.8NH_3)$.

Roux and Tets [25] produced very thin, yellowish ADU platelets. For this they mixed 2 ml dimethyl formamide and 50 ml water with 3 ml 0.5M UO_2Cl_2. Then solution was kept in a ampoule. Then ampoule was kept in an oven at $80^{O}C$ for 30 days. They studied X-ray powder diffraction using CuKα source and hexagonal structure was observed by them.

Chen_Yeh et al. [26] reported that ammonium diuranate, produced by reaction of NH_4OH and uranyl nitrate in a pH 3.7 buffer solution, had similar orthorhombic XRD pattern as observed by Debets and Loopstra for type I but had different DR- FTIR spectra characteristics.

Narsimha et al. [27] observed that the consumption of ammonia for complete precipitation of uranium is sufficiently lower than stoichiometric quantity. This indicated that the actual requirement of ammonia for complete precipitation of uranium was considerably less than that dictated by equation:

$$2UO_2(NO_3)_2 + 6NH_4OH \longrightarrow (NH_4)_2U_2O_7 + 4NH_4(NO_3) + 3H_2O \quad \ldots\ldots\ldots\ldots (3)$$

They proposed following alternative equations:

$$3UO_2(NO_3)_2 + 7NH_4OH \longrightarrow (UO_3)_3.NH_3.4H_2O + 6NH_4(NO_3) \quad \ldots\ldots\ldots\ldots (4)$$

$$2UO_2(NO_3)_2 + 5NH_4OH \longrightarrow (UO_3)_2.NH_3.3H_2O + 4NH_4(NO_3) \quad \ldots\ldots\ldots\ldots (5)$$

Das [28] also observed the ammonia to uranium mole ratios was 0.4. He referred the precipitated cake as ammonium polyuranates rather than ammonium di-uranate.

Suton [29] and Notz [30] also reported that polymeric ions were produced during precipitation.

$$2UO_2^{2+} + H_2O = U_2O_5^{2+} + 2H^{+} \text{ and} \quad \ldots\ldots\ldots\ldots (6)$$

$$U_2O_5^{2+} + UO_2^{2+} + H_2O = U_3O_8^{2+} + 2H^{+} \quad \ldots\ldots\ldots\ldots (7)$$

Some evidence has been produced to show that partial degeneration of these polymers occurs during washing and is accompanied by the formation of more crystalline material.

Whether the form of ammonia present in ammonium uranate is NH_3 (ammoniate) or NH_4^+ (ammonium) has been the subject of arguments for a long time. Deane [19] concluded from an I.R. study that ammonia was present as coordinated NH_3 molecules. Garner [21] and Hermans and Markkestein [24] also proposed a similar view. Debets and Loopstra [23] suggested that ammonia was combined as the NH_4^+ ion, but did not present direct experimental evidence to support this opinion. Brusset and Daostated [31] pointed out that the I.R. spectrum of an ammonium uranate ($2UO_3$. NH_3. $3H_2$ O) showed absorbance bands characteristic of $NH_4{}^+$. Stuart and Whateley [32] have used I.R. spectrophotometry, thermo gravimetric analysis (TGA) and differential thermal analysis (DTA) to show that ammonia present as NH_4^+ ion in all ammonium uranates. They prepared ammonium diuranates by equilibration of $UO_3.2H_2O$ and NH_4OH solution, or by addition of NH_4OH solution to uranyl nitrate solution. The dihydrate $\beta UO_3.2H_2O$ was prepared by hydrating UO_3 in water vapour at room temperature and UO_3 was obtained by decomposition of $UO_4.2H_2O$ at 470°C. Precipitates were washed with ethanol until free of nitrate. They concluded that ammonia is present as the NH_4^+ ion in all ammonium uranates. They also explained that the previous I.R. studies might have been confused by the presence of nitrate impurities, which exhibit some absorbance bands in the same regions as do coordinated NH_3 molecules. Also, I.R. data indicate the non existence of four distinct compounds as mentioned by Cordfunke [22] and Debets and Loopstra [23], but rather that the ammonium urinate system is a single phase in which the NH_3:U ratio can be varied continuously. In an aqueous environment the variation of NH^+_4 content occurs by a cation exchange mechanism. They studied the interaction of $UO_2(OH)_2.H_2O$ and solutions of ammonium nitrate and ammonium acetate. These results are consistent with a cation exchange mechanism of the type:

$$UO_2(OH)_2+xNH_4{}^+ \longrightarrow UO_2(OH)_{2\ -x},\ (O^-NH_4^+)_x.+\ xH^+ \qquad \text{..........}\ (8)$$

They opined that the ammonium uranate system was similar in many ways to a zeolite or lamellar clay type material, in which a continuous range of composition can be induced by exchange of cations interposed within an aluminosilicate lattice. By analogy they proposed that ammonium uranates involve a fairly constant uranium-oxygen lattice with exchangeable H^+ or NH_4^+. Changes in diffraction pattern could then arise from slight variations in the positions of oxygen or uranium atoms, or from replacement of H^+ by NH_4^+, leading to changes in symmetry.

On the other hand Urbanek and Moravec [33] suggested that both NH_3 and NH_4^+ can be present depending on the conditions under which the uranates were prepared. ChenYeh [26] finally concluded that when ammonium uranate was obtained at a pH of 3.7, ammonia in the form of NH_3 is predominant. For ammonium uranate obtained by reaction over concentrated NH_4OH, however, most of the ammonia is bonded as NH_4^+.

2.3. Precipitation kinetics

Reactive precipitation or reactive crystallization of sparingly soluble materials is an important industrial operation that is widely used to produce fine and bulk chemicals, pharmaceuticals, biochemicals, catalysts, pigments, ceramics, etc. Precipitation is a very complex process, because it is complicated by several interacting phenomena, and for this reason, it has attracted much attraction. In the process supersaturation is achieved by adding individual reagents to the precipitator and reaction product forms at a concentration higher than its solubility. Reaction, nucleation, growth, agglomeration and breakage are the steps or kinetics of precipitation. Product is formed by chemical reaction. Frequently, reactions are fast or very fast and product is less soluble. Nucleation is the first formation of the solid phase. There are two modes of nucleation. In a primary mode, nucleation occurs without crystalline matter. Primary nucleation may be (a) homogeneous nucleation, which occurs spontaneously from clear solution and (b) heterogeneous nucleation, which occurs in the presence of ‘dust’ particles in suspension, or solid surfaces. It occurs at lower levels of supersaturation than that is required for homogeneous nucleation. Secondary nucleation is induced by presence of existing crystals. At still lower level of super saturation secondary nucleation takes place, which occurs due to aggregation, attrition/breakage and abrasion. Of these types of nucleation, heterogeneous and secondary nucleation is generally the most important for industrial crystallizers. Crystal growth is a diffusion and integration process, modified by the effect of the solid surfaces on which it occurs [1]. Solute molecules/ions reach the growing faces of a crystal by diffusion through liquid phase. At the surface, they must become organized into the space lattice through an adsorbed layer [34]. Agglomeration is a particle size enlargement process by which fine particles, rather than ions or molecules, are joined in an assembly. Agglomeration of ammonium diuranate (ADU) like materials depends on also zeta potential barrier [35]. Existing particles are broken down into a larger number of smaller fragments due to breakage. Breakage largely depends upon the interaction of particles with surrounding particles, impeller and wall. It also depends on the fluid shear. The breakage process is also related to secondary nucleation. Both nucleation and crystal growth rates are function of super-saturations. Higher the supersaturation, higher is the rate of both. The mean crystal size and morphology is determined by the competition between nucleation and growth, both of which depend on supersaturation. Theoretically, nucleation should initiate when solute concentration passes the saturation point and the solution becomes supersaturated [36]. However, it does not occur instantly, and excess of solute remains in solution until a sufficiently high level of supersaturation is generated to induce nucleation [12]. The extent of this supersaturation is referred to as metastable zone width (MSZW). Determination of MSZW is important to avoid or minimize spontaneous nucleation and obtain narrow particle size distribution [37]. At very high supersaturation above the critical value of supersaturation (above metastable zone) at which homogeneous nucleation starts to predominate over heterogeneous nucleation. This causes formation of very small size crystallites. Whereas in metastable zone crystal growth occurs and bigger size crystallites are formed [1]. These crystallites are connected with each other and form primary and secondary agglomerates. However, many times these agglomerates may undergo breakage to smaller agglomerate due to impeller shear. A production process, having high levels of both growth and nucleation result in a very broad crystal size distribution (CSD), which is undesirable from a downstream handling perspective [10]. Therefore, controlling supersaturation profile inside the reactor over the entire time of crystallization is expected to control the levels of nucleation, crystal growth, agglomeration and breakage, thereby control the morphology and crystal size distribution [11].

Ammonium diuranate, material for present research work, is produced by reactive precipitation process. The reaction is very fast and ADU is sparingly soluble in solution. Because of the high supersaturation levels due to very low solubility of ADU, the involved mechanisms of primary nucleation, crystal growth, aggregation and breakage proceed nearly simultaneously [38]. Producing a material with the desired quality often requires a sound knowledge of the elementary steps involved in the process: creation of supersaturation, nucleation, crystal growth, aggregation and other secondary processes [6]. This kinetics has an effect on the particle size distribution, particle morphology and other properties. The kinetic parameters involved in precipitation depend upon many process parameters [10]. Many of them are coupled and hard to study separately. Given vast complexity, it is very important to study different component individually and gradually couple the phenomena.

2.4. Effect of process parameters on characteristic of ADU

Doi and Ito [39] reported the effect of uranium concentration in uranyl nitrate on ADU precipitate and this affected in turn behaviour of particles in the subsequent heat treatments, i.e. calcination in air to higher oxide (UO_3 or U_3O_8) and the subsequent reduction of the higher oxide to UO_2. ADU-precipitates were prepared by adding 28 % NH_4OH to $UO_2(NO_3)_2$ solutions of U-concentrations of 1 and 52 g/l, the addition being invariably stopped at pH 6-7. The precipitates were filtered, dried at 100° C, and ground to – 30 mesh size. Conversion of ADU to UO_3 was carried out by calcination in air. The UO_3 was fired in hydrogen for 3 h at temperatures 900 °C -1700 °C. The resulting UO_2 was disintegrated to -550 mesh size before physical inspections. The samples were inspected by (1) electron microscopy, (2) sedimentation analysis of particle-size distribution, (4) surface area determination by BET method utilizing adsorption of krypton. They also reported that the ADU precipitate usually consists of two or three types of particles. The smallest particles are very thin elementary platelets and size increases directly with the uranium concentration. Larger particles are formed when the elementary platelets are attracted to each other by weak intermolecular forces and, subsequently, bonded by chemical forces into stable primary aggregates. In addition to these two types of particles, secondary agglomerates may be formed when panicles are attracted to each other by weak surface forces. Doi and Ito described polymeric uranyl ions are formed in hydrolysis of uranyl ion during ADU precipitation. All positively charged ions in aqueous solution tend to associate with water (hydration) and a large proportion of such ions tend in turn to associate with other co-ordinating groups (complex ion formation). The hydrolic data of UO_2^{2+} can be best accounted for by the formation of sheet-like complexes with double OH bridges $(UO_2((OH)_2UO_2)_n)^{2+}$. Very thin single crystal line ADU-platelets which are observed in the present experiment must be three-dimensional polynuclear complexes formed by the “corelink” mechanism of this kind. These platelets may be attracted by each other, plane to plane, by weak intermolecular forces, leading to the formation of primary agglomerate.

It was observed by them that when uranium concentration of initial $UO_2(NO_3)_2$ solution was low, the size of the elementary platelets of ADU (ADU(A)) was small and comparatively uniform (0.1-0.2μ), and they built up small agglomerated particles (primary agglomeration) of comparatively uniform size (0.2-0.3μ). They reported that larger size ADU agglomerate (ADU (B)) with wide particle size distribution was obtained when uranium concentration was high. Fig. 2.1 shows the morphology of the ADU (A) and ADU (B) by electron microscopy. Furthermore, they reported that, ADU (A) had appreciably larger particle size than ADU(B). Consequently, they concluded that the formation of larger particles of more homogeneous secondary agglomeration was characteristic of ADU (A) as compared with ADU (B).

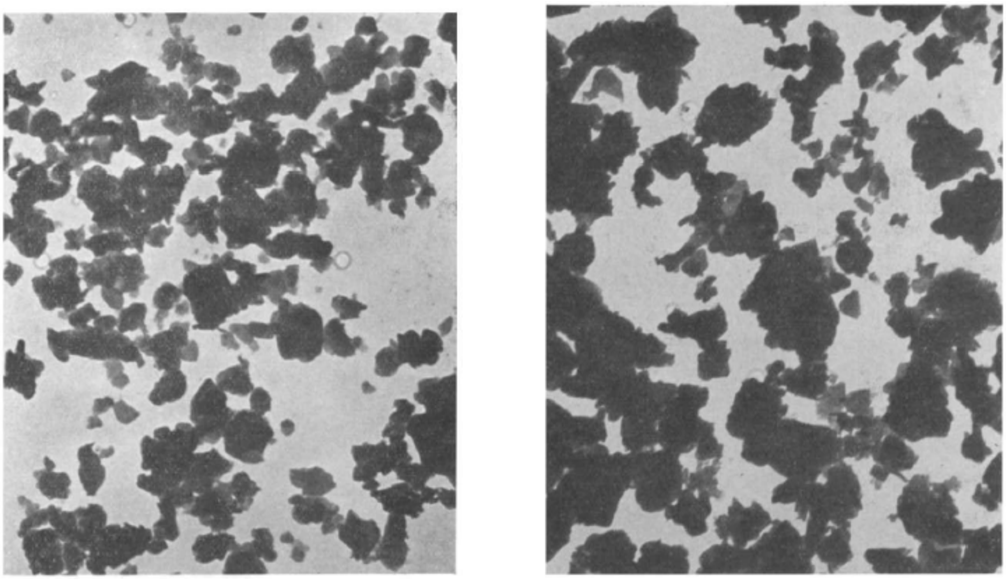

a) b)

Fig. 2.1: Morphology of ADU: (a) ADU (A) and (b) ADU (B) [39]

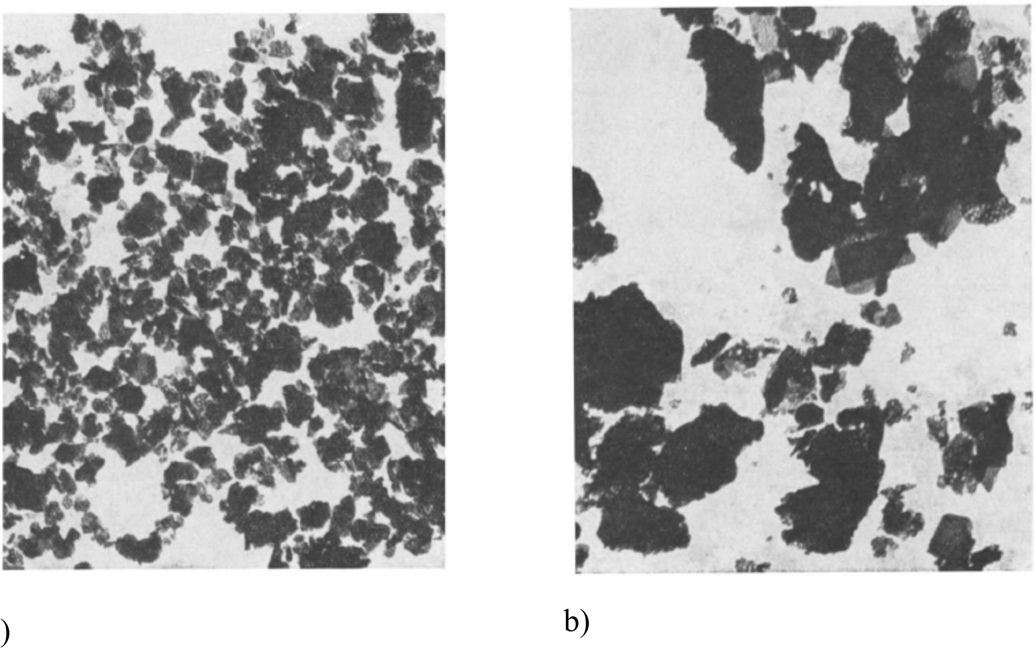
a) b)

Fig. 2.2: Morphology of UO_3: a) UO_3 (A) and b) UO_3 (B) [39]

Fig. 2.2 shows the morphology of the UO_3 produced from ADU (A) and ADU (B). Calcination of ADU precipitate to UO_3 and subsequent reduction to UO_2 at low temperatures did not involve significant modification in microstructure of agglomeration introduced by precipitation. They observed that extensive sintering of resulting UO_2 during firing the UO_3 in hydrogen at elevated temperatures. Lowering of U-concentration in initial UO_2 $(NO_3)_2$ solutions produced smaller elementary ADU platelets and more homogeneous agglomerate. This resulted in improved homogeneity in microstructure of resulting UO_2 at early stage of sintering, and consequently, at more elevated temperatures, sintering of powder aggregate proceeded homogeneously and rapidly to coarse, dense UO_2 particles. This homogeneity in microstructure of UO_2 resulting from natural agglomeration in ADU-precipitate produced even more rapid grain growth as compared to any kind of UO_2 powders compacted beforehand by cold pressing. Fig. 2.3 shows the morphology of the UO_2 produced from UO_3 (A) and UO_3 (B).

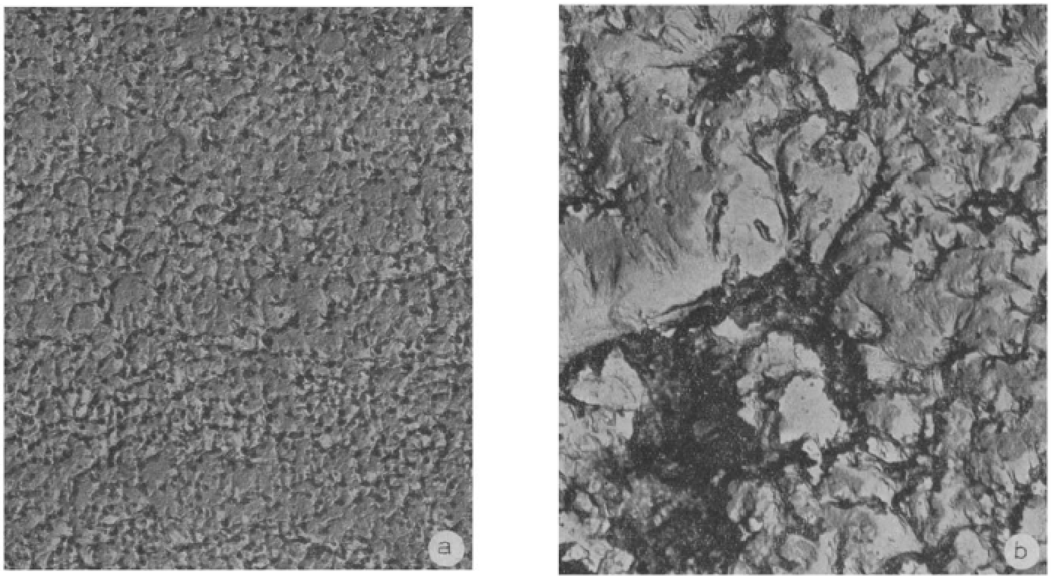

a) b)

Fig. 2.3: Morphology of UO_2: a) UO_2 (A) and b) UO_2 (B) [39]

Janov et al. [40] have investigated effect of final pH of slurry on the properties of ADU precipitates and the sinterability of subsequent UO_2 powders in pellet fabrication. ADU was produced by reaction between uranyl nitrate with analytical grade 11 (N) ammonium hydroxide. The concentration of uranium in uranyl nitrate was adjusted to 70 ± 2 g/l in all experiments and the acidity varied in the range 0.05 to 0.15 N. The uranyl nitrate contained a total of less than 150 ppm cation impurities. After precipitation, the ADU was washed three times by allowing the precipitate to settle, decanting the mother liquor, and then reslurrying precipitate in the demineralised water. The washing reduced the amount of nitrate in the solids to a level below which it was difficult to remove any further nitrate (approximately 0.3 wt %). The washed ADU was filtered in a Buchner funnel and dried in an air oven at 50 ^{O}C to constant weight. UO_2 powders produced from a range of ADU powder by reduction at 600 $^{\circ}$C. They measured surface areas of both ADU and UO_2 by the BET method using nitrogen adsorption. Before nitrogen adsorption, the ADU was cleaned at 50 $^{\circ}$C and the UO_2 at 300 $^{\circ}$C for 18 h. They reported that the conditioning temperature was not critical for ADU and the measured value of surface area did not vary for conditioning temperatures over the range of 50 °C -200 °C. They further reported that the measured UO_2 surface area was a function of the conditioning temperature chosen. Below 300 °C the surface of the UO_2 was not cleaned thoroughly and above surface diffusion processes presumably began to reduce the surface area 300 °C.

The ADU produced at pH 3.5 settled very rapidly and filtered fast but as the pH of precipitation increased above 6.6, the settling rate fell and predictably the slurry became more difficult to filter. They reported that the specific filtration resistance of ADU precipitated at pH 8.4 was 49 times that of ADU precipitated at pH 3.5.

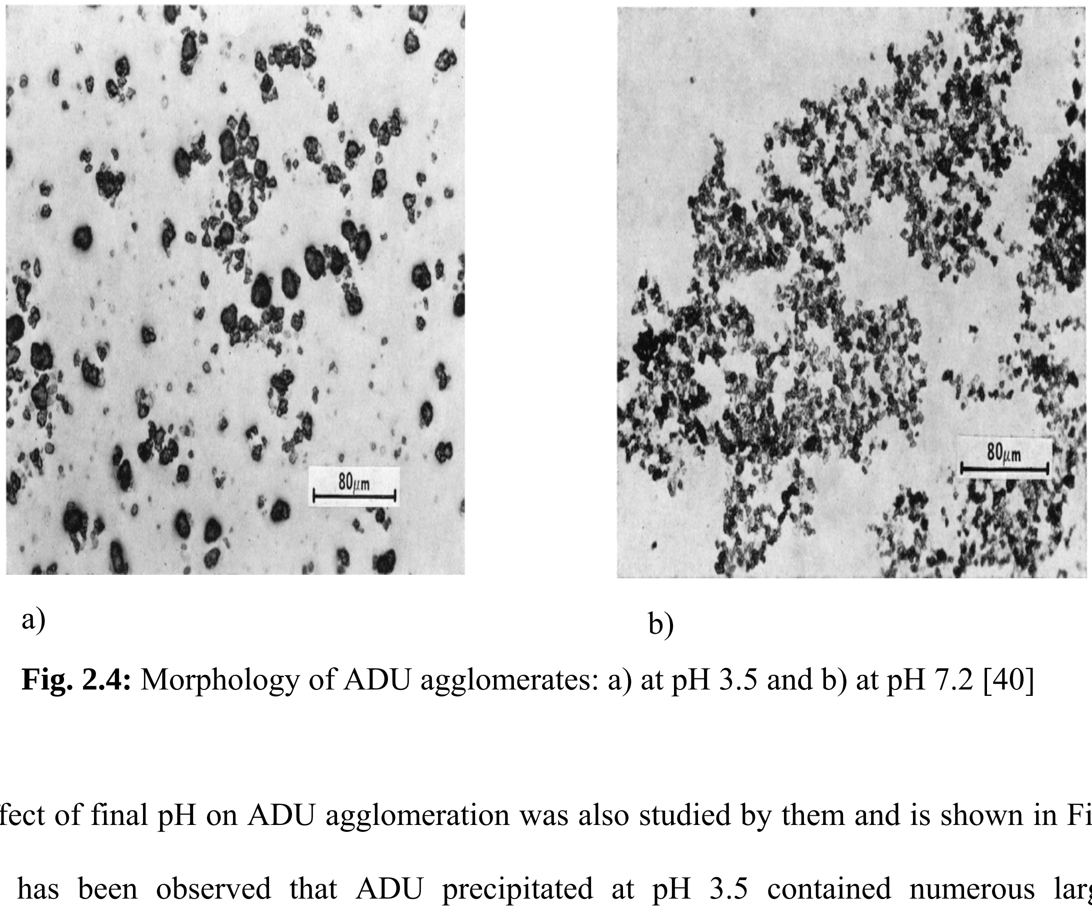

a)

b)

Fig. 2.4: Morphology of ADU agglomerates: a) at pH 3.5 and b) at pH 7.2 [40]

The effect of final pH on ADU agglomeration was also studied by them and is shown in Fig. 2.4. It has been observed that ADU precipitated at pH 3.5 contained numerous large agglomerates of size 20-24 μm while ADU precipitated at pH 7.2 contained agglomerates of approximately 3 μm which were further connected together into chains and secondary clusters. The size of ADU crystallites which make up the agglomerates also decreases with increasing pH, but they are an order of magnitude smaller than the respective agglomerates and hence do not control the rate of settling of ADU slurries. The filterability of ADU slurries could, however, is affected by both crystallite size and agglomerate size.

In unwashed ADU, significant amounts of ammonium nitrate may have prevented the nitrogen gas, used for measuring the surface area, from reaching all the ADU surfaces. Washing removed some of the ammonium nitrate and the measured ADU surface area increased as more of the ADU surfaces became accessible to the nitrogen gas. Most of the surface area change occurred during the first wash when 75% of the ammonium nitrate was removed. After the first wash the measured ADU surface area remained essentially constant.

They reported that the size of UO_2 agglomerates was determined by the manner in which the parent ADU was precipitated. The ADU was chemically converted to UO_2 during reduction at about 600 ^{O}C and caused changes in the size of crystallites but the agglomerates remained essentially intact. This dependence of UO_2 agglomerate size on the ADU can be seen by comparing Fig. 2.4 and Fig. 2.5. The Fig. 2.4 a shows the ADU produced at pH 3.5. This was a fast settling, readily filterable ADU and contained many agglomerates of 20-24 μm in diameter. Fig. 2.5 a is a scanning electron micrograph of UO_2 powder produced from this ADU by reduction at 600 $^{\circ}$C. The powder is aggregated into discrete spherical agglomerates of mean size approximately 10 to 15 μm. In the case of ADU precipitated at pH 7.2, the agglomerates were up to 2-3 μm in diameter but less distinct because they tended to cluster and form loosely bound groupings (Fig. 2.4 b). UO_2 produced from this material was observed using SEM (Fig. 2.5 b). Agglomerates were not as distinct in this type of UO_2 as UO_2 produced from ADU at pH 3.5. But clearly no large agglomerates were present.

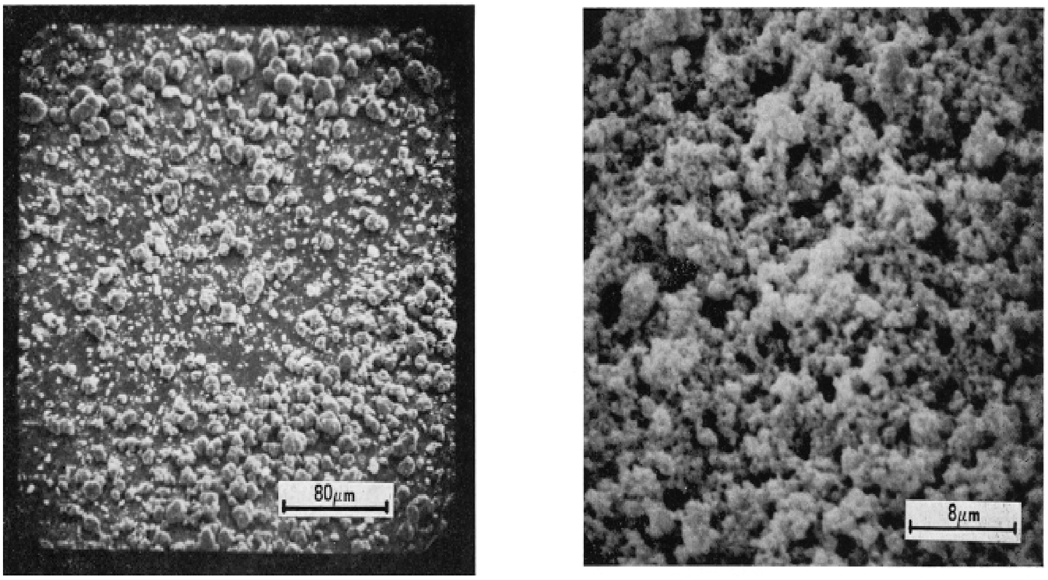

a) b)

Fig. 2.5: Morphology of UO_2 powder: a) from ADU precipitated at pH 3.5 and b) from ADU precipitated at pH 7.2 [40]

However, they also reported that the surface area of UO_2 powder is largely independent of the parent ADU and is mainly governed by the reduction temperature They further reported that the large agglomerates produced poorly sinterable UO_2 powder affected the microstructure of the sintered pellets (Fig. 2.6 a). Numerous isolated dense areas greater than 10 µm in diameter were visible in the etched polished section of the pellet and these were probably produced by sintering within large single UO_2 agglomerates. After the initial sintering within agglomerates, the contact between adjacent agglomerates was apparently not intimate enough to facilitate further sintering to high overall pellet densities and extensive inter-granular porosity remains. Pellets fabricated from UO_2 containing only small agglomerates have much smaller grains and generally a denser pellet with uniform microstructure is obtained (Fig. 2. 6b). They noted that the size of the agglomerates in the powder was found to be a more important parameter than surface area. They finally concluded that the pH at which precipitation occurred was the most important parameter in determining the size of ADU agglomerates and the settling rate and filterability of the slurry. The higher the pH of precipitation, the smaller was the agglomerates. Powders containing large agglomerates gave sintered pellets with low densities and non-uniform microstructures.

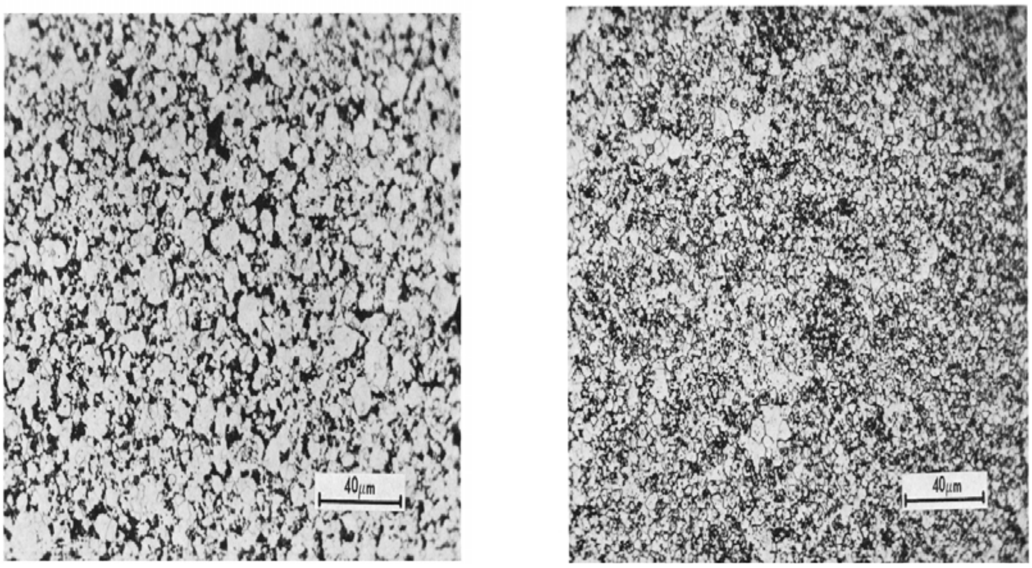

a) b)

Fig. 2.6: Morphology of UO_2 pellet a) from ADU precipitated at pH 3.5 and b) from ADU precipitated at pH 7.2 [40]

Steeper and Zink [41] studied the effect of pH (4, 5 and 6) of the slurry and uranium concentration in uranyl nitrate (100 g/l and 120 g/l) on the particle size distribution of ADU. The temperature was maintained at 50 °C. Particle size distribution was determined by the Andreasen piper sedimentation technique using a dilute ammonium hydroxide solution as the suspending medium. They noticed that particle size distribution followed log normal function.They reported that particle size distribution became narrower with an increase in the slurry pH and an increase in the uranium concentration of the feed. The uranium concentration, at least for the range of values investigated, has more effect the distribution than does the pH.

Roy et al. [42] carried out ADU precipitation by reaction between uranyl nitrate and ammonia diluted with air. They reported that the dilution provide more homogeneous distribution of ammonia in liquid reaction media. This prevents the localized precipitation, increase the number of nucleation and thereby reduce crystalinity. They got finer and lesser flow-able ADU powder when they created similar turbulence by only mechanical agitation.

Narsimha et al. [27] reported influence of temperature of precipitation on characteristics of ADU. They produced ADU by reaction between uranyl containing 120 g/l uranium and 0.25 (N) FA with 7 (N) aqueous NH_4OH solutions in a 1 lit batch. The precipitation was carried out at various temperatures, as 15 °C, 30 °C, 40 °C, 50 °C and 60 °C and various flow rate of ammonia solution as 26 ml/h and 87 ml/h. They reported that in the case of precipitation at 60 °C, though the onset of turbidity (starting of precipitation) took place early compared to that at 30 °C, the completion of precipitation (time to reach pH 8) is delayed considerably as reflected in the length of the plateau. In the case of precipitation at 30 °C, the rate of change of pH of the slurry was fast and continues almost in the same pace till it attained the value of 8.00. While for precipitation at 60 °C though there was a sharp change in pH immediately after the plateau region, the rate of change in pH after this point was relatively very slow and it deteriorated more and more as the pH of the slurry approached the final pH. The slurry obtained at a higher temperature of precipitation settled faster compared to that obtained at a lower temperature. However, the difference in settling rates was considerable only when the rate of addition of ammonia is slow (26 ml/h). At high flow rates (87 ml/h) of addition of ammonia, the settling rate of the ADU slurry did not seem to be dependent on the temperature. The moisture content in the ADU obtained at higher temperature of precipitation was found to be more compared to that obtained at a low temperature. Again, the difference in the moisture contents of ADU obtained at two distinct temperatures was quite high when the flow rate of addition of ammonia was low.

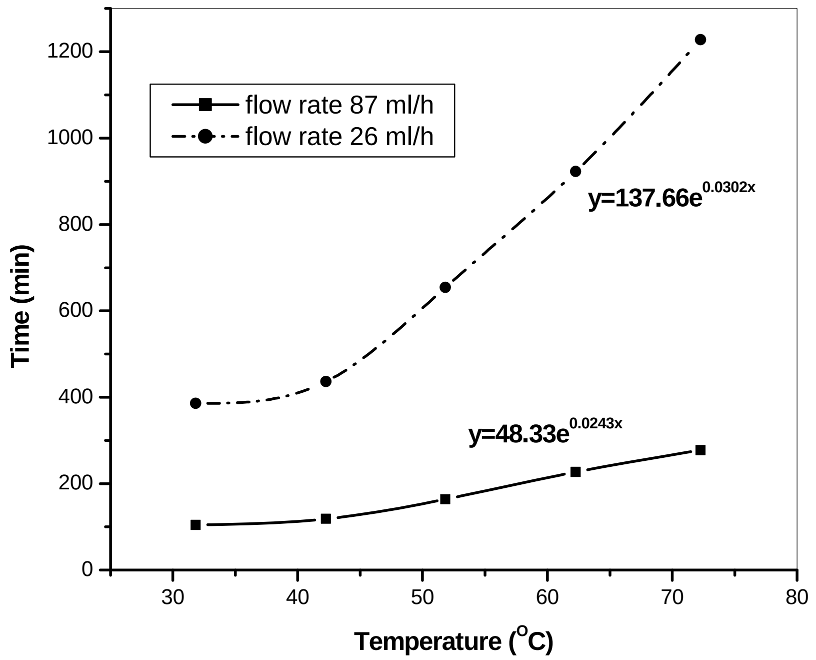

Fig. 2.7: Dependence of total time required on temperature in a batch precipitation process [27]

They observed that the temperature of precipitation of ADU and the time required for reaching pH of 8.00 in a batch precipitation ADU experiment at a given flow rate of addition of ammonia followed an exponential relation. A plot of elapsed time of precipitation vs. temperature of precipitation shown in Fig. 2.7 reveals this fact.

Das [28] investigated effect of process parameters like of uranium and ammonia, pH, temperature of precipitation, form of ammonia (solution or gas), and washing on the properties of ADU. ADU was prepared by reaction between uranyl nitrate containing 100 gpl uranium and ammonia solution containing 25 % w/w ammonia. Surface area was measured based on the physical adsorption of nitrogen gas, at liquid nitrogen temperature. Nitrate in the samples was determined by reduction with Devers's alloy, followed by steam distillation. They carried out ruggedness test to study relative importance of the three process parameters: pH, uranium concentration and concentration of ammonia solution on settling rate and surface area of the ADU. For this he carried out four experiments involving three conditions (concentration of uranium: 100 or 60 g/l, concentration of ammonia: 10 or 8 N and pH: 3.3 or

7). In each case, to 250 ml of uranium solution, maintained at a constant temperature of 50 °C (± 1-2 °C), ammonia was added at a constant rate of 0.5 ml/min with constant stirring. After the precipitation, the stirring was stopped and the settling rate of the precipitates layer was noted down. The pH of the supernatant liquid was noted again after about 30 minutes. The slurry was divided approximately into two halves and filtered through a 540 filter paper. One half was washed two three times on the filter paper with water, while the other half was left unwashed. All the precipitates were dried simultaneously at 105 °C for 4 hours and preserved in desiccators for the other measurements. They concluded that pH is most important parameter compare to others and low pH slurry is sluggish in settling compare to higher pH slurry.

In precipitation or reactive crystallization, supersaturation is achieved by adding individual reagents to the crystallization vessel and reaction product forms at a concentration higher than its solubility. Crystallization at different super-saturations causes different particle sizes and morphology. Different authors [14, 43-62] reported that fluid dynamics or mixing plays an important role in controlling supersaturation profile, hence determining particle sizes and morphology. Both mixing between fluid and particles, and particles and particles affect the crystallization process. The mixing effect is mainly considered on two scales of mixing. One is macromixing, i.e. residence time distribution, which defines retention time of the elementary volumes, and the other is micromixing, which describes communication between elementary volumes [63]. Nature of mixing depends on hardware of the reactor. Though there are different kinds of reactors used in reactive crystallization like stirred tank, jet mixer, forced circulation evaporator, Taylor Coutte reactor; stirred vessel (CSTR) is most commonly used in reactive crystallization. Parameters like reactor and impeller shapes, aspect ratio of the reactor vessel, number, type, location and size of impellers, degree of baffling, etc., provide effective handles to control the performance of stirred reactors [10]. In baffled stirred vessels, flow generated by the rotating impeller interacts with stationary baffles and generates complex, three-dimensional, re-circulating turbulent flow. The mean flow generated by the impeller causes bulk motion of the constituents, which is responsible for the convective transport of momentum, heat and mass. The generated turbulence determines the eddy diffusion of momentum, heat and mass. Hence the overall performance of the stirred vessel depends strongly on the flow field and the associated turbulence characteristics produced by the impeller. There is no published literature on effect of mixing on properties of ADU. But there are several literatures on effect of mixing on properties of product produced by reactive crystallization or precipitation. Most of studies were reported on $BaSO_4$ precipitation. Leeuwen et al. [64] showed that the effect of impeller speed on crystal size was limited and could be negligible for impeller speeds larger than 100 rpm. Wong et al. [65] revealed that, in the concentration range applied, impeller speed had small effect on crystal size and morphology. Pohorecki et al. [66] observed a decrease in the mean particle size with an increase of impeller speed for batch precipitation. Tosun [67] observed particle size first decreases then increases with an increase of impeller speed. Fitchett and Tarbell [9] used an MSMPR crystallizer and found the nucleation rate to decrease and particle size to increase with increased mixing. Wei et al. [68] concluded that impeller speed significantly affects the supersaturation distributions and mean crystal size. They also reported that the feed location is another important operating parameter controlling CSD. Feeding into the region where mixing is poor may lead to a larger average crystal size with a more widely spread distribution. Jaworski et al. [69] reported that agitator speed had little effect on crystal size. Zheng et al. [70] studied effect of mixing and draft tube in a continuous stirred tank reactor with a six bladed rushton turbine impeller. They found that the presence of the draft tube can advantageously enhance the mixing of feed fluids with the reactor environment and provide lower level of the local supersaturation and more uniform distribution in the tank. They concluded the presence of the draft tube increases the mean crystal size. Kamyabia et al. [71] observed increase in mean particle size with an increase in rotational speed of impeller and bigger particle size is obtained in the centre of reactor than other points. Aslund et al. [7] reported that an increase in feed point mixing intensity favor the production of larger crystals based on benzoic acid precipitation. Rousseaux et al [72] reported that higher energy dissipation (i.e. higher rotating speed) generally leads to a specific surface increase and to a slight crystallite size decrease. Feed point locations have a major influence on product properties based on precipitation of pseudo-boehmite.

2.5. Thermal decomposition of ADU

ADU produced then calcined to uranium oxide (UO_3+U_3O_8) and then reduced to UO_2. The thermal decomposition of ADU takes place through different stages. Woolfrey [13] reported that morphology of UO_3 and UO_2 are inherited from the precursor material. Woolfrey prepared ADU powders by precipitation from a uranyl nitrate solution with gaseous ammonia. He reported stage wise thermal decomposition during the calcination of ammonium diuranate and the final reduction to UO_2. The initial dehydration (20^O to 200°C) occurred by a two-stage process involving concurrent removal of coordinated water molecules and some de-hydroxylation. Thermal decomposition of the ADU (stage III) occurred between 200 °C and 350 °C with the loss of NH_3 and H_2O to form “amorphous” UO_3 (UO_3 “A”) and βUO_3, but some of the ammonia is retained within the structure in the form of ammoniate ($UO_3 . xNH_3$). Any nitrate present also gets decomposed. Stage IV (350 °C to 450 °C) was a process of self-reduction by the ammonia retained within the solid to form U_3O_8 and U_4O_9. In the presence of a reducing atmosphere, a final reduction to UO_2 occurred between 450 °C and 500 °C. The specific surface area observed during the decomposition of a powder is generally a function of two competing processes; surface generation due to decomposition and surface loss due to sintering. They observed specific surface area was increased during the dehydration and decomposition stages of the calcination of ADU and reaches a maximum during self reduction.

He also reported that thermal decomposition of ADU in hydrogen was affected by the initial composition (ammonia and nitrate content) and the morphology of the ADU powders. The amount of self-reduction increases with increasing combined ammonia content. The specific surface area of the decomposed powder was increased with increasing total ammonia content and initial surface area of the precursor ADU. Individual ADU platelets retained their external shape when heated below 600 °C. However, subsequent thermal treatment of the decomposed powder was a profound effect on the observed properties and can be used to modify and minimize the effect of precursor powder properties on the final product. In commercial powder production, it is the final thermal treatment of the decomposed powder rather than the precursor ADU properties which controls the final UO_2 powder properties.

Price [73] reported that ADU contained 0.3-0.7 moles ammonia per gram atom of uranium and occluded nitrate ions amounts up to about 0.2 g ion per g atom of uranium. He noted that a significant amount of the contained ammonia was not expelled as gaseous ammonia on heating and the retained ammonia reduced the uranium oxide to approximately U_3O_8. They further observed that even when ADU is reduced in hydrogen, self reduction occurs as the first step. He produced nitrate-free ADU by absorption of ammonia in nitrate free UO_3 di-hydrate (UO_3. $2H_2O$). ADU samples were heated at 5 ^{O}C/min to temperature between 350-430 ^{O}C. A sharp drop in the concentration of ammonia in the solid occurred in the vicinity of 400 ^{O}C, but very little extra gaseous ammonia evolved. Corresponding exothermic peak was also observed. It indicated the reduction of ADU with evolved ammonia. He reported that the uranium oxide powder formed by reduction of ADU was more reactive than that from the parent UO_3 di-hydrate and the surface area of the ADU derived UO_2 was almost twice that of the UO_2 from the parent UO_3 di-hydrate.

Doi and Ito [39] studied the calcination of ADU at 400 °C and 800 °C. They concluded that the calcination at lower temperatures is more effective for rapid growth of resulting UO_2. Their results have been tabulated in Table 2.

Table 2.2: Effects of calcination temperature upon UO_3 [39]

Uranium concentration in uranyl nitrate, (mole/l)	0.022	
Calcination Temperature (°C)	400	700
Calcined product	UO_3	UO_3O_8
Specific surface area of calcined product (m^2/g)	8.4	3.8

Das [28] studied thermal decomposition of ADU using TGA and DTA. For this they heated only 0.1 g sample at a slow and constant rate of 10 °C /min. When ADU is heated / calcined at 650 °C, the surface area of residue uranium oxide is 5 to 6 m^2/ gm but when the ADU was heated to about 960 °C instead of 650 °C the surface area was dropped considerably to 1.4 m^2g^{-1}. . It was also noticed by in the thermal analysis that no loss in weight (no change in composition), but a gradual and continuous endothermic change in this region of 650 °C - 960 °C. They correlate these two and inferred that a sintering process of the oxide started at temperature above 650 °C. They reported that there are three main stage of change in ammonium polyuranate in the temperature range of ambient to 670 °C (i) dehydration (60-225 °C), (ii) decomposition of anhydrous di-uranate to UO_3 (150 °C -500 °C) and (iii) Conversion of UO_3 to U_3O_8 (575 °C -670 °C).

2.6. Effect of properties of ADU on properties of its subsequent products

Uranium production processes are categorized in four groups: 1) reduction of uranium halides with metals, 2) reduction of uranium oxides with metal and carbon 3) electrolytic reduction and 4) disproportionate or thermal decomposition of uranium halides [74]. The reduction of uranium tetrafluoride by magnesium is one of the main industrial methods for producing commercial pure uranium ingot [14-15, 75, 76]. Performance of metallothermic reaction and recovery of uranium largely depends on properties of UF_4 [15] which are inherited from its precursors UO_2, UO_3 and ADU. Doi and Ito [39] and Janov [40] reported effect of properties of ADU on properties of UO_3 and UO_2.

2.7. Summary

Detailed review on chemistry of Ammonium Diuranate (ADU), precipitation kinetics, effect of process parameters on characteristics of ADU, effect of calcination temperature on properties of its calcined product and effect of properties of ADU on properties of its subsequent products have been presented in this Chapter. Different authors reported that molar ratio of NH_3 and U was varying 0.2 to 0.8 depending on operating condition, though the name suggests that ratio should be 1:1. Different authors also reported different crystal structures of ADU depending on production process. Morphology is an important and interesting physical attribute because of its potential impact on downstream filtration, washing, drying, further processing and the final product quality. These characteristics mainly depend on different process parameters like temperature, pH of solution, uranium concentration, NH_3 feed rate and mixing mechanism. An understanding of effect of different process parameters on morphology of ADU is very much desired, which is studied here using high resolution SEM. Recovery of uranium and concentration of uranium in filtrate is another important aspect, which has not been addressed by earlier researchers. Different authors presented mechanism of ADU calcination but no one reported the morphology of its calcined product and effect of calcination temperature on morphology of its calcined product. This is important for selection of calcination temperature. Commercial pure uranium metal in massive form is produced in nuclear industries by Magnesio-thermic Reduction (MTR) of uranium tetra fluoride (UF_4). Performance of metallothermic reaction and recovery of uranium largely depends on properties of UF_4. Still no literature is available on the study of effect of ADU properties on properties UF_4. As ADU is first intermediate product in powder form in the process flow sheet for uranium metal production, its morphology controls morphology of subsequent products. Further research and development is required for better understanding ADU precipitation process to understand its morphology and its effect on subsequent products. These studies would not only provide useful scientific information but also useful for industrial production of uranium metal and uranium base fuel.

CHAPTER 3

CHAPTER 3

EXPERIMENTAL

3.1. Introduction

In this chapter, experimental details of ADU precipitation, ADU calcination to UO_3, UO_3 reduction to UO_2 and hydrofluorination of UO_2 to UF_4 along with different product characterization methods used in the present research work are described. ADU was produced via both uranyl nitrate route and via uranyl fluoride route. Pure uranyl nitrate solution (UNS) was obtained by purification of crude uranyl nitrate solution, produced by dissolution of impure uranium oxide in nitric acid, by 32% Tri-Butyl-Phoshphte (TBP). Whereas, pure uranyl fluoride solution (UFS) was obtained by dissolution of nuclear grade UF_6 in DM water.

3.2. Experimental Set Up

Experimental set up for the present research work is broadly divided in four categories:

a) ADU precipitation system, b) ADU calcination system, c) UO_3 reduction system and

d) UO_2 hydrofluorination system.

3.2.1. ADU precipitation system

ADU precipitation reactor or precipitator is an agitated 4 l glass reactor (10) with dished bottom. Schematic drawing and photograph of the precipitator are shown in Fig 3.1 a and b respectively. The reactor was of 150 mm inner diameter and fitted with different type of impeller (11), motor (12) connected with variable frequency drive (VFD) (13) and 4 number equal spacing 15 mm width baffles. Gaseous ammonia (99.9% pure) from commercial grade ammonia cylinder (1) was mixed with air from compressor (4) at the ratio of 1:10 and the mixture gas was introduced through ring sparger (14). Pressure of ammonia and air was regulated using PRV (2) and pressure regulator (5) respectively. Similar pressure of both ammonia and air was maintained before respective rotameters as indicated by respective pressure gauge (3 and 6). The flow rates of ammonia and air were continuously controlled using two separate valves and calibrated rotameters (7, 8). One non return valve (NRV) (9) was provided in gas feeding line just prior to entering the reactor to prevent reverse flow of liquid in gas line. pH and temperature of the solution were continuously measured using pH electrode (16) and RTD (17) respectively and indicated in pH meter (18).

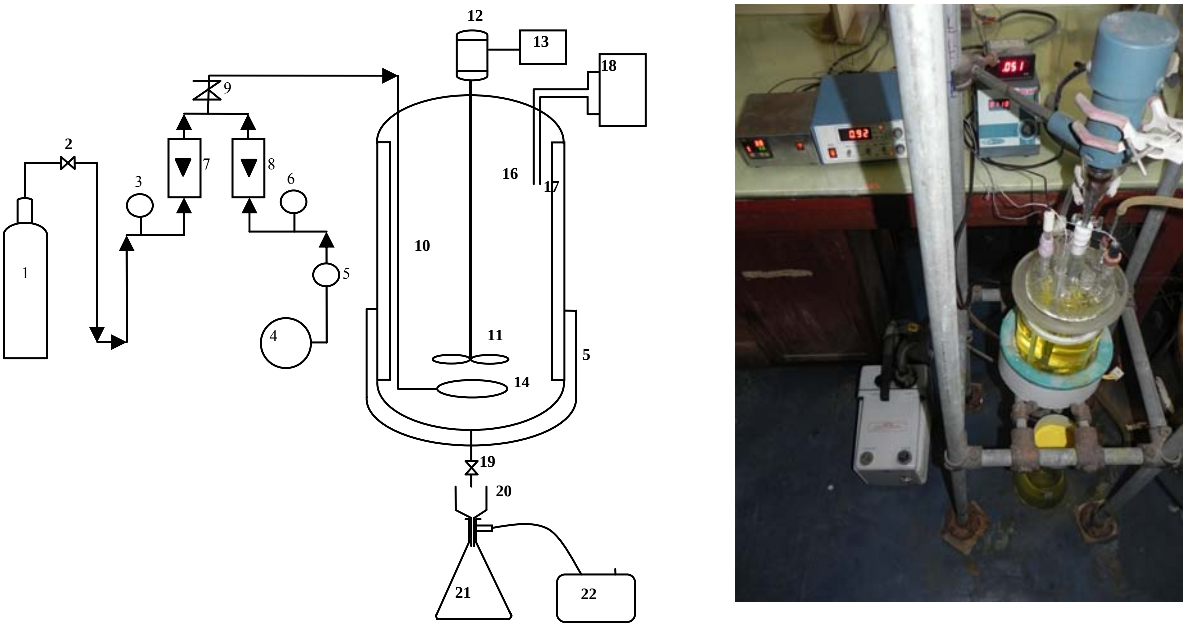

1. Ammonia Gas Cylinder
2. Pressure Reducing Valve
3. Pressure Gauge
4. Air Compressor
5. Pressure regulator
6. Pressure Gauge
7. NH_3 Rotameter
8. Air Rotameter
9. NRV
10. Glass Reactor
11. Impeller
12. Motor
13. VFD
14. Sparger
15. Muffle Heater
16. pH Electrode
17. PT 100 RTD
18. pH Meter
19. Bottom valve
20. Buchner Funnel
21. Conical Flask
22. Vacuum Pump

Fig. 3.1: (a) Schematic diagram and (b) pictorial image of ADU precipitation system

After completion of reaction the slurry was filtered under vacuum using the Büchner funnel (20) and 542 grade Whatman filter paper. Vacuum pump (22) was used to create vacuum. Flush bottom valve (19) was used to prevent chocking at bottom nozzle. Filtrates were collected in conical flask (21).

3.2.2. ADU calcination system

Calcination of ADU was carried out in a static bed box type muffle furnace. Schematic drawing and photograph of the ADU calcination system are shown in Fig 3.2 a and b respectively. ADU powder was kept inside a tray and tray was kept inside the furnace. The furnace is a resistive heating furnace with K-type thermocouple was inserted on a thermowell from outside of the muffle. The temperature of the furnace was controlled through PID temperature controller. The calcination was done at 550 °C for four hours. The exhaust of the furnace was discharged into the atmosphere after scrubbing through a wet scrubber.

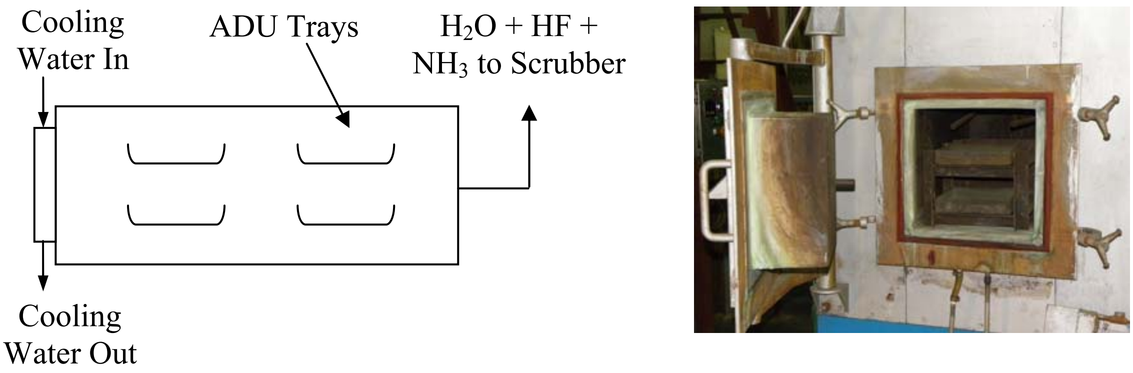

Fig. 3.2: (a) Schematic diagram and (b) pictorial image of ADU calcination system

3.2.3. UO_3 reduction system

UO_3 reduction system is basically a static bed tubular muffle furnace with hemispherical trays of 160 mm diameter and 480 mm length inside it. Schematic drawing and photograph of the UO_3 reduction system are shown in Fig 3.3 a and b respectively. Similar to calcination furnace the furnace was a resistive heating furnace with K-type thermocouple inserted on a thermowell from outside of the muffle and the temperature of the furnace was controlled through PID temperature controller. Provision of Argon purging inside the reactor was made. The reduction was done at 750 °C for four hours. The exhaust of the furnace was discharged into the atmosphere after passing through a wet scrubber.

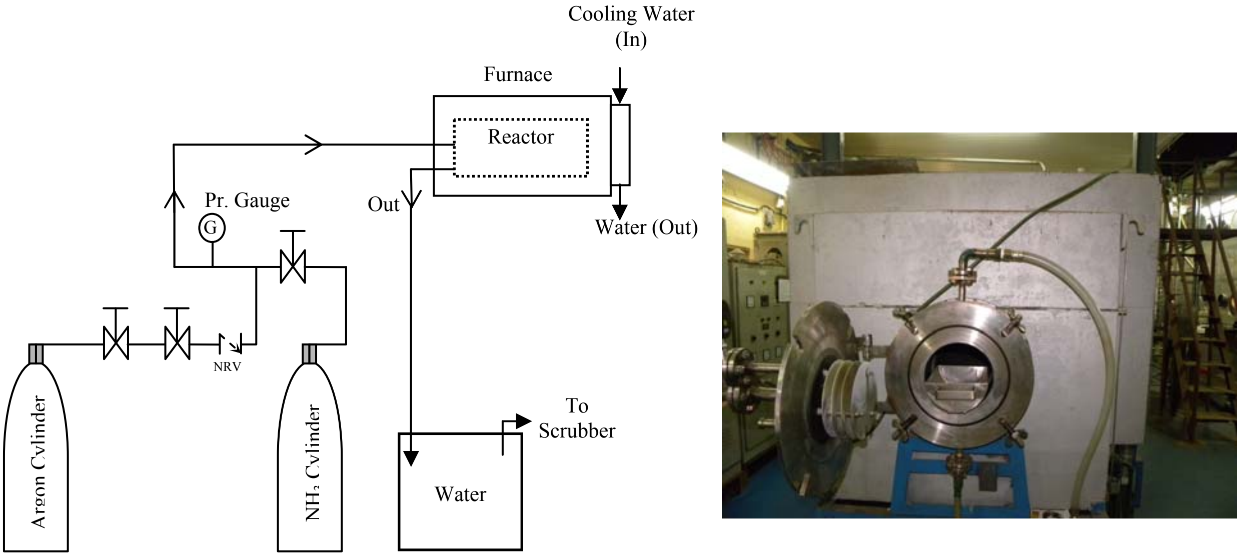

Fig. 3.3: (a) Schematic diagram and (b) pictorial image of UO_3 reduction system.

3.2.4. UO_2 hydrofluorination system

UO_2 hydro-fluorination system was consisted of a rectangular cross section reactor of inconel 600. Schematic drawing and photograph of the UO_2 hydro-fluorination system are shown in Fig 3.4 a and b respectively. The reactor is then loaded into a resistive heating furnace with K-type thermocouple inserted on a thermowell from outside of the reactor. The temperature of the furnace was controlled through PID temperature controller. The hydrofluorination was carried out at 750 °C for four hours. The exhaust of the furnace was discharged into the atmosphere after passing through a wet scrubber.

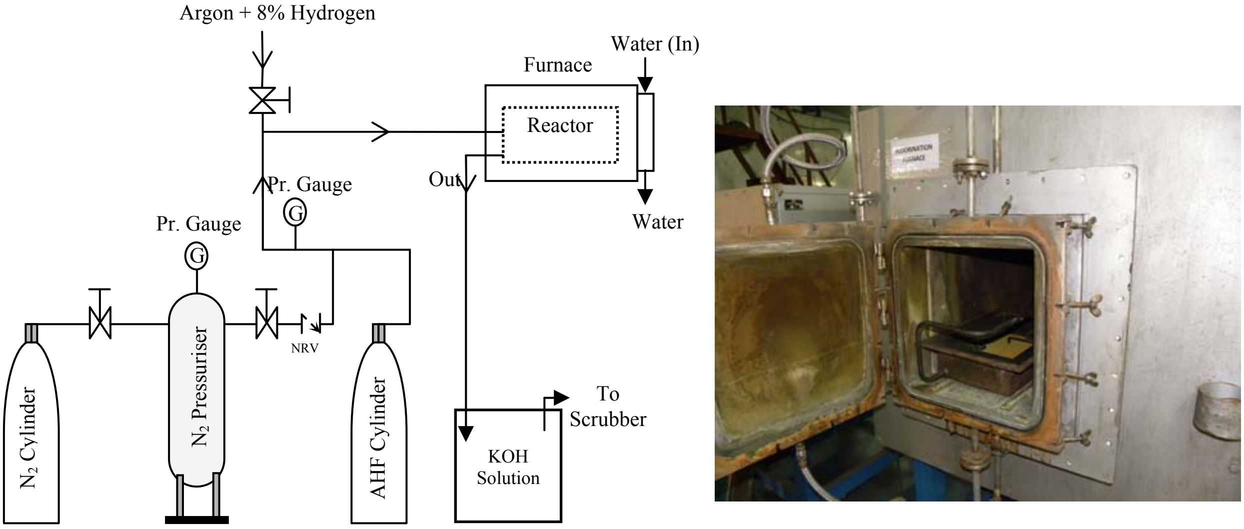

Fig. 3.4: (a) Schematic diagram and (b) pictorial image of UO_2 hydro-fluorination system.

3.3. Experimental procedure

In the present research work, experiments were carried out to study a) effect of process parameters and mixing on characteristics of ADU, b) Effect of ADU calcination temperature on morphology and physical properties of its calcined product UO_3, c) Study on progress of ADU precipitation via both UNS and UFS route and d) Study on effect of ADU produced from different route on subsequent products.

3.3.1. Changes in pH, uranium concentration in solution and composition of ADU with progress of precipitation reaction

During this study, ADU was produced by addition of gaseous ammonia in both UNS and UFS with special attention on first appearance of the precipitate and changes in crystal structure and morphology with pH. Uranium concentration and temperature of both the feed solutions were 65 g/l and 50 °C respectively. PBT type impeller was used as impeller and rotational speed of the impeller was maintained at 8.33 r/s. Air purging was continued both the cases. During ADU precipitation the reaction pH of the solution was continuously monitored through pH meter. Samples (aliquot) were withdrawn after regular intervals. The samples collected were filtered using Büchner funnel and 542 grade (pore size 2.7 μm) Whatman filter paper and then washed with distilled water. Cakes were then naturally dried. The pH and uranium concentration in the filtrate were measured. The cake obtained was washed twice with total 100 ml distilled water. Then, the cake was dried in an oven at 100 °C for 4 h. Morphology and crystal structure of dried ADU was measured.

3.3.2. Effect of process parameters and mixing on characteristics of ADU

Study on effect of process parameters (uranium concentration in feed and feed temperature) and mixing (type of impeller and rotational speed of impellers) was carried out based on ADU precipitation from UNS only. Experiments were performed for six concentrations of uranium in UNS: 20 g/l, 40 g/l, 60 g/l, 80 g/l, 100 g/l and 120 g/l to observe the effect of uranium concentration. To generate UNS of different uranium concentration, UNS containing 50 g/l uranium was either evaporated (to increase uranium concentration) or diluted with required DM water (to reduce uranium concentration). To study the effect of initial temperature of UNS, UNS was heated up using muffle heater (15) to preset temperature. Once the set temperature was reached heater was automatically switched off. To reduce the temperature below the room temperature, ice blocks were used. Experiments were carried out at four different temperatures: 10 °C, 30 °C, 50 °C and 70 °C. To study the type of impeller (11), three impeller design were used (a) six bladed disc turbine (DT), (b) six 45° pitched blade turbine(PBT) and (c) three bladed hydrofoil (HF). Pictorial images of these impellers are shown in Fig. 3.9. In all the three cases the impeller sweep diameter was 0.4 times the tank diameter (150 mm). The impeller speed was varied from 5 r/s to 10 r/s using variable frequency drive (VFD) to study effect of impeller speed. For all the experiments ammonia was added until pH of the solution reached to 7.5. After pH 7.5, the addition of ammonia was stopped. The final slurry was then filtered under vacuum using the Büchner funnel (20) and 542 grade Whatman filter paper. Uranium concentration in the filtrate was measured. The cake obtained was washed twice with total 100 ml distilled water. Then, the cake was dried in an oven at 100 °C for 4 h. Morphology, crystal structure, particle size and surface area of ADU powder were studied.

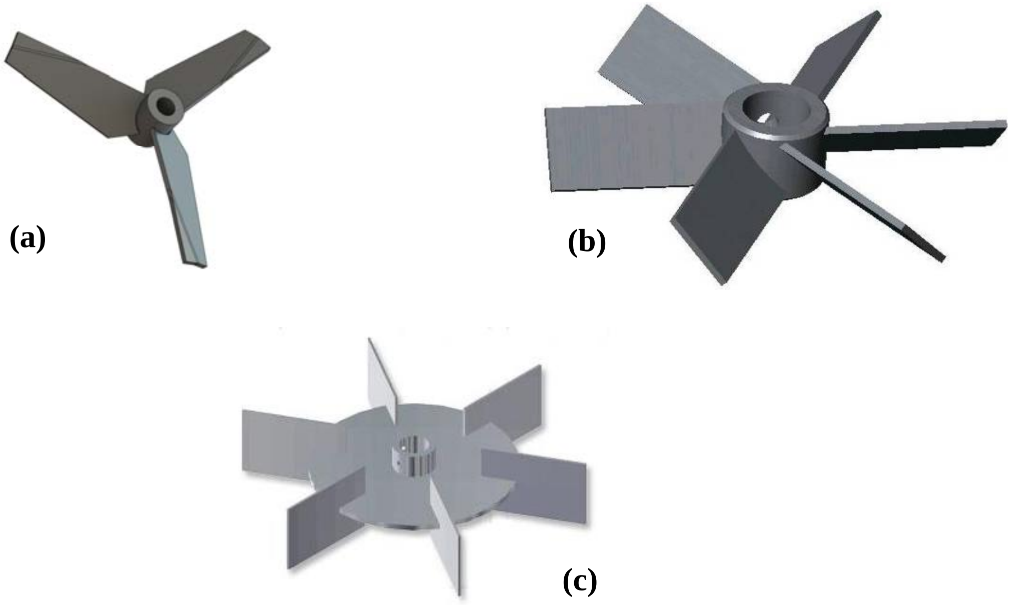

Fig. 3.5: Pictorial image of (a) three bladed hydrofoil (HF), (b) six 45° pitched blade (PBT) and (c) six bladed disc turbine (DT)

3.3.3. Effect of ADU calcination temperature on morphology and physical properties of its calcined product UO_3

ADU produced by reaction of UNS and gaseous diluted ammonia was dried in an oven at 100 ^{O}C for 4 h. 100 g of dried cake was taken in a porcelain crucible. Calcination was carried out in a muffle furnace at the temperatures of 450 °C, 550 °C, 650 °C and 750 °C for a period of 4 h. Slightly negative pressure (50-100 mm water column) has generally been maintained in the furnace to remove release gas. The rate of gas release increases with an increase in vacuum. High level of vacuum doe not used as chance of carryover loss of calcined product of ADU increases at high vacuum. Morphology, crystal structure, O/U, density particle size, and surface area of calcined product of ADU powder were studied.

3.3.4. Study on effect of properties of ADU produced from UNS and UFS on properties of subsequent products

ADU produced from both UNS and UFS by addition of gaseous were calcined to UO_3, further reduced to UO_2 and hydroflorinated to UF_4 at similar conditions. Effect of two different process routes of ADU precipitation on the characteristics of ADU, UO_3, UO_2 and UF_4 were studied here.

ADU was produced by reaction of ammonia with UNS and UFS in agitated vessel. Uranium concentration and temperature of both the feed solutions were 65 gpl and 50 ^{O}C respectively. PBT type impeller was used as impeller and rotational speed of the impeller was maintained at 8.33 rps. Air purging was continued both the cases. ammonia was added until pH of the solution reached to 8.5 for both routes. The final slurry was then filtered under vacuum using the Büchner funnel (20) and 542 grade Whatman filter paper. Uranium concentration in the filtrate was measured. The cake obtained was washed twice with total 100 ml distilled water. Then, the cake was dried in an oven at 100 $^{\circ}$C for 4 h. Crystal structure, fluoride content, particle size and specific surface area of ADU powder were studied.

UO_3 was produced by calcination of two types of ADU in similar condition. Calcination was carried out in box type furnace. Temperature was increased from room temperature to 550 $^{\circ}$C @ 5 $^{\circ}$C per min and then maintained 550 $^{\circ}$C for 4 h. Then heating was stooped. Crystal structure, fluoride content, particle size, specific surface area and O/U of UO_3 were measured. Further, UO_3 was reduced by passing NH_3 gas over the static bed of UO_3 at 750 $^{\circ}$C inside a box furnace. The furnace was first evacuated three times and back flushed with argon. The furnace was heated at a ramp rate of 6.25 $^{\circ}$C /min and argon flow was continued till 750 $^{\circ}$C.

NH_3 gas was then fed over UO_3 @ 8-10 LPM. Similar operating conditions were maintained both the cases. Crystal structure, fluoride content, particle size, specific surface area and O/U of UO_2 were measured.

UF_4 was produced thereafter by passing anhydrous HF gas over the static bed of UO_2 at 450 °C inside a box furnace. The furnace was evacuated three times and back flushed with argon. The furnace was heated at a ramp rate of 5°C/min. Argon was purged till 450 °C and after that reducing gas (Ar-8%-H_2) was purged at the rate of 5-7 lpm for 30 minutes. HF was then purged for 30 minutes at 450 °C. Similar operating conditions were maintained both the cases. Morphology, crystal structure, particle size, TD, FA, % moisture, UO_2F_2 and AOI content of UF_4 were measured.

3.4. Methods of Analysis

Different analytical and characterization techniques for measurement of properties of ADU and its subsequent products UO_3, UO_2 and UF_4 have been described here.

3.4.1. Uranium concentration

Determination of uranium is carried out by three techniques viz. UV-Visible Spectrophotometry, Energy Dispersive X-Ray Fluorescence (EDXRF) and Volumetry. These three methods cover determination of uranium from ppm to moles/l. In spectrophotometric method absorbance of uranium-thiocyanate complex formed in organic medium is measured. This method has a precision of ±2 - 3 %. For EDXRF measurements, the L-alpha fluorescence X-Ray line of uranium having energy 13.6 eV is used. The instrument is calibrated using a set of matrix matched standards. Strontium is used as internal standard. The minimum determination limit is 10 ppm and the precision is ±2 - 3 %. Volumetric method involves a redox titration procedure. U (VI) is reduced to U (IV) by Fe (II) in presence of concentrated phosphoric acid and the excess Fe (II) is oxidized to Fe (III) with nitric acid. on dilution, the potentials reverse and an equivalent amount Fe (II) is generated which is titrated with standard potassium dichromate solution. The precision is ± 0.5. Pictorial image of EDXRF and spectrophotometer is shown Fig 3.6 a and b respectively.

Fig. 3.6: Pictorial image of (a) Energy Dispersive X-Ray Fluorescence (EDXRF) and (b) spectrophotometer

3.4.2. pH

PH analysis is carried out by electrochemical method using hydrogen ion selective electrode (PH electrode). When pH electrode is in contact with a solution containing hydrogen ion, an electrode potential is develops. This potential is measured against a constant reference potential with digital pH meter. The pH measuring system used here is consisting of a 10PHM 11 meter, 10PHM 90 electrode and an automatic thermal compensator. The electrode was calibrated with standard buffer solution over the pH range of measurement prior to every experiment.

3.4.3. % Fluoride

Fluoride is measured by electrochemical method using Ion Selective Electrode (ISE). The range of analysis is 0.02 ppm to saturation concentration of fluoride. The fluoride ISE consists of sensing element bonded in to epoxy body. When sensing element is in contact with a solution containing fluoride ion, an electrode potential is develops across the sensing element. This potential, which depends on free fluoride ion in the solution, is measured against a constant reference potential with digital ion/millvolt meter. Thermo Orion make Orion 720+ Advanced ISE/PH/mV/ORP meter (Fig: 3.7) was used for fluoride analysis.

Fig. 3.7: Pictorial image of Fluoride measurement instrument

3.4.4. O/U ratio

O/U ratio is determined by gravimetric method, where uranium oxide sample is converted in to stable uranium oxide U_3O_8 at 800 $^{\circ}$C and uranium content in the sample is calculated. From the quantity of oxygen & uranium present in the sample, molar concentration and then ratio is calculated.

3.4.5. Tap density

Tap density is determined physically by using simple formula d=m/v. The volume of previously weighed powder sample is measured by tapping of powder in measuring cylinder as per ASTM B-527, 1976.

3.4.6. UO_2F_2 content

UO_2F_2 Content in the sample is determined by spectrophotometry. Sample is leached into methanol at 60 °C and optical density of leached solution is measured against blank (methanol). The concentration is calculated by comparing optical density of sample with optical density of standard solution. Spectrophotometer UNICAM-UV 500 was used for measurement of optical density/absorbance.

3.4.7. Ammonium Oxalate Insoluble (AOI) content

AOI indicated unconverted uranium oxides in UF_4. UF_4 $_s$ample is dissolved in 6% hot ammonium oxalate solution. The insoluble is filtered, dried and weighed.

3.4.8. % FA content

Free acid is determined by acid-base titrimetry. Sample is leached in water, filtered and titrated against std. solution of NaOH. From the normality and NaOH volume consumed, free acid content is calculated.

3.4.9. % Moisture content

Moisture determination is carried out by gravimetric method. Sample is dried at 105 °C & from weight difference moisture content is calculated. Moisture is also determined by moisture analyser which works on the basis of weight loss after drying at 105 °C. Sartorius make MA100 moisture analysis is used for moisture determination.

3.4.10. Crystal structure

Crystal structure of ADU was studied by X-Ray diffractometer. It is consisted of three basic elements: (a) X-ray tube, (b) a sample holder, and (c) an X-ray detector. X-rays are generated in a cathode ray tube by heating a filament to produce electrons, accelerating the electrons toward a target by applying a voltage, and bombarding the target material with electrons. When electrons have sufficient energy to dislodge electrons from the inner shell of the target material, characteristic X-ray spectra are produced. These spectra consist of several components, the most common being Kα and Kβ. Kα consists, in part, of $K\alpha_1$ and $K\alpha_2$. Kα1 has a shorter wavelength and twice the intensity as $K\alpha_2$. The specific wavelengths are characteristic of the target material (Cu, Fe, Mo and Cr). Filtering, by foils or crystal monochrometers, is required to produce monochromatic X-rays needed for diffraction. Copper is the most common target material for single-crystal diffraction, with Cu $K\alpha$ radiation = 1.5418Å. The sample and detector are rotated; the intensity of the reflected X-rays is recorded. When the geometry of the incident X-rays impinging the sample satisfies the Bragg's equation, $2d\sin\theta = n\lambda$, constructive interference occurs and the peak intensity of the diffracted beam is observed. For typical powder patterns, data is collected at 2θ from $\approx 10°$ to 70° angles that are preset in the X-ray scan. The d-spacing of each peak is then obtained by solution of the Bragg equation for the appropriate value of λ. Because each material has a unique set of d-spacings, matching these d-spacings provides an identification of the unknown sample. Files of d-spacings for hundreds of thousands of inorganic compounds are available from the International Centre for Diffraction Data as the Powder Diffraction File (PDF). In the present study 'Match' software was used to indexing the peaks.

In the present study crystal structure of ADU was studied by X-Ray Diffraction using INEL Equinox 3000 powder diffractometer in Bragg-Brentano geometry with monochromatic Cu-Kα radiation (λ = 1.54056 Å). The x-ray data was taken from 10°–100° of 2Θ using curved position sensitive detector having resolution of 0.029°. Yttrium oxide was used to check the calibration of the diffractometer. The phases were identified using the database compiled by Joint Committee on Powder Diffraction, International Centre for Diffraction (JCPDS ICDD 1999).

Fig. 3.8: Pictorial image of X-Ray Diffractometer

3.4.11. Particle size

Particle size distribution and mean particle size of ADU and its subsequent products were measured using laser particle size analyzer. Figure 3.9 shows the actual photograph of a laser particle size analyzer. The operation of laser particle size analyzer is based on the principle of light scattering that the angle of scattered light is inversely proportional to the particle size (i.e. the smaller the particle size, the larger the scattering angle). As particle size decreases, the observed scattering angle increases logarithmically. Scattering intensity is also dependent on particle size and diminishing with particle volume. Large particles therefore scatter light at narrow angles with high intensity whereas small particles scatter at wider angles but with low intensity. Mean diameter (also called mean size) is the statistical mean value diameter of particles contained in the sample. Designated amount of powder is dispersed in distilled water and passed through the optical prism, where laser interacts with particles. Multiple detectors located at different angles in order to measure the number of counts. In the present study CILAS 1090 was used for measuring the mean particle size and its distribution of starting powders.

Fig. 3.9: Pictorial image of instrument used for measuring PSD

3.4.12. Morphology

Morphology or shape of the powders were measured by scanning electron microscope (SEM). Figure 3.10 shows photograph of SEM. SEM is an instrument to study the microstructure of the materials. In a typical SEM, electron is thermionically emitted from an electron gun fitted with a tungsten filament cathode. The electron beam, which typically has an energy ranging from 0.5 to 40 keV, is focused by one or two condenser lenses to a very small spot. The beam passes through pairs of scanning coils or pairs of deflector plates in the electron column, typically in the final lens, which deflect the beam in the *X* and *Y* axes so that it scans over a rectangular area of the sample surface. When the primary electron beam interacts with the sample, the electrons lose energy by repeated random scattering and absorption within a teardrop-shaped volume of the specimen known as the interaction volume, which extends from less than 100nm to around 5μm from the surface. The size of the interaction volume depends on the electron's landing energy, the atomic number of the specimen and the specimen's density. The energy exchange between the electron beam and the sample results in the reflection of high-energy back scattered electrons by elastic scattering, emission of secondary electrons by inelastic scattering and the emission of electromagnetic radiation, each of which can be detected by specialized detectors. Secondary electrons are emitted from the sample by interaction of primary electrons of incident electron beam. They are mainly loosely bounded electron of the atom. The secondary electrons of energy < 50 ev come from a small layer on the surface (50-500 Å) and yield the best resolution. The secondary electrons are used in SEM to study topological contrast. Whereas, back scattered electron (BSE) are the original primary electrons which are scattered back from the sample. The energy of BSE is almost equal to the incident primary electron. BSEs are mainly used for Z contrast. The image may be captured by digitally and displayed on a computer monitor and saved to a computer's hard disk [77, 78]. In the present study Zeiss make FESEM (model: Auriga) was used for SEM.

Fig. 3.10: Pictorial image of Scanning Electron Microscope

Conductive coating is needed to prevent charging of a specimen with an electron beam in conventional SEM (high vacuum, high voltage) as ADU, UO_3, UO_2 and UF_4 along with its subsequent products are non conductive material. The coating has been carried out by sputter coating equipment. Figure 3.11 is actual photograph of a sputter coating equipment. Sputter coating is a process of covering the specimen with a very thin layer of a conducting material, typically a metal, such as silver, gold - palladium (Au - Pd) alloy. Sputter deposition is a physical vapor deposition (PVD) method of depositing conductive material by sputtering, that is ejecting, material from a target, that is source, which then deposits onto a substrate, such as a samples to be analyzed in electron microscopes [77, 78]. In the present study, SEC make Magnetron Coating machine was used for sputter coating.

Fig. 3.11: Pictorial image of a sputter coating equipment

3.4.13. Specific surface area

Surface area is measured based on BET (Brunner-Emmet-Teller) principle. The concept of the BET theory is an extension of the Langmuir theory, which is a theory for monolayer molecular adsorption, to multilayer adsorption with the following hypotheses: (a) gas molecules physically adsorb on a solid in layers infinitely; (b) there is no interaction between each adsorption layer; and (c) the Langmuir theory can be applied to each layer. The specific surface area of a powder is determined by physical adsorption of a gas on the surface of the solid and by calculating the amount of adsorbate gas corresponding to a monomolecular layer on the surface. Physical adsorption results from relatively weak forces (van der Waals forces) between the adsorbate gas molecules and the adsorbent surface area of the test powder. The determination is usually carried out at the temperature of liquid nitrogen. The amount of gas adsorbed is measured by a volumetric procedure. Thermo Scientific make SURFER was used for surface area analysis. Fig. 3.12 shows pictorial image of the instrument.

Fig. 3.12: Pictorial image of instrument used for measuring surface area

3.5. Summary

Experimental set up and production procedure of ADU and its subsequent products UO_3, UO_2 and UF_4 are explained here. Further, different measurement techniques for properties of these products are described in the Chapter.

CHAPTER 4

CHAPTER 4

STUDY ON PROGRESS OF ADU PRECIPITATION REACTION VIA URANYL NITRATE ROUTE

4.1. Introduction

Ammonium diuranate (ADU) is the first intermediate product in solid powder form in flow sheet of uranium metal ingot production. ADU was produced by the reaction of uranyl nitrate containing 62 g/l uranium and gaseous ammonia diluted with air. Changes in pH, uranium concentration in filtrate, morphology of ADU and crystal structure of ADU are discussed in this Chapter.

4.2. Results and discussions

ADU precipitation reaction was carried out in an agitated glass reactor at 50 $^{\circ}$C. Downward 45° pitched six bladed impeller was used for mixing. Experimental set up, experimental procedure and measurement techniques are already described in details in Chapter 3. Variation in pH and uranium concentration in filtrate with time during ADU precipitation reaction has been plotted in Fig. 4.1a. It was observed that initially there was slow increase of pH and then there was sudden small reduction in pH, followed by almost flat zone and then there was a sharp increase in pH followed by slow increase in pH. The first precipitation point was detected by inception of permanent turbidity which was found to coincide with the reduction of pH. To get clarity in reduction of pH at the starting of precipitation a selected portion (in between point A at time 13 min to D at time 22 min) of Fig. 4.1a has been enlarged in Fig. 4.1b. pH was increased very fast in between A to B from 2.95 to 3.19. No reaction took place in this zone as no change in uranium concentration was observed. Reduction in both the uranium concentration and pH was observed after point B.

pH was reduced from 3.19 to 3.18 and uranium concentration was reduced from 62 g/l to 56.22 g/l from point B to C. With further addition of NH_3, pH and uranium concentration were further reduced to 3.15 and 40.08 g/l respectively at point D. No reduction in pH was observed after point D, but reduction in uranium concentration was continued.

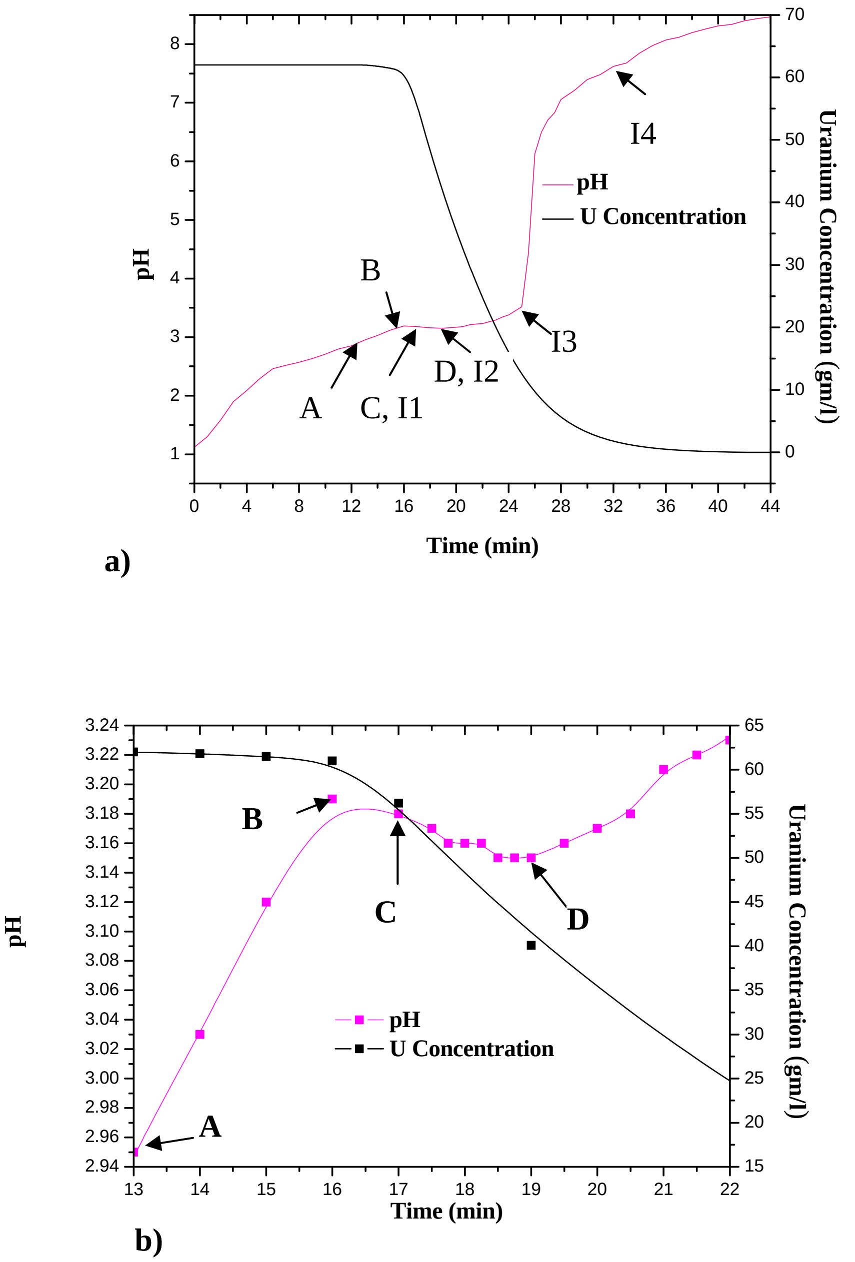

Fig. 4.1: Changes in pH and uranium concentration with time a) across the total duration of precipitation b) across the selected duration (13 min to 22 min) of the precipitation.

Initial increase in pH can be explained due to neutralization of free acid present in UNS. Small reduction of pH was occurred due to generation of H^+ ion at the inception of precipitation [79]. It was further notices from uranium concentration vs time plot that precipitation started only after reaching certain pH. It was also observed that around 90% recovery of uranium was took place at the end of flat zone. Recovery was further increased to 99.98 % when pH reached to 7.5. Almost no improvement in recovery was observed when pH was further increased to 8.5.

Slurry samples were collected at the first precipitation point (I1) (pH 3.18), in between (I2) (pH 3.15) the flat zone, end point (I3) (pH 3.52) of the flat zone and at pH 7.5 (I4). ADU I1 was very sticky and became hard lump on drying. ADUI2 and ADUI3 were not sticky but they also became soft lumps on drying. ADUI4 was very easily filterable and converted to powder on drying.

Morphology of ADU has been observed using high resolution Scanning Electron Microscope (SEM) and Transmission Electron Microscope (TEM). ADU powder was coated with very thin (40-50 nm) gold layer by magnetic scattering technique to prevent charge deposit during the study of morphology using high resolution SEM. For TEM analysis, the ADU powder was dispersed in alcohol using ultrasonic bath and one drop of the dispersed solution was poured on carbon coated cupper grid. The morphology of final ADU at different magnification has been shown in Fig. 4.2. The SEM images exhibit that the final ADU powder basically consists of primary platelets. These primary platelets form primary agglomerates. These agglomerates are also connected with each other to form secondary agglomerates. The TEM image (Fig. 4.3 a) also confirm that the plate like structure of the final ADU. The selected area diffraction (SAD) pattern of ADU (Fig. 4.3 b) indicates that the ADU particle is made of agglomerates of both nano-crystals and larger crystals. The nano crystals produce ring pattern whereas larger crystals give bright spots.

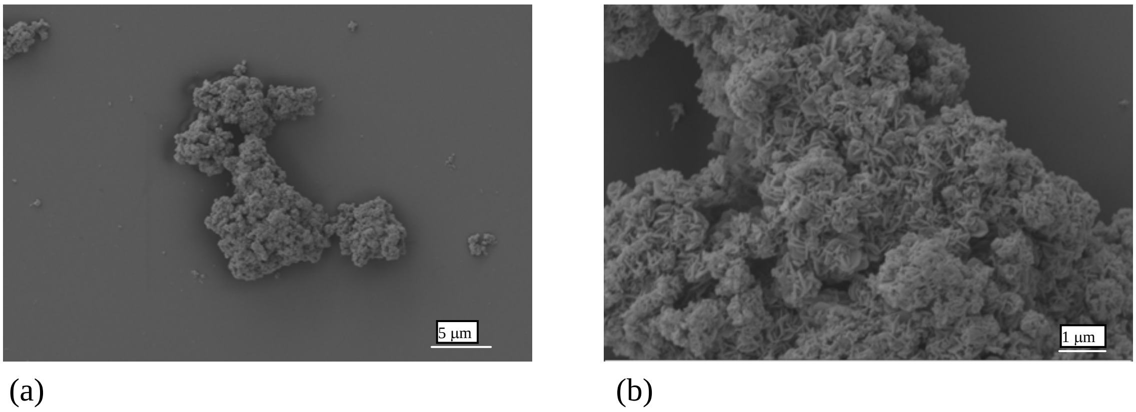

Fig. 4.2: SEM images of final ADU at different magnifications (a) 5,000x and (b) 25,000x

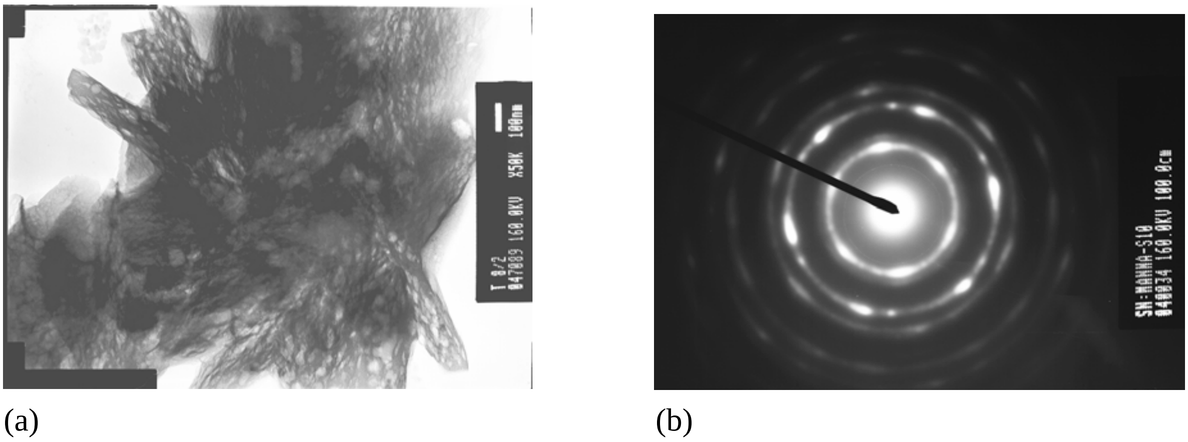

Fig. 4.3: TEM images of final ADU (a) microstructure and (b) diffraction pattern

The SEM images of ADU at different stages of precipitation have been shown in Fig. 4.4. Fig. 4.4 a indicates platelet like structure of ADU at inception. In the course of reaction platelets has been connected with each other to form agglomerates. As reaction proceeds, the size of both platelets and agglomerates are increased.

X-Ray diffraction pattern of these ADU are shown in Fig 4.5. Colour of the ADU at every stage of reaction was yellowish. ADUI1 and ADUI2 were found to be orthorhombic $3UO_3.NH_3.5H_2O$ (JCPDF 043-0365) [23]. It was also noticed that another phase appeared with further increase of ammonia. It was studied that ADUI3, ADUI4 and ADUI5 were multi-phasic compound and consisted of orthorhombic $3UO_3.NH_3.5H_2O$ and hexagonal $2UO_3.\ NH_3.\ 3H_2O$ (JCPDF 044-0069) [23].

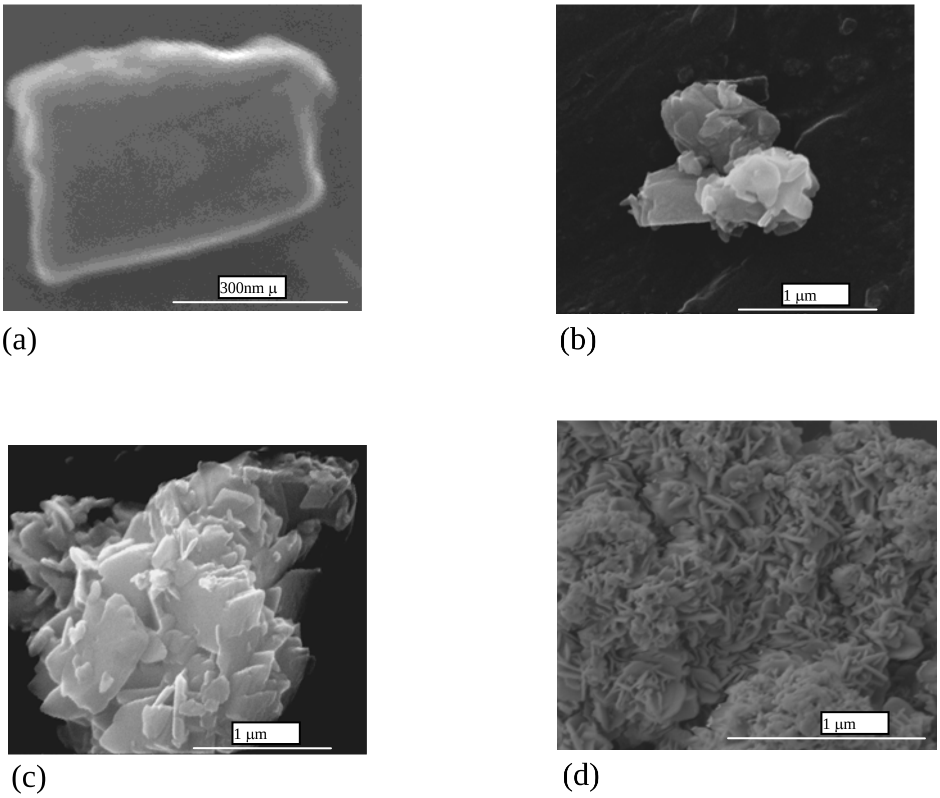

(a) (b)

(c) (d)

Fig. 4.4: Microstructure of ADU at different stages of ADU precipitation (a) inception (ADUI1), (b) intermediate, (ADUI2), (c) intermediate (ADUI3) and (d) Final ADU (ADUI4).

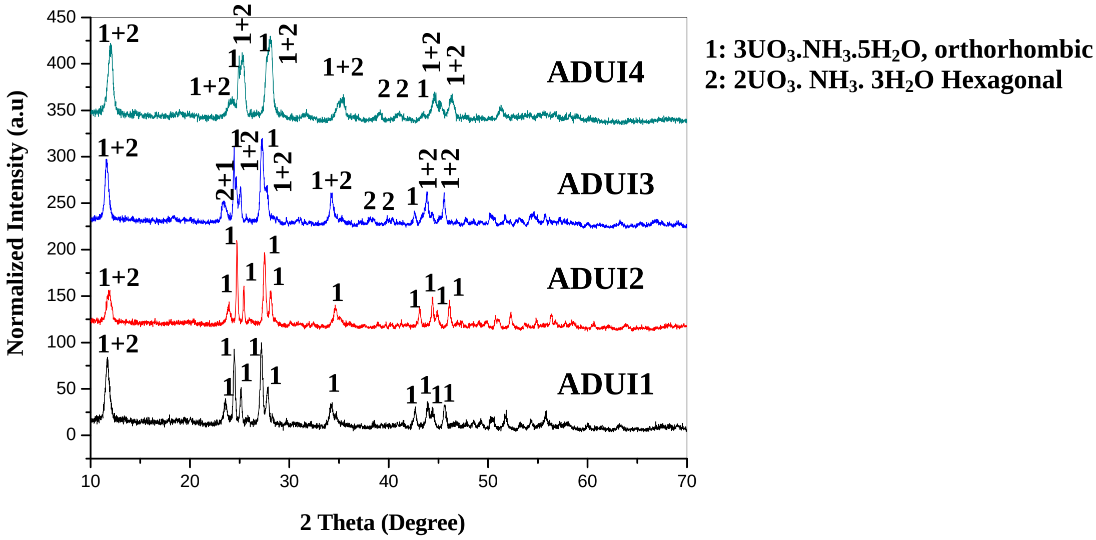

Fig. 4.5: XRD images of ADU produced at different time during ADU precipitation by reaction of UNS with gaseous ammonia

It was further observed that with an increase of ammonia addition dominancy of hexagonal structure was increased. It indicates that ADU is not monotropic in nature. At lower pH only orthorhombic $3UO_3.NH_3.5H_2O$ is stable and at higher pH both orthorhombic $3UO_3.NH_3.5H_2O$ and hexagonal $2UO_3$. NH_3. $3H_2O$ are stable.

4.3. Summary

Ammonium Di Uranate (ADU) was produced by the reaction of ammonia with uranyl nitrate solution (UNS) at 50 °C in an agitated reactor. Changes in pH and uranium recovery were noted after regular interval. Further, changes in morphology and crystal structure of ADU staring from inception to end of precipitation were studied. It was observed that, initially pH was increased slowly. Then there was small reduction in pH, followed by almost flat zone and then sharp increase in pH followed by slow increase in pH. The first precipitation point was detected by inception of turbidity which was further found to be coinciding with the reduction of pH. ADU powder basically consists of primary platelets. These primary platelets form primary agglomerates, which are further connected with each other to form secondary agglomerates. At the inception ADU platelets are formed. In the course of reaction platelets are connected with each other to form agglomerates. As the reaction proceeds, the size of both platelets and agglomerates has been increased. ADU obtained at inception via UNS route was consisted of orthorhombic $3UO_{3.}$ $NH_{3.}$ $5H_2O$. Another hexagonal phase ($2UO_{3.}$ $NH_{3.}$ $3H_2O$) were appeared in ADU with further addition of NH_3.

CHAPTER 5

CHAPTER 5

STUDY ON EFFECT OF PROCESS PARAMETERS AND MIXING ON MORPHOLOGY OF AMMONIUM DIURANATE FROM URANYL NITRATE

5.1. Introduction

Ammonium diuranate (ADU) which is an important intermediate for production of uranium base fuel, is produced by precipitation or reactive crystallization process where ammonia is mixed with stirred uranyl nitrate solution and the solid product (ADU) is formed by a chemical reaction in concentrations exceeding the solubility. The reaction is very fast [42] and ADU is sparingly soluble in solution. Production process and properties of uranium oxide, which is used as fuel in power reactor and uranium metal, which is used as fuel in research reactor, largely depend on ADU characteristics, as morphology of ADU is retained by its subsequent products [13]. Morphology typically refers to the appearance of powder particles rather than its internal structure. It represents shapes of powder [11]. Morphology of ADU powders controls their flow-ability which is required for further material movement through different equipment. In addition, the property of surface area is required for the chemical reactivity of powder, the particle size distribution (PSD) decides the carryover losses occurring during the gas-solid counter current reaction and the properties of tap density is required for effective capacity determination. Very small particles may give very high surface area, but very high surface area or reactivity also may damage product due to sintering as a result of high heat of reaction. ADU particles with larger platelets and high surface area due to porosity are favorable. Over all rounded shape is also helpful to increase the flow-ability. Morphology of ADU particle largely depends on the process parameters like temperature, pH of solution, uranium concentration, feed free acidity, NH_3 feed rate and mixing mechanism.

5.2. Results and discussion

ADU was produced here by reaction of uranyl nitrate solution (UNS) and gaseous ammonia diluted with air. The reaction was carried out in an agitated glass reactor equipped with different kind of impeller, motor with VFD, muffle heater. In the present work, an effort has been given to study the effects of uranium concentration, temperature, impeller type and impeller speed on the morphology and the other properties of ADU.

5.2.1. Effect of Uranium concentration

To study the effect of uranium concentration in UNS, experiments were carried out with six different uranium concentration: 20 g/l, 40 g/l, 60 g/l, 80 g/l, 100 g/l and 120 g/l at room temperature. pH of the solution were continuously monitored during experiments. Changes in pH of the solution with time have been shown in Fig. 5.1.

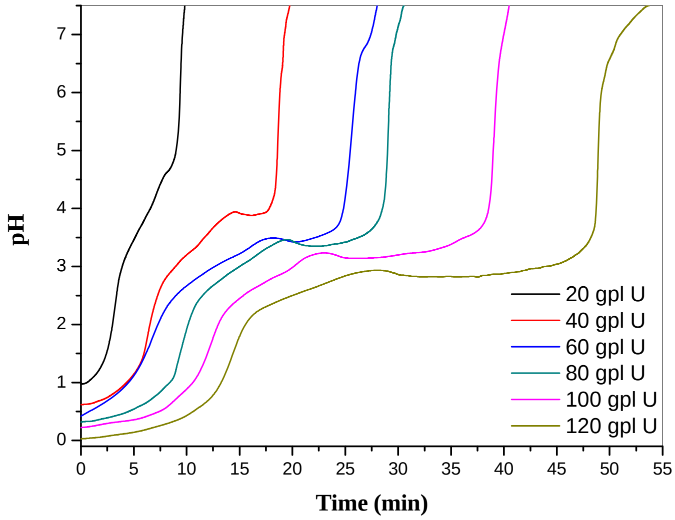

Fig. 5.1: Variation of pH with time for different uranium concentration in UNS

It was observed that initially there was slow increase of pH and then there was sudden small reduction in pH, followed by almost flat zone and then there was a sharp increase in pH followed by slow increase in pH. The first precipitation point was detected by inception of turbidity which was found to coincide with the reduction of pH. After reaching certain pH, ammonia was started to react with uranyl nitrate present in the solution. This is why there is a flat zone in the pH curve. More than 90% reaction took place in this zone. Similar nature of pH vs time curve was observed in all the cases. As uranium concentration in UNS was increased by evaporation of base UNS and uranium concentration was reduced by dilution with DM water, initial pH of the UNS was reduced with an increase of uranium concentration in UNS. It was observed that starting pH for precipitation was also reduced with an increase in uranium concentration. It was also observed that the time duration of flat zone in pH curve got increased with an increase in the uranium concentration. Concomitantly the time to reach pH 7.5 also got increased from 9.83 min for 20 g/l uranium concentration to 54 min for 120 g/l uranium concentration. It was noticed that, the rate of change of pH was fastest and there was almost no flat zone when the uranium concentration in UNS was 20 g/l. Filterability of ADU slurry was very poor when uranium concentration in UNS was 20 g/l and ADU cake was gelatinous. Lumps were formed instead of powder during drying. Filterability and nature of cake improved with an increase of uranium concentration. Filterability of ADU slurry was good (filtration rate more than 700 ml/min) and ADU powder was formed from cake on drying when uranium concentration in UNS was 60 g/l or above.

Morphology of oven dried ADU powders produced from UNS of different uranium concentrations were studied using SEM (Fig. 5.2). SEM images show that ADU basically consists of primary platelets. These primary platelets form primary agglomerates. These agglomerates are also connected with each other to form secondary agglomerates. As ADU is sparingly soluble (solubility <10 mg/l), very high level of local super saturation (degree of super saturation in the order of 6000) occurs during precipitation. It causes primary nucleation. But crystals are not able to grow at very low uranium concentration. This is why platelet like structure was not observed in case of ADU obtained from UNS containing 20 g/l uranium (Fig. 5.2 a).

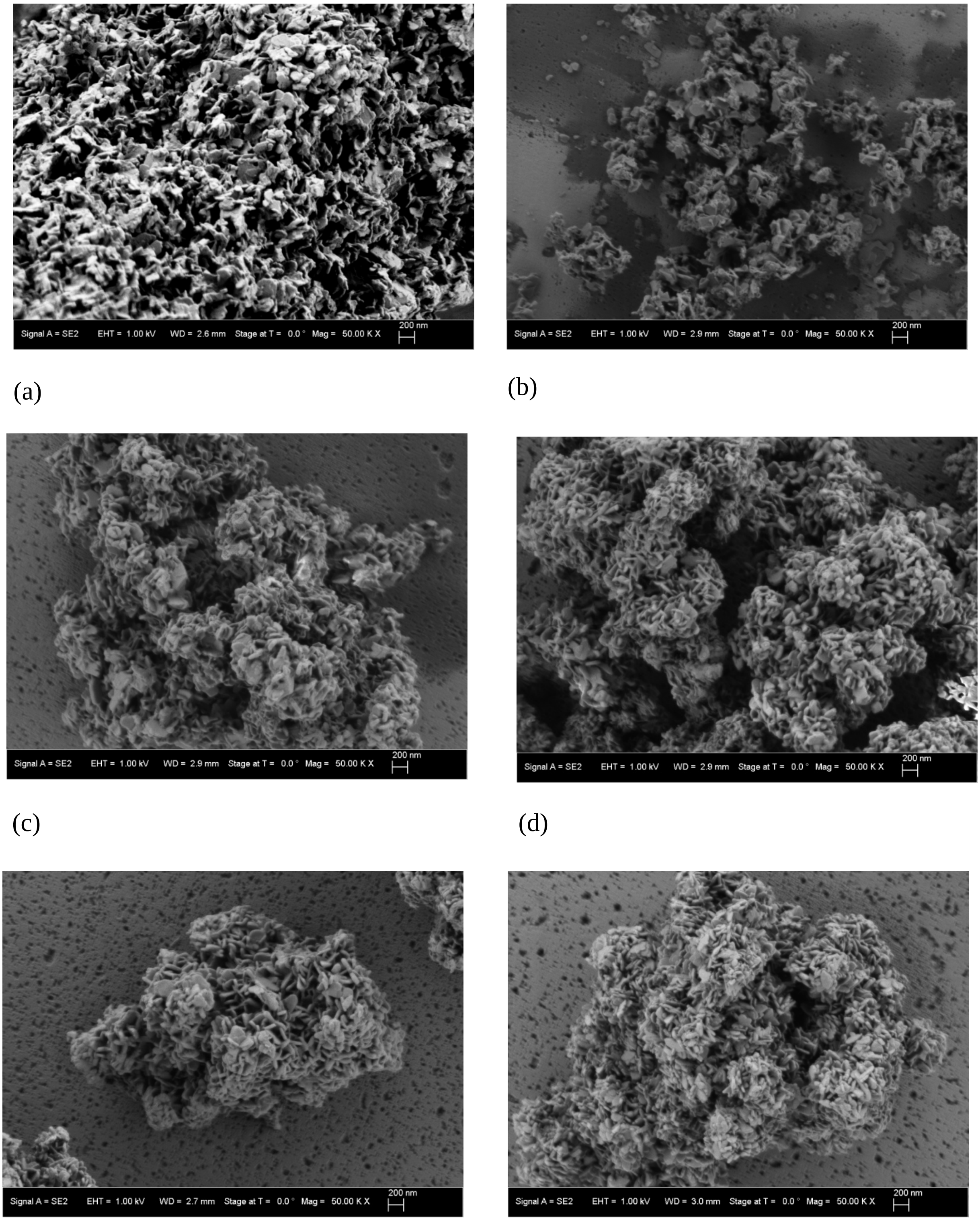

(a) (b)

(c) (d)

(e) (f)

Fig. 5.2: Morphology of ADU produced from UNS of different uranium concentration (a) 20 g/l, (b) 40 g/l, (c) 60 g/l, (d) 80 g/l, (e) 100 g/l and (f) 120 g/l

With an increase of uranium concentration crystals grow due to increase in diffusion flux and platelet like structure becomes prominent. Agglomeration has also been increased due to reduction of zeta potential barrier with increase of uranium concentration [35]. As a result, both mean particle size (mean agglomeration size) and specific surface area (SSA) of ADU were increased with an increase of uranium concentration. Some of the observations are tabulated in Table 5.1. It shows that the conversion of uranium is more than 99% in all the cases.

Fig. 5.3 shows XRD pattern of ADU samples obtained with UNS having different uranium concentrations. The ADU with low uranium concentration of 20 g/l and 40 g/l at room temperature were found to be matching with hexagonal phase (a=14.087 Å, c=14.494 Å) [23]. Whereas, XRD patterns of ADU obtained from 60 g/l, 80 g/l, 100 g/l and 120 g/l exhibited both hexagonal and orthorhombic (a=7.142 Å, b=12.198 Å and c=15.07 Å) structure [23]. It was further observed that dominancy of orthorhombic structure increases with an increase of uranium concentration.

Table 5.1: Study of effect of uranium concentration in UNPS on ADU precipitation

Uranium concentration in UNPS (g/l)	20	40	60	80	100	120
Initial Temperature of UNPS	30	30	30	30	30	30
Time to reach pH 7.5 (min)	9.833	19.75	28	30.58	40.5	54
% conversion	>99%	>99%	>99%	>99%	>99%	>99%
Mean size (μm)	13.94	15.06	16.01	19.57	20.75	22.27
Surface Area (m^2/gm)	7.44	11.38	15.32	17.21	17.54	18.35

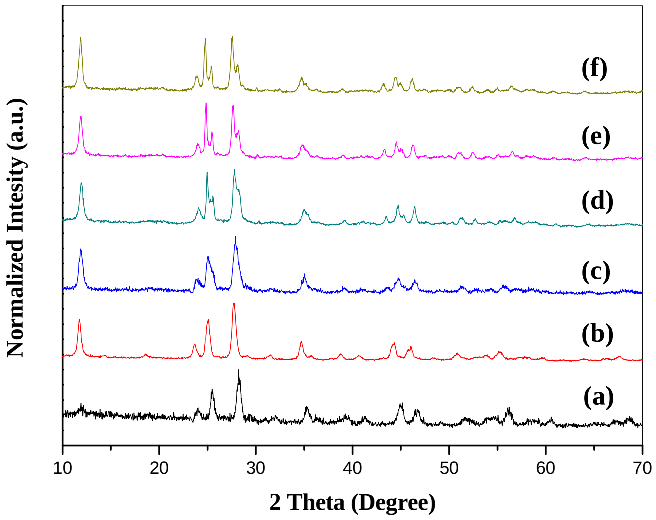

Fig. 5.3: Effect of uranium concentration of UNS on XRD pattern of ADU (a) 20 g/l, (b) 40 g/l, (c) 60 g/l, (d) 80 g/l, (e) 100 g/l and (f) 120 g/l

5.2.2. Effect of temperature of UNS

To study the effect of UNS temperature, experiments were carried out at four different temperatures: 10 °C, room temperature (RT, 28 °C), 50 °C and 70 °C. pH of the solution was continuously monitored during experiments. Changes in pH of the solution with time are shown in Fig. 5.4. It was observed in all the four experiments that the pH variation was similar to that shown in Fig. 5.1.

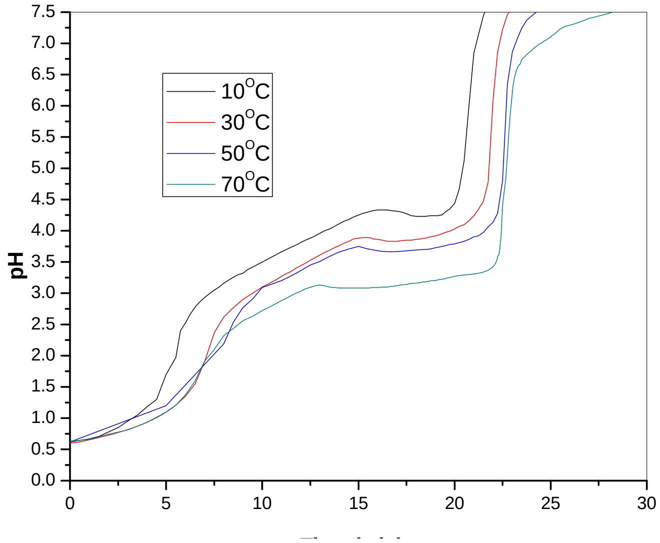

Fig. 5.4: Variation of pH with time for UNS at different temperature

Further, it was seen that the pH, at which precipitation started was reduced with an increase of temperature. As a consequence, the time to start precipitation was reduced with an increase of UNS temperature. However, total time to reach pH 7.5 was almost the same. It was also observed that, the duration of flat zone in the pH curve was increased with an increase of temperature. Filtration rate of ADU slurry produced at 10 °C was very poor and cake produced was very sticky in nature. Filtration rate of ADU slurry was improved with an increase of UNS temperature and became good when temperature of UNS was 50 °C or above. Some observations of the study are given in Table 5.2. It shows that, as far as, there is no effect of temperature on conversion of uranium during ADU precipitation.

Fig. 5.5 shows SEM images of ADU produced from UNS at different initial temperatures. Prominent platelet like structure was not visible in ADU produced at 10 °C and 28 °C (Fig. 5.5 a and b) due to lack of crystal growth of ADU platelets. Visible growth of ADU platelets was observed due to the increase in rate of diffusion at higher temperature and concomitantly size of platelet was increased with an increase of temperature. However, overall morphology of ADU powders obtained both at 50 °C and 70 °C was almost similar (Fig. 5.5 c and d). It has been studied that the SSA increases by about 38.5% with increase of temperature from 28 °C (RT) to 50 °C and about 10% with further increase of temperature from 50 °C to 70 °C. Whereas, energy required to increase temperature to 70 °C is twice than increase temperature to 50 °C. So, it may be optimized to operate ADU precipitation process at 50 °C.

Table 5.2: Study of effect of initial temperature of UNPS on ADU precipitation

Uranium concentration in UNPS (g/l)	50	50	50	50
Initial Temperature of UNPS ($^{\circ}$C)	10	30 (RT)	50	70
Time to reach pH 7.5 (min)	24.583	22.833	24.25	28.25
% conversion	>99%	>99%	>99%	>99%
Mean size (μm)	12.50	13.51	17.11	19.57
Surface Area (m^2/gm)	12.23	15.17	21.01	23.17

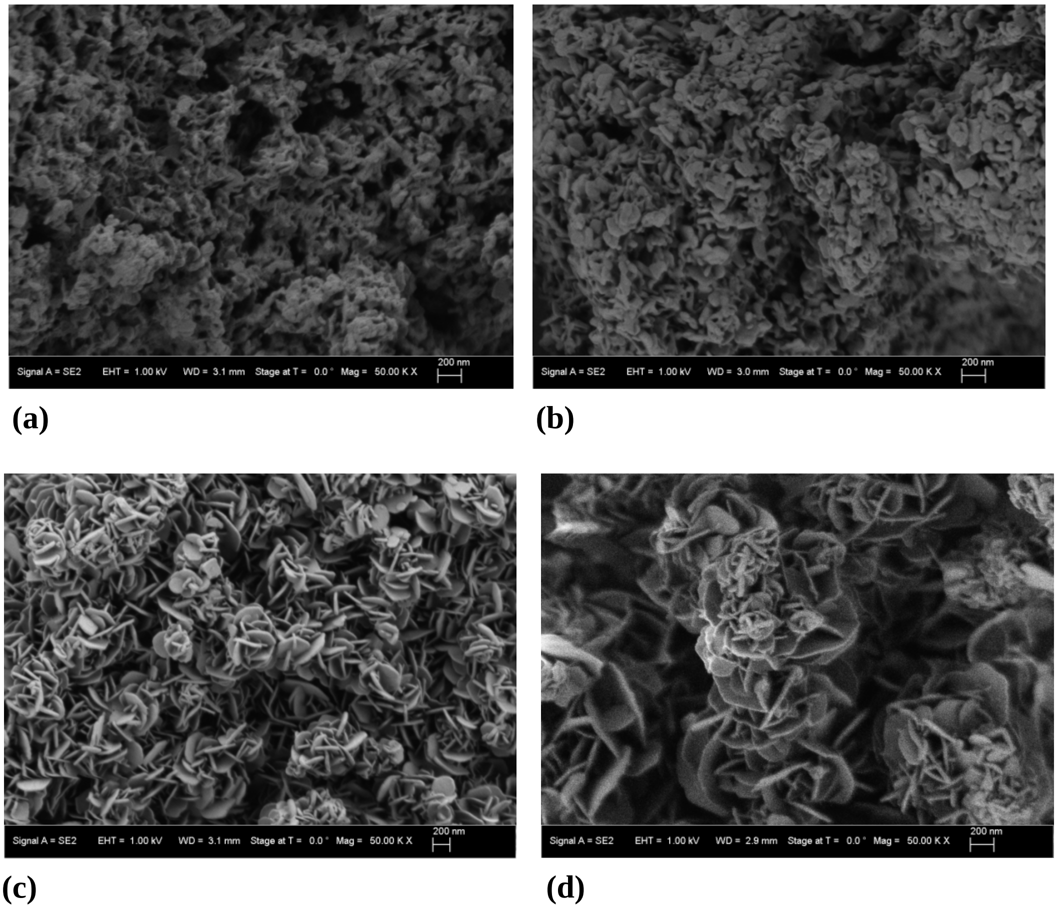

Fig. 5.5: Morphology of ADU produced from UNS at different temperature (a) 10 $^{\circ}$C, (b) 28 $^{\circ}$C, (c) 50 $^{\circ}$C and (d) 70 $^{\circ}$C

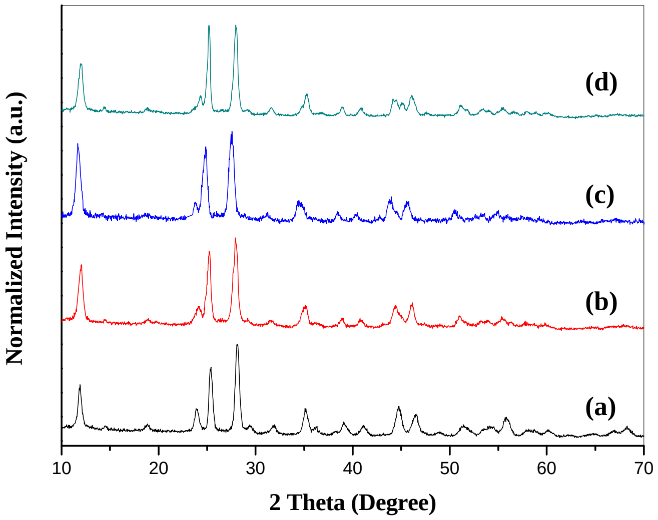

Fig. 5.6: Effect of temperature of UNS on XRD pattern of ADU
(a) 10 °C, (b) 28 °C, (c) 50 °C and (d) 70 °C

Fig. 5.6 shows XRD pattern of ADU obtained from UNS with different initial temperatures. Almost no change in crystal structure can be seen with a change in temperature and all the XRD patterns show hexagonal structure as reported by Debets et al. [23].

5.2.3. Effect of type of impellers

Three types of impellers were used to study the effect of impeller design. Power number (N_P) of the hydrofoil (HF), 45° pitched blade turbine (PBT) and disc turbine (DT) are 0.27 [80], 1.73 [81] and 5.18 [81], respectively. To study effect of impeller speed on morphology and other properties of ADU, impellers rotational speed were fixed at 8.33 r/s. Effect of type of impeller on pH vs time curve is shown in Fig. 5.7. It can be seen that the pH variation was similar to that shown in Fig. 5.1 in all cases.

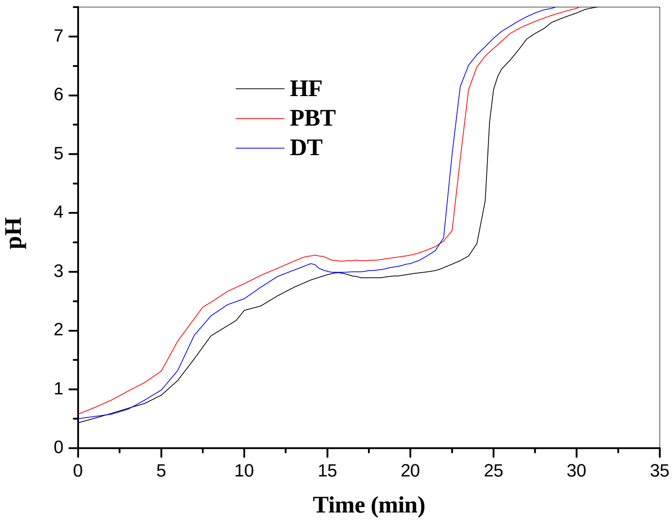

Fig. 5.7: Variation of pH with time for different impeller design

It was observed that the reaction time and the total precipitation time were slightly reduced with an increase of N_P. Though filtration rate was good in all the cases, the filtration rate was improved with an increase N_P. Power input to the reaction solution increases with an increase in Np as $P=N_P\rho N^3D^5$, where P is the power consumption (W), N_P is power number, ρ is the liquid density (kg/m^3), N is the impeller speed (rps) and D is the impeller diameter (m). Power input per unit volume increases with an increase of N_P as reactor solution volume is same (3 l) in all the three cases. With an increase of power input per unit volume, mixing inside the reactor is also increased and concomitantly, bulk convection inside the reactor is also increased. As ADU reaction kinetics is very fast and ADU is sparingly soluble in solution very high level of local super saturation occurs near the NH_3 feeding zone. It causes primary nucleation. But supersaturation level reduced to the level at metastable zone due to mixing, as a results crystal growth dominates. Simultaneously agglomeration and breakage also occur. In this way mixing plays role in morphology, particle size distribution and other physical properties. Fig. 5.8 shows SEM images of ADU produced using HF, PBT and DT type of impeller respectively. It was observed that numbers of platelets were more and sizes of platelets were very small due to more nucleation and lesser crystal growth in case of HF type impeller (Fig. 5.8 (a)). In the case of PBT (Fig. 5.8 (b)), the size of individual platelets were seen to be increased due to increase of crystal growth and number of platelets were reduced. Porosity in ADU was increased. Fig. 5.8 (c) shows morphology of ADU produced using DT. It shows platelets size was smaller than that produced by PBT but larger than HF.

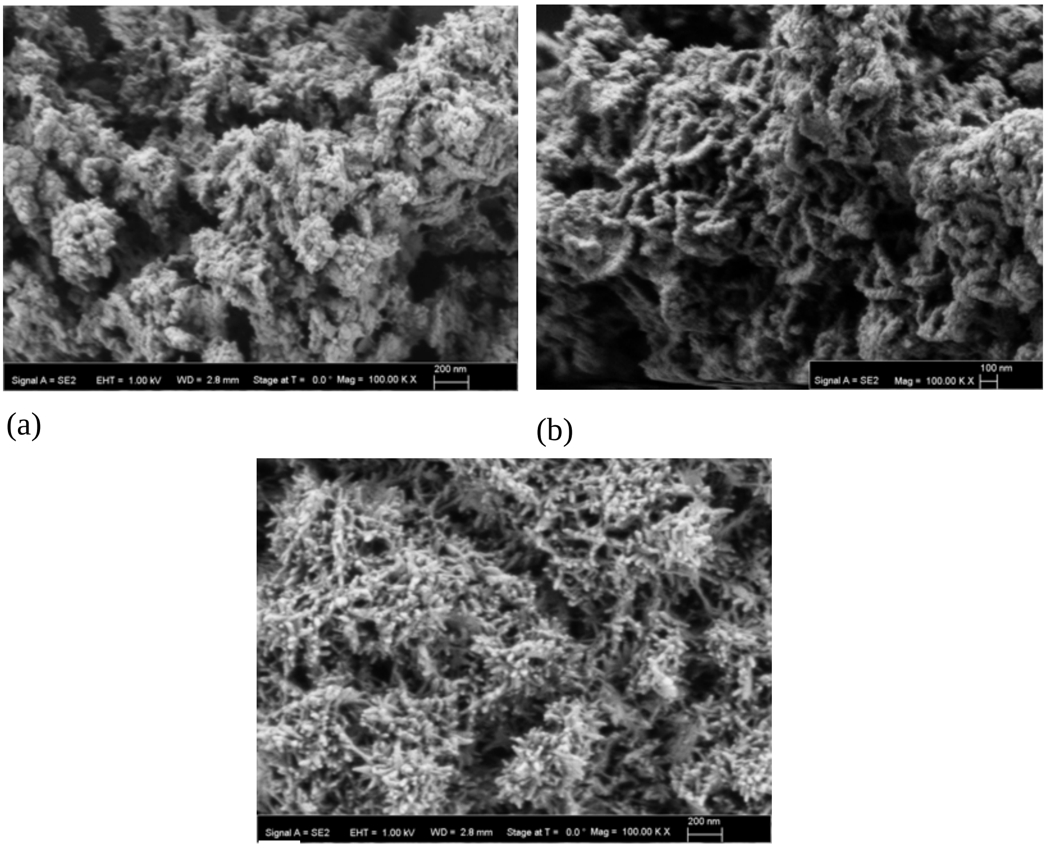

(a) (b)

(c)

Fig. 5.8: Effect of impeller design on morphology of ADU
(a) Hydrofoil, (b) Pitched Blade Turbine and (c) Disc Turbine

Some observations of the study are given in Table 5.3. More breakage of agglomerates takes place with an increase of Np. This is why mean particle size (basically agglomerate size) decreases with an increase of N_P. SSA of ADU substantially increases with PBT than with DT.

Table 5.3: Study of Effect of impeller design on ADU precipitation

Type of mixing	Hydrofoils	PBT	DT
Power Number (Np)	0.27	1.73	5.18
Power /unit volume (W/m^3)	40.5	259.5	777
Total precipitation time (min)	31.25	30.167	28.75
% conversion	>99%	>99%	>99%
Mean particle size (µm)	18.95	16.96	15.82
Surface Area (m^2/gm)	14.98	21.74	22.13

Fig. 5.9 shows XRD pattern of ADU obtained with different types of impeller. All XRD patterns were found to be matched with hexagonal phase as reported by Debets et al. [23] though, a broadening of the peaks were observed in the pattern of ADU with DT impeller. It shows that there is small contribution of the orthorhombic phase. It was also studied that conversion of UNS was more than 99% and irrespective of the impeller design.

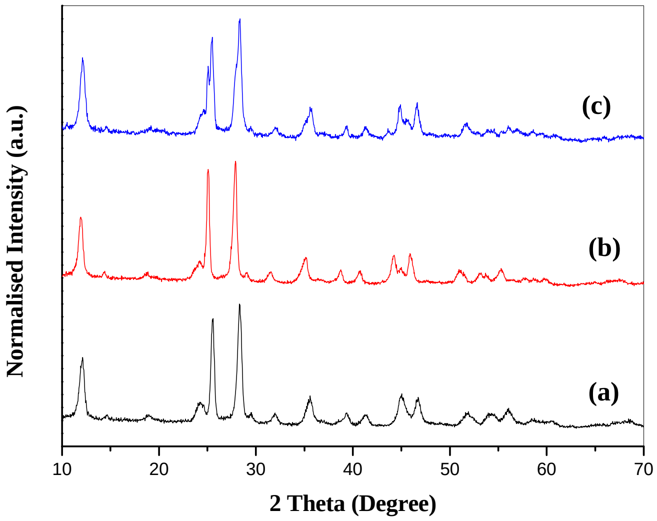

Fig. 5.9: Effect of impeller design on XRD pattern of ADU
(a) Hydrofoil, (b) Pitched Blade Turbine and (c) Disc Turbine

5.2.4. Effect of impeller speed

To study the effect of impeller speed, experiments were carried out with four different impeller speed (5, 6.66, 8.33 and 10 r/s) with PBT impeller. Fig. 5.10 shows the effect of impeller speed on pH vs time curve. It was observed that the pH variation was similar to that shown in Fig. 5.1 in all the cases. It was further noticed that reaction time and total precipitation time were slightly reduced with an increase in impeller speed. Though filtration rate was found to be good in all the cases, the filtration rate improves with an increase of RPM. Power input per unit volume increases with an increase of impeller speed. With an increase of power input per unit volume, mixing inside the reactor is also increased and concomitantly, bulk convection inside the reactor is also increased. Fig. 5.11 shows SEM image of ADU produced with different impeller speed. At lower RPM (5 and 6.66 r/s) bulk convection was less so nucleation was more and crystal growth was less. This is why platelet size was relatively small. SEM images (Fig. 5.11 c and d) show growth of platelets in ADU produced at 8.33 and 10 r/s. However, increase in impeller speed, breakage of agglomerates and platelets was also occurred. This can clearly be seen in Fig. 5.11 (d).

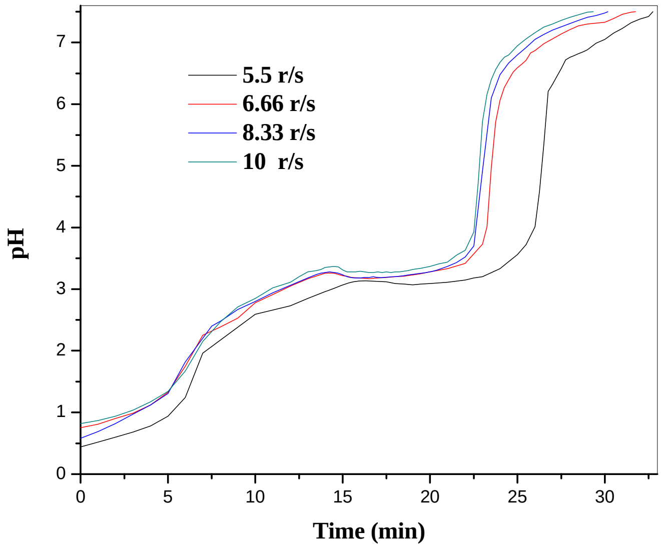

Fig. 5.10: Variation of pH with time for different impeller speed

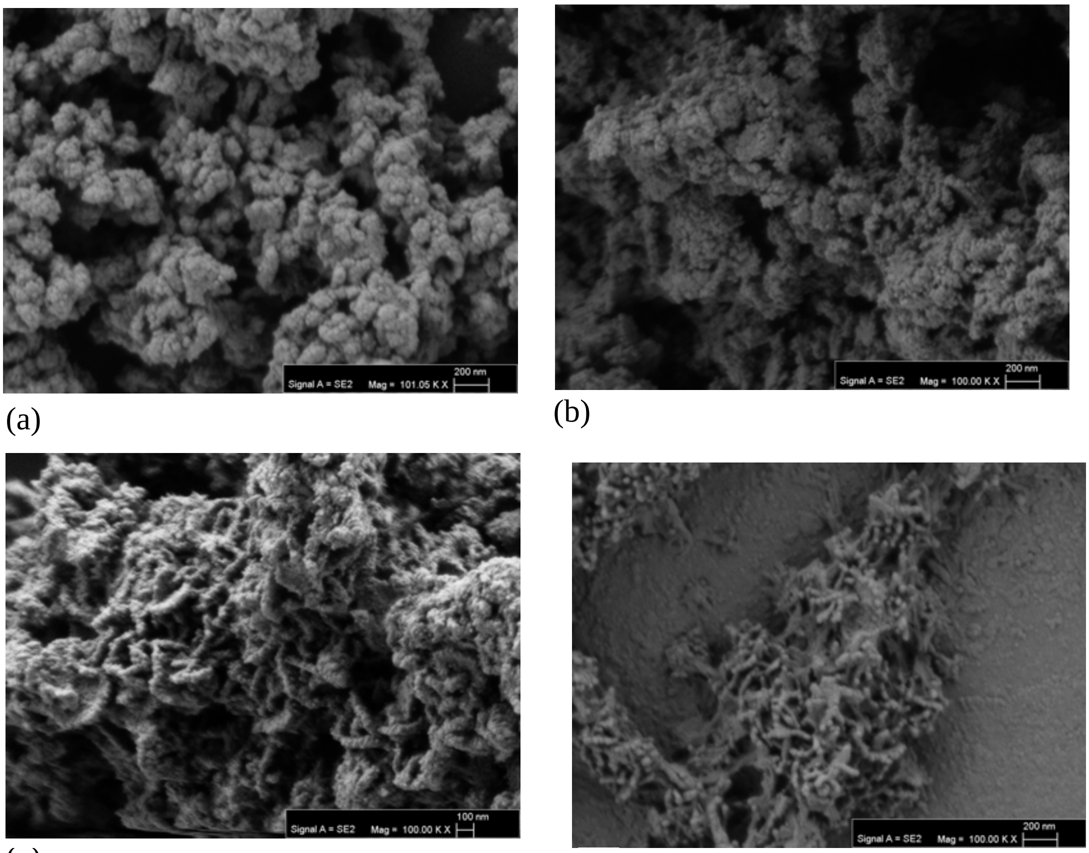

(a) (b)

(c) (d)

Fig. 5.11: Effect of impeller speed on morphology of ADU

(a) 5 r/s, (b) 6.66 r/s, (c) 8.33 r/s and (d) 10 r/s

Table 5.4: Study of Effect of rotational speed of impeller on ADU precipitation

RPM	300	400	500	600
Power /unit volume (W/m^3)	56.052	132.864	259.5	448.416
Total precipitation time (min)	32.75	31.75	30.167	29.33
% conversion	>99%	>99%	>99%	>99%
Mean particle size (µm)	18.79	17.25	16.96	16.19
Surface Area (m^2/gm)	14.48	20.53	21.74	22.63

Table 5.4 shows a decrease in particle size and an increase of SSA with an increase in impeller speed. Power per unit volume increases 173% with an increase in impeller speed

from 8.33 to 10 r/s, whereas increase in SSA is only 4% and SSA obtained at 8.33 r/s is of good quality ADU. So, impeller speed may be optimized at 8.33 r/s.

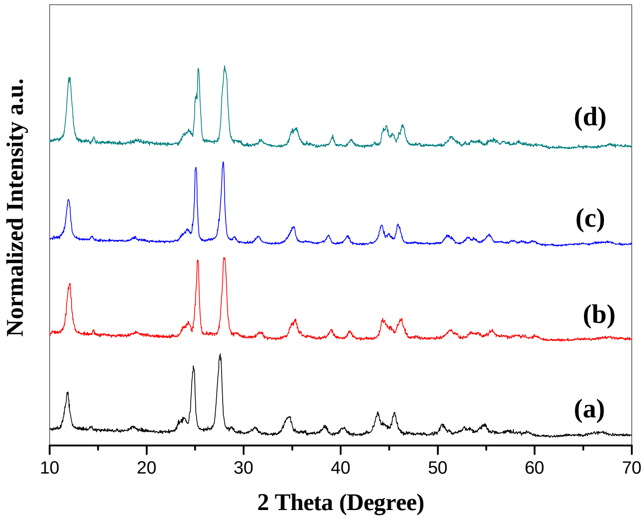

Fig. 5.12: Effect of impeller speed on XRD image of ADU
(a) 5 r/s, (b) 6.66 r/s, (c) 8.33 r/s and (d) 10 r/s

Fig. 5.12 shows XRD pattern of ADU produced from UNS containing 50g/l at $50^{O}C$ at different impeller speed. No significant change in the XRD pattern was observed as seen. Phase analysis shows that all ADU have hexagonal structure as reported by Debets et al. [23]. It may be pointed out that the overall conversion was more than 99% irrespective of impeller speed.

5.3. Summary

ADU is first intermediate product in solid powder form in flow sheet of uranium metal or uranium oxide fuel production. Its morphology and other properties are important as subsequent products are also retaining the morphology of ADU. Morphology of ADU powders controls their flow-ability required for further material movement through different equipment, surface area required for chemical reactivity of powder, carryover losses occurred during gas solid counter current reaction and tap density required for effective capacity determination. Very small particles may give very high surface area, but very high surface area or reactivity also damages product due to sintering due to high heat of reaction and small particles cause carryover losses occurred during gas solid counter current reaction. ADU particles where growth of platelets occurs and high surface area generated due to porosity are required. Over all rounded shape is also helpful to increase flow-ability. Effect of uranium concentration of UNS, temperature of UNS, type of impeller and rotational speed of impeller on the morphology, particle size, specific surface area and crystal structure has been systematically studied. Though growth of platelets increases with an increase of uranium concentration, temperature power number and rotational speed, effect of temperature is found to be more dominant. Considering required morphology and properties and power consumption per unit volume, UNS temperature, type of impeller and impeller speed are optomised as 50 °C, PBT and 500 RPM respectively.

CHAPTER 6

CHAPTER 6

STUDY ON EFFECT OF CALCINATION TEMPERATURE ON MORPHOLOGY OF CALCINED PRODUCT OF ADU

6.1. Introduction

Oxide fuel for Nuclear Power Plant is produced from ammonium diuranate (ADU). ADU is calcined to UO_3 (basically mixture of UO_3 and U_3O_8) in rotary kiln furnace where ADU is fed at a controlled rate in the furnace at a pre set temperature. Properties of uranium oxide depend on temperature of the rotary kiln i.e. calcinations temperature.

6.2. Results and discussion

ADU produced by reaction of uranyl nitrate solution and gaseous ammonia was calcined in a muffle furnace at different temperature: 450 °C, 550 °C, 650 °C and 750 °C. Effect of calcination temperature on the properties of uranium oxide was studied here.

Morphology of ADU and uranium oxides has been studied at different magnification in high resolution Scanning Electron Microscopy (Fig 6.1). It has been observed that overall morphology of ADU is retained in its calcined product: UO_3. Similar to ADU, UO_3 is also consisted of primary platelets. These primary platelets form primary agglomerates. These agglomerates are also connected with each other to form secondary agglomerates. SEM micrograph at 50000X indicates presence of pores on the primary platelet of uranium oxide calcined at 550 °C and at higher temperatures, but no pores have been observed in uranium oxide produced at 450 °C. These pores were generated due to release of gaseous NH_3 and water vapor during calcination. The micrographs clearly indicate that sintering of UO_3 powder took place at 650 °C onwards. It clarifies that initial increase of surface area was occurred due to generation of pores whereas a reduction of surface area was occurred because of sintering. This is why surface area and porosity pass through a maximum value at 550 °C and then reduces.

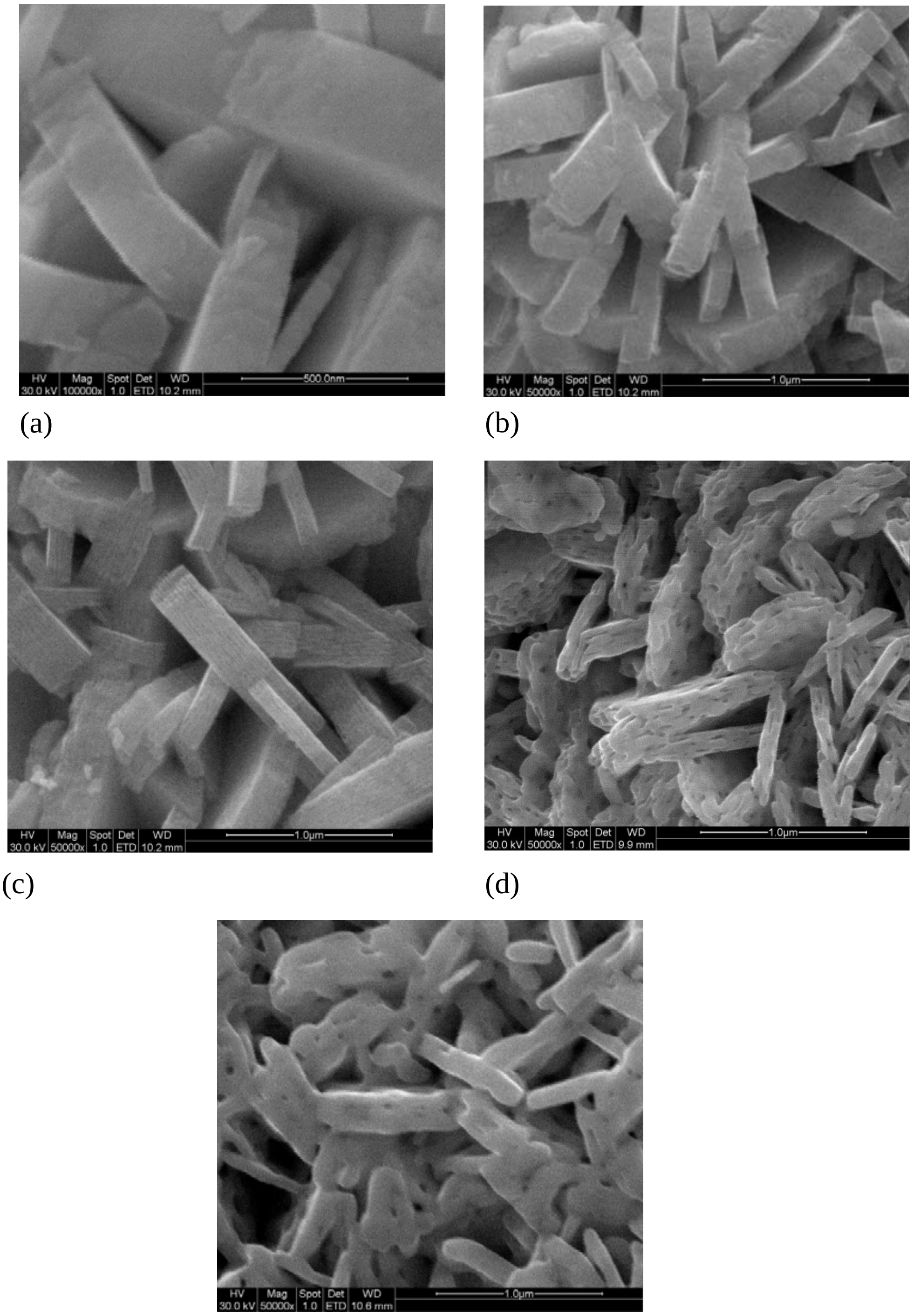

(a) (b)

(c) (d)

(e)

Fig. 6.1: SEM image (a) ADU, (b) Uranium oxide produced at 450 °C, (c) Uranium oxide produced at 550 °C, (d) Uranium oxide produced at 650 °C and (e) Uranium oxide produced at 750 °C

The values of surface area and porosity of uranium oxide are given in Table 6.1. Further, effect of calcination temperature on O/U, bulk density, tap density, mean particle size, specific surface area (SSA), porosity & color of uranium oxide has been shown in Table 6.1.

Table 6.1: Effect of calcination temperature on properties of uranium oxide

Sr. No.	Temp. (°C)	O/U Ratio	Bulk Density (g/ cm^3)	Tap Density (g/ cm^3)	Mean Particle Diameter (μ)	SSA (m^2/g)	Porosity (cm^3/g)	Color
1	450	2.82	1.92	2.26	24.68	22.5	0.07	Reddish Black
2	550	2.77	1.89	2.24	25.09	35.39	0.17	Black
3	650	2.71	1.88	2.22	22.83	12.15	0.04	Black
4	750	2.67	1.77	1.90	24.27	7.24	0.03	Black

It was noticed that the O/U ratio, bulk density and tap density of the uranium oxide is reduced with an increase of calcinations temperature. Colour of the uranium oxide produced at 450 °C is reddish black whereas it was found to be black when produced at temperatures, higher than 450 °C.

6.3. Summary

This study establishes the effect of calcination temperature on the properties of uranium oxide produced from ammonium diuranate. High resolution SEM has revealed that pores are generated due to release of gases and closed due to sintering at higher temperature during calcination. As a results porosity and surface area of uranium oxide first increases with temperature and then reduces after passing through a maximum. It has also been observed that the O/U ratio, bulk density and tap density of the uranium oxide are reduced with an increase in the calcination temperature.

CHAPTER 7

CHAPTER 7

STUDY ON PROGRESS OF ADU PRECIPITATION REACTION VIA URANYL FLUORIDE ROUTE

7.1. Introduction

Ammonium diuranate (ADU) is produced by reaction of uranyl fluoride solution (UFS) with ammonia during production of Low Enriched Uranium (LEU) metal. In the present work, a systematic study has been carried out to understand changes in composition of precipitate with progress of reaction with special attention of first appearance of precipitate.

7.2. Results and discussions

ADU was produced from UFS in a glass reactor at 50 °C. Uranium concentration in UFS was 65 g/l. During the course of reaction pH of the solution was continuously monitored using pH meter and uranium concentration in solution was also measured simultaneously. Experimental set up, experimental procedure and measurement techniques are described in Chapter 3 in details. Variation of pH and uranium concentration with time during ADU precipitation by reaction between UFS and gaseous ammonium has been shown in Fig. 7.1. Unlike Fig. 4.1 pH of the solution was increased continuously and no flat zone was observed in the graph. However, precipitation started only after reaching certain pH as earlier, but at higher pH compared to precipitation from uranyl nitrate solution (UNS). The recovery of uranium at any pH in UFS route was lower than that in case of UNS route. It was further observed that recovery is only 60% and 98 % at pH 7.5 and 8.5 respectively. More than 99% recovery is observed only at pH 9.

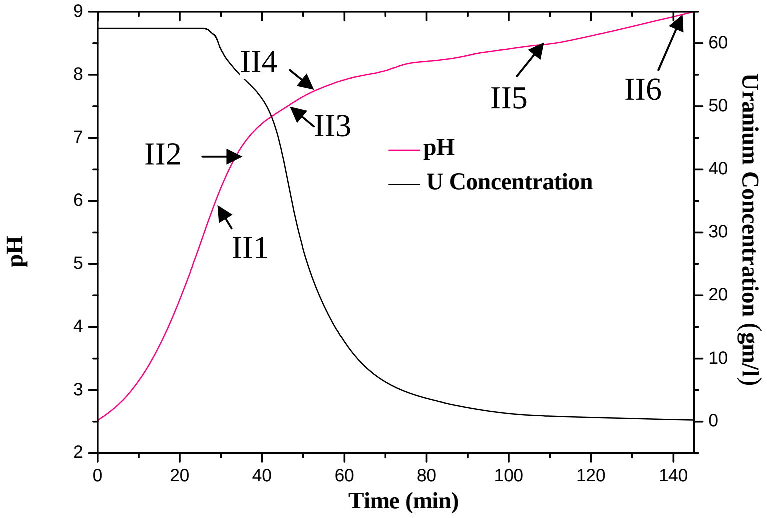

Fig. 7.1: Changes in pH and uranium concentration with time during ADU precipitation by reaction of UNS with gaseous ammonia

Slurry samples were collected at the first precipitation point (II1) (pH 5.98), at pH 6.74 (II2), at pH 7.5 (II3), at pH 7.85 (II4), at pH 8.5 (II5) and at pH 9 (II6). Green gelatinous precipitate (ADU II1) was obtained at inception. ADUII2 and ADUII3 were little sticky and became hard lumps on drying. ADUII4 was not sticky and became soft lumps on drying. ADUII5 and ADU II6 were easily filterable and became powder on pressing during drying. Colour of the ADU was nicely changed from green to khaki to brownish to greenish yellow. X-Ray diffraction pattern of these ADU is shown in Fig 7.2. It has been observed that ADU produced at inception (ADU II1) was consisted of orthorhombic $(NH4)_3UO_2F_5$ (JCPDF 021-0802) [82]. ADU II2 was consisted of orthorhombic $(NH_4)_3UO_2F_5$ and (NH_4) $(UO_2)_2F_5.4H_2O$ (hexagonal) (JCPDF 026-0095) [83] with dominancy of $(NH_4)_3UO_2F_5$. ADU II3 was consisted of $(NH_4)_3UO_2F_5$, $(NH_4)(UO_2)_2F_5.4H_2O$ and hexagonal $2UO_3.\ NH_3.\ 3H_2O$ (JCPDF 044-0069) [23] with dominancy of $(NH_4)_3UO_2F_5$. ADU II4-ADUII6 were consisted of $(NH_4)_3UO_2F_5)$, (NH_4) $(UO_2)_2F_5.4H_2O$ and $2UO_3.NH_3.3H_2O$ with dominancy of $2UO_3.NH_3.3H_2O$ increased with ammonia addition.

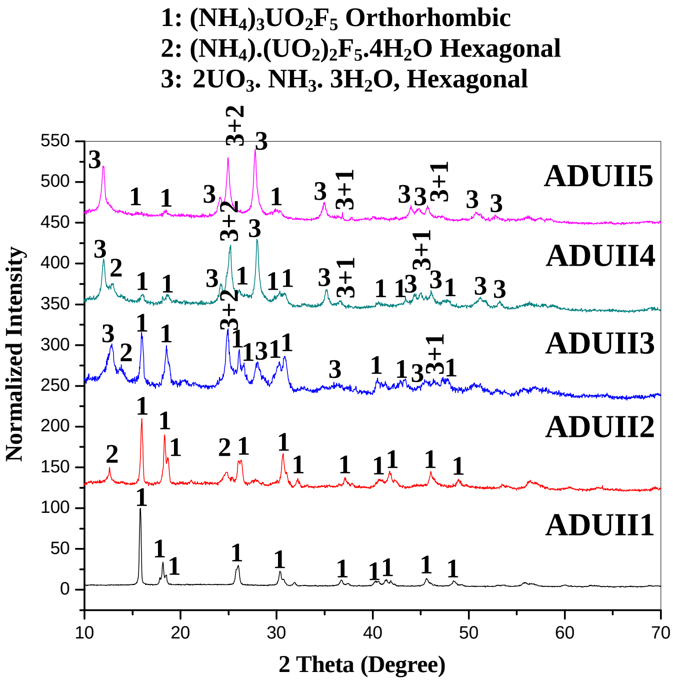

Fig. 7.2: XRD images of ADU produced at different time during ADU precipitation by reaction of UFS with gaseous ammonia

7.3. Summary

Ammonium Di Uranate (ADU) was produced here by the reaction of ammonia with uranyl fluoride solution (UFS) at 50 °C in an agitated reactor. In the present work, study of the progress of ADU precipitation was carried out to study changes in recovery of uranium and structure of ADU with pH with special attention on first appearance of the precipitate. It was observed that pH of the solution was continuously increased during ADU precipitation via UFS route. But precipitation started at higher pH and uranium recovery was lesser compared to production via UNS route. It was further studied that ADU produced at inception via UFS route was consisted of $(NH_4)_3UO_2F_5$ (orthorhombic) and with further addition of ammonia composition of ADU was changed and it became mixture of $(NH_4)_3UO_2F_5$ (orthorhombic), $2UO_3.NH_3.3H_2O$ (hexagonal) and (NH_4) $(UO_2)_2F_5.4H_2O$ (hexagonal). Extent of $2UO_3.NH_3.3H_2O$ (hexagonal) was increased with progress of reaction.

CHAPTER 8

CHAPTER 8

STUDY ON EFFECT OF PROPERTIES OF ADU PRODUCED FROM UNS AND UFS ON PROPERTIES OF SUBSEQUENT PRODUCTS

8.1. Introduction

The role of research reactors for the development of nuclear programme of any country is well established [84-86]. Research reactors are utilized to produce radioisotopes and offer irradiation facilities for testing various nuclear fuel and structural materials [87, 88]. Radioisotopes like Co^{60}, Cs^{137}, I^{131} are used for medicine, industries, agriculture, food processing [89]. Apart from these, the research reactors are also used for neutron beam research activity, testing neutron detectors, testing material for mew power plant, training of manpower etc. With rapid expansion of nuclear program in India, more research reactors are needed for nuclear technology as they contribute to creation of essential infrastructure for research and for building capabilities. Very high pure metallic uranium has been used for production of fuel of the research reactor. Uranium production processes are categorized in four groups: 1) reduction of uranium halides with metals, 2) reduction of uranium oxides with metal and carbon 3) electrolytic reduction and 4) disproportionate or thermal decomposition of uranium halides [74]. The reduction of uranium tetrafluoride by magnesium is one of the main industrial methods for producing commercial pure uranium ingot. A simplified flow sheet for production of uranium metal ingot is given in Fig. 8.1. Ammonium Diuranates (ADU) is first intermediate product in solid powder form in flow sheet of uranium metal ingot production. ADU is generally produced either via uranyl nitrate route or via uranyl fluoride route. In both the production process uranyl solution (either nitrate or fluoride) react with ammonia (either gaseous or aqueous form) and precipitation occurs when concentration of product (ADU) exceeding the solubility. The process is called reactive precipitation or crystallization. Reaction, nucleation, growth, agglomeration and breakages are the kinetics of reactive precipitation. Recovery of uranium during ADU precipitation is an important for selection of process. ADU is calcined to UO_3. The UO_3 is then reduced to UO_2 followed by hydrofluorination of UO_2 to UF_4. Uranium metal ingot is produced by metallothermic reduction (MTR) of UF_4. Performance of metallothermic reaction and recovery of uranium largely depends on properties of UF_4 [15, 90]. UF_4 normally contains small amount of uranyl fluoride (UO_2F_2), known as water soluble content, mixed oxides, known as AOI (ammonium oxalate insoluble), moisture and little bit of free acid (HF). UO_2F_2 in UF_4 plays major role in the reduction reaction. UO_2F_2 when heated in presence of moisture hydrolyses to UO_3 and HF. UO_3 remains unreduced during the MTR and naturally bomb yield decreases. HF reacts with magnesium and forms refractory MgF_2 film on magnesium, which hinders the vaporization of the magnesium chips and the triggering of the reaction is delayed. Hydrogen generated by this side reaction reacts with UO_2F_2, produce harmful HF again. AOI content of the green salt is a mixture of all the un-hydro-fluorinated oxides. These oxides neither get reduced during the course of the reaction nor they get dissolved in the slag and as a result reduce the fluidity of the slag and metal and slag separation. Tap density of UF_4 is also important parameters for performance of MTR operation [88, 90]. Properties of UF_4 are inherited from its precursor materials UO_2, UO_3 and ADU [13]. In the present studies, ADU was produced from both uranyl nitrate and fluoride route using gaseous ammonia. Then ADU were calcined to UO_3, further reduced to UO_2 and hydroflorinated to UF_4 at similar condition. Both chemical and physical properties of the products are analyzed carefully to understand how properties of UF_4 are inherited from its precursors.

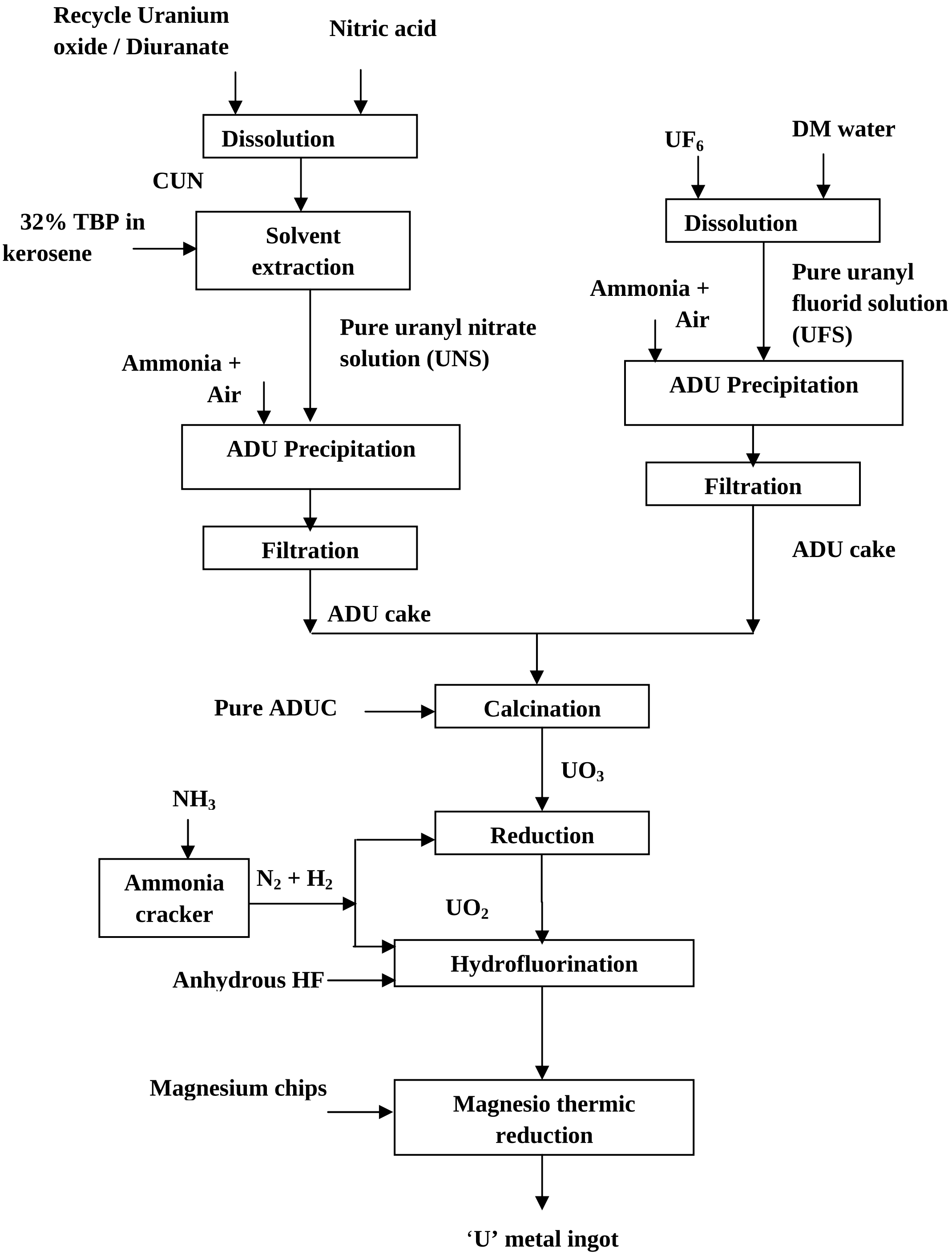

Fig. 8.1: Process flow sheet for production of natural uranium metal ingot**.**

8.2. Results and discussion

ADU, UO_3, UO_2 and UF_4 produced via UNS route is written as ADUI, UO_3I, UO_2I and UF_4I and ADU, UO_3, UO_2 and UF_4 produced via UFS route is written as ADUII, UO_3II, UO_2II and UF_4II. It has been observed from Table 8.4 that UO_2F_2 and AOI content was more in UF_4

obtained via UFS route than via UNS route. UO_2F_2 has been generated due to reaction of HF with unconverted UO_3 presence in UO_2, which depends on conversion of UO_3 to UO_2 and indicated by O/U ratio of UO_2. More the O/U ratio of UO_2, more the presence of UO_3 in UO_2. Conversion of UO_3 to UO_2 depends on specific surface area (SSA) of UO_3 and O/U ratio of UO_3. Table 8.2 indicates that SSA of UO_3 obtained from UNS is more than that of UFS route. SSA of UO_3 mainly depends on particle size of UO_3 and morphology of UO_3. It has been noted from Table 8.2 that mean particle size of UO_3 obtained from UFS is more than that of UNS route. Ammonia released during calcination reduces UO_3 [13, 73]. Reduction of calcined product of ADU produced via UFS route is lesser due to presence of fluoride in ADU. As a result O/U ratio of UO_3 from UNS is lesser than UFS route. AOI in UF_4 indicates conversion of UO_2 to UF_4 which depends on SSA of UO_2. Table 8.3 shows that SSA of UO_2 obtained from UNS are more than that of UFS route. Similarly, SSA of UO_2 mainly depends on particle size of UO_2 and morphology of UO_2. It has been observed from Table 8.3 that mean particle size of UO_2 obtained from UFS is more than that of UNS route. It is further noticed that tap density (TD) of UF_4 obtained from UNS is more than that of UFS route (Table 8.4). It has been observed from Table 8.1 that mean particle size of ADU obtained from UFS is more than that of UNS route and SSA of DU obtained from UNS is more than that of UFS route. It is further noted that particle size was reduced from ADU to UO_3 to UO_2 to UF_4.

Table 8.1: Physical and chemical properties of ADU

Sr. No.	ADU sample No.	% Fluoride	Mean Particle Size (μm)	SSA (m^2/gm)	TD (gm/cc)
1	ADU I	-	19.91	20.93	2.26
2	ADU II	2.21	23.88	17.72	2.18

Table 8.2: Physical and chemical properties of UO_3

Sr. No.	UO_3 sample No.	% Fluoride	O/U	Mean Particle Size (μm)	SSA (m^2/gm)	TD (gm/cc)
1	UO_3 I	-	2.70	19	27.59	2.31
2	UO_3 II	0.15	2.79	23.28	21.03	2.19

Table 8.3: Physical and chemical properties of UO_2

Sr. No.	UO_2 sample No.	% Fluoride	O/U	Mean Particle Size (μm)	SSA (m^2/gm)	TD (gm/cc)
1	UO_2 I		2.06	16.34	19.21	2.53
2	UO_2 II	0.0323	2.09	21.03	15.36	2.41

Table 8.4: Physical and chemical properties of UF_4

Sr. No.	UF_4 sample No.	UO_2F_2	AOI	MPS (μm)	TD (gm/cc)
1	UF_4 I	0.64	0.17	17.53	2.45
2	UF_4 II	1.13	0.52	22.75	2.37

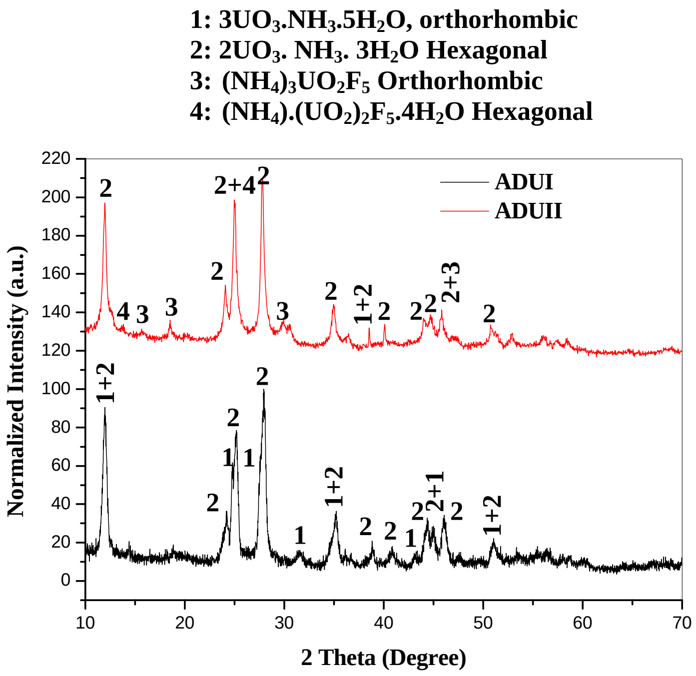

Fig. 8.2: XRD pattern of ADU produced from UNS and UFS

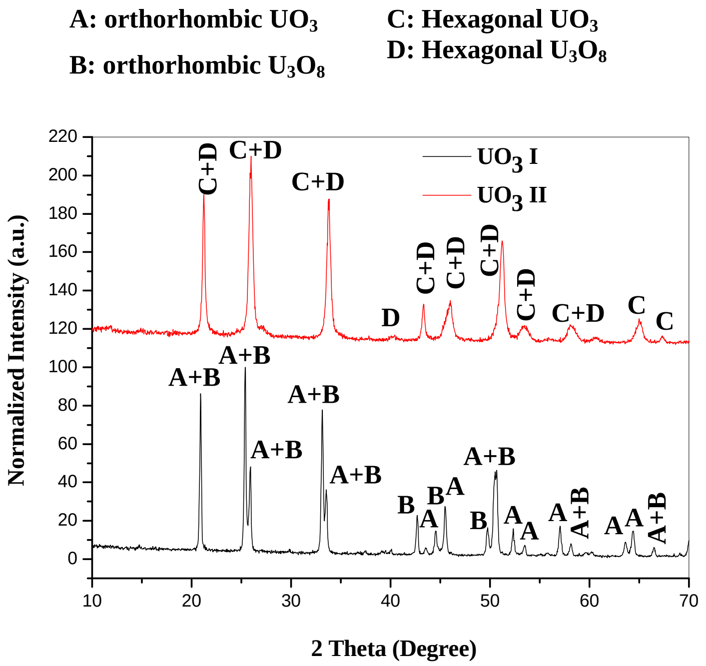

Fig. 8.3: XRD pattern of UO_3 produced via UNS and UFS route

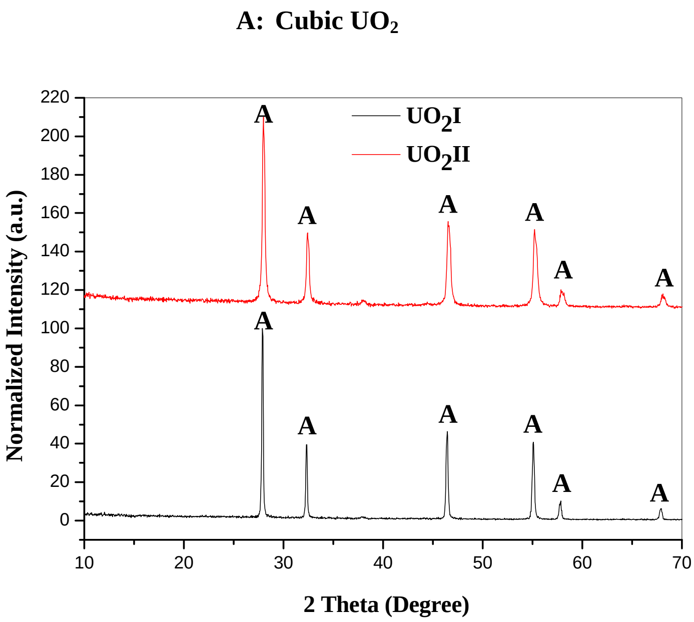

Fig. 8.4: XRD pattern of UO_2 produced via UNS and UFS route

XRD pattern (Fig. 8.2) shows that ADUI is consisted of orthorhombic $3UO_3.NH_3.5H_2O$ (PDF 043-0365) [23] and hexagonal $2UO_3$. NH_3. $3H_2O$ (PDF 044-0069) [23] and ADUII is consisted of orthorhombic $(NH_4)_3UO_2F_5$ (JCPDF 021-0802) [82], hexagonal $(NH_4).(UO_2)_2F_5.4H_2O$ (PDF 026-0095) [83] and hexagonal $2UO_3.NH_3.3H_2O$ with dominancy of $2UO_3.NH_3.3H_2O$. XRD patterns of calcined product of ADU produced from both UNS and UFS route are shown in Fig. 8.3. Both the UO_3 is basically mixture of UO_3 and U_3O_8 which is clearly indicated by O/U ratio of UO_3 (Table 8.2). It is further observed from XRD patterns that UO_3I is consisted of orthorhombic UO_3 (PDF 072-0246) [91] and orthorhombic U_3O_8 (PDF 047-1493) [92] and UO_3II is consisted of hexagonal UO_3 (PDF 031-1416) [93] and hexagonal U_3O_8 (PDF 074-2102) [94]. But both the pattern (Fig. 8.4) of UO_2 are matched to those reported in the ICDD database (PDF number 00-041-1422) [95] for the cubical structure. X-ray phase analysis (Fig. 8.5) of UF_4I and UF_4II are matched to those reported in the ICDD database (PDF number 082-2317) [96] for the monoclinic structure.

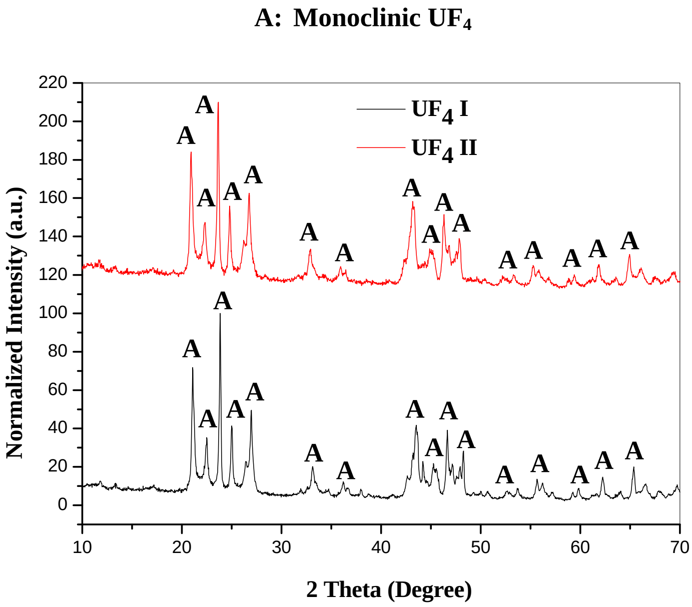

Fig. 8.5: XRD pattern of UF_4 produced via UNS and UFS route

8.3. Summary

Uranium metal used for fabrication of fuel for research reactor is generally produced by metallothermic reduction of UF_4. Performance of metallothermic reaction and recovery of uranium largely depends on properties of UF_4. Properties of UF_4 are inherited from its precursor materials UO_2, UO_3 and ADU. Uranium recovery during ADU precipitation via UNS route is more than that of via UFS route. Reduction of UO_3 to UO_2 is lesser in UFS route than UNS route due to presence of fluoride in ADU and subsequent UO_3.This causes more presence of UO_2F_2 in UF_4 produced via UFS route. SSA of UO_2 obtained from UFS is lesser than that of UNS route. This is why UF_4 produced via UFS route content more AOI than UF_4 produced via UNS route. Crystal phase analysis shows that inspite of different composition of ADU produced by two routes, crystal structure of UO_2 and UF_4 produced by two different routes are similar.

CHAPTER 9

CHAPTER 9

SUMMARY AND SCOPE FOR FUTURE WORK

9.1. Summary of Present Research Work

Ammonium diuranate (ADU) is first intermediate product in solid powder form in the process flow sheet of uranium metal or uranium oxide fuel production. ADU is generally produced from uranyl nitrate solution (UNS) for natural uranium fuel and from uranyl fluoride solution (UFS) for low enriched uranium fuel production. ADU has been produced by continuous adding of ammonia in uranyl solution contained in an agitated reactor. In the present work, change in pH, uranium concentration in filtrate (% recovery) and composition with progress of reaction has been studied. In UNS route, it has been observed that, initially pH increases relatively slowly then there is sudden small reduction in pH, followed by almost flat zone. With further addition of ammonia, pH is sharply increased followed by slow increase in pH. Inception of precipitation was found to coincide with the sudden reduction in pH. More than 90% recovery of uranium was observed to be completed by the end of the flat zone. Recovery of uranium was further increased even more than 99.5%, when ammonia addition was continued up to pH 7.5. However, pH of the solution was continuously increased during ADU precipitation via UFS route. Precipitation starts at higher pH and uranium recovery was lesser compared to production via UNS route. ADU obtained at inception via UNS route was found to consist of orthorhombic $3UO_{3.}\ NH_{3.}\ 5H_2O$. Another hexagonal phase ($2UO_{3.}\ NH_{3.}\ 3H_2O$) appeared in ADU with a further addition of NH_3. It was further studied that the ADU produced at inception via UFS route was consisted of $(NH_4)_3UO_2F_5$ (orthorhombic) and with further addition of ammonia, the composition of ADU was changed and it became mixture of $(NH_4)_3UO_2F_5$ (orthorhombic), $2UO_3.NH_3.3H_2O$ (hexagonal) and $(NH_4).(UO_2)_2F_5.4H_2O$ (hexagonal). The content of $2UO_3.NH_3.3H_2O$ (hexagonal) was found to increase with the progress of reaction.

Morphology and other properties of ADU are important as subsequent products are also retaining the morphology of ADU. Morphology of ADU powders controls their flow-ability required for further material movement through different equipment, surface area required for chemical reactivity of powder, carryover losses occurred during gas solid counter current reaction and tap density required for effective capacity determination. Very small particles may give very high surface area, but very high surface area or reactivity also damages product due to sintering due to high heat of reaction. Further, small particles cause carryover losses during gas solid counter current reaction. Over all rounded shape is also helpful to increase the flow-ability. Producing a material with the desired quality often requires a sound knowledge of the elementary steps involved in the process: creation of supersaturation, nucleation, crystal growth, aggregation and other secondary processes. These elementary steps depend on reaction chemistry, process parameters, fluid dynamics, heat and mass transfer. Effect of uranium concentration of UNS, temperature of UNS, type of impeller and rotational speed of impeller on the morphology, particle size, specific surface area and the crystal structure has been systematically studied. SEM images show that ADU basically consists of primary platelets. These primary platelets form primary agglomerates. These agglomerates are also connected with each other to form secondary agglomerates. At the inception, ADU platelets are formed. In the course of reaction platelets connect each other forming agglomerates. As reaction proceeds, the size of both platelets and agglomerates get increased. It is desired that ADU platelets grow and they form spherical agglomerate. Though, the growth of platelets increases with an increase in the uranium concentration, the impeller power number and rotational speed, effect of temperature were found to be more dominant. Considering the desired morphology and the properties, the UNS temperature, the type of impeller and the impeller speed are optimised as $50^{O}C$, pitched blade turbine (PBT) and 500 RPM respectively.

Further, research work has been extended to study the effect of ADU calcination temperature on properties of its calcined product (uranium tri oxide). Specific surface area (SSA) of uranium tri oxide, produced by the calcination of ammonium diuranate is a function of two competing processes: generation of surface area due to generation of pores because of the evolution of gaseous products (NH_3, H_2O vapour) and the loss of surfaces due to sintering. As a consequence, pores are closed and sometimes the pores are combined to make a larger pore and result into reduction in the specific surface area. High resolution SEM has revealed that the pores are generated during calcination and at higher temperature sintering of powder takes place. As a results surface area increases with temperature and then reduces after passing through a maxima at $550^{O}C$. Further, it has been observed that the O/U ratio of the uranium oxide is reduced with an increase in the calcination temperature. However, the temperature was not found to have a significant effect on the tap density, the bulk density and the mean particle size.

Uranium metal ingot is produced by metallothermic reduction of UF_4. The performance of metallothermic reaction and the recovery of uranium largely depend on the properties of UF_4. It may me pointed out that the properties of UF_4 are inherited from its precursor materials UO_2, UO_3 and ADU. Uranium recovery during ADU precipitation via UNS route is more than that via UFS route. Reduction of UO_3 to UO_2 is lesser in UFS route than UNS route due to the presence of fluoride in ADU and subsequent UO_3.This causes more presence of UO_2F_2 in the UF_4 produced via UFS route. SSA of UO_2 obtained from UFS is lesser than that of UNS route. This is why UF_4 produced via UFS route content more AOI than UF_4 produced via UNS route.

XRD pattern shows that the ADU produced via UNS route consists of orthorhombic $3UO_3.NH_3.5H_2O$ and hexagonal $2UO_3.\ NH_3.\ 3H_2O$. On contrast, the ADU produced via UFS route consists of orthorhombic $(NH_4)_3UO_2F_5$, hexagonal $(NH_4).(UO_2)_2F_5.4H_2O$ and hexagonal $2UO_3.NH_3.3H_2O$ with dominancy of $2UO_3.NH_3.3H_2O$. UO_3 produced by calcination of ADU obtained from both the routes is basically a mixture of UO_3 and U_3O_8 which is also clearly indicated by O/U ratio of UO_3. It is further observed from XRD patterns that the UO_3 via UNS route consists of orthorhombic UO_3 and orthorhombic U_3O_8 and UO_3 via UFS route consists of hexagonal UO_3 and hexagonal U_3O_8. Crystal phase analysis shows that, inspite of different compositions of ADU produced by the two routes, crystal structure of UO_2 and UF_4 produced by two different routes are similar.

9.2. Scope for Future Work

In the present research work, it has been observed that the ammonium diuranate obtained from the reaction from both the uranyl nitrate and the uranyl fluoride is not a single compound. It is a mixture of compounds and composition of the mixture is varied with pH. The future study should be focused on the understanding of the underlying chemistry and the mechanism of ADU precipitation. It is also desirable to understand the reaction kinetics.

It has been observed that the morphology and other physical properties of ADU depend on the process parameters of operation, hydrodynamics, heat and mass transfer inside the reactor. In the present research work of UNS route, the effect of uranium concentration of feed, temperature of feed, type of impeller and rotational speed of impeller have been investigated on the morphology and the other physical properties. However, the effects of spurger design, ammonia to air ratio and individual flow rate on properties of ADU were not covered in the present research work. Similar study can be carried out for ADU precipitation via UFS route. These unexplored areas should be considered as future work.

It is reported in the thesis that, ADU precipitation process is basically a reactive precipitation process. Reaction kinetics and precipitation kinetics control the properties of the ADU. The most significant factors affecting the kinetic parameters are reaction kinetics, degree of supersaturation, flow field pattern, mixing, residence time, temperature, concentration, and suspension density. Several authors reported the effect of mixing on particle size distribution and morphology in reactive precipitation. The hydrodynamic situation in a turbulently stirred tank is complex. The mixing is due to the transport of the energy provided by the agitator through a cascade of vortices to the smallest scales where the energy is dissipated as heat. Mixing takes place on all the levels from the largest scales of the flow to the molecular scale, but, in particular, three levels are distinguished: macromixing, mesomixing, and micromixing. Macromixing describes mixing at the scale of the tank; that is, how fluid lumps are distributed over the whole tank volume. It controls global mixing times and mean concentration fields. Micromixing describes mixing at molecular scale (below Kolmogorov micro scale. It controls molecular diffusion. Mesomixing is often referred to as the intermediate mixing time scale. It describes the coarse-scale turbulent exchange between the fresh feed and its surrounding environment. It is most frequently evident at the feed pipe scale of semi-batch reactors. In reactive precipitation micromixing controls the generation of supersaturation, mesomixing describes the interaction of plume of fresh feed with it surrounding and macromixing determine the environment in which micromixing take pace. Quantification of these time scale is not only providing proper understanding of mixing but also it is essential for future optimization and scale up for the process. Detailed experimental as well as mathematical studies need to be carried out to understand relative importance these time scale. This can be considered as another future work.

One of the major challenges in industrial precipitator is to control the particle size distribution and the morphology and to predict the influence of vessel geometry, operating conditions, and the effect of scale on the process behaviour. A complex variety of different processes occur in crystallizers, such as reaction, nucleation, crystal growth, attrition and agglomeration of crystals, fluid dynamics, and heat and mass transfer. Some of these processes are not yet well understood in spite of their need for design and operation of large-scale crystallizers. Process time scale, reactor opacity and the inconvenience and intrusive nature of in-situ experimental assessments are some of the formidable obstacles that prevent full understanding of the process dynamics within the stirred tank crystallizers. The geometrical complexity of crystallizers has rendered theoretical flow field study impractical. Experimental study, on the other hand, is difficult, expensive, and time consuming. Computational Fluid Dynamics (CFD) is a method to understand the hydrodynamics and was successfully used to the fluid mechanics in a crystallizer. CFD can give a quantitative engineering insight into the effects of the impeller configuration on the flow pattern and micro-mixing, which in turn, governs the crystallization rates and the crystal size distribution as well as power consumption. However, it requires additional capabilities to account for the coupled effects of fluid mechanics, reaction kinetics and precipitation phenomena in order to analyze the crystal population balance in the tank. The crystal population balance alters the local fluid properties and hence the hydrodynamics, which in turn influence the CSD. Population balance models that quantitatively monitor nucleation, growth, dissolution, aggregation and breakage make it possible to account for the coupling between the CSD and hydrodynamics. Mathematical modelling and simulation of ADU precipitator including reaction kinetics, fluid dynamics and population balance should be considered as another future work.

REFERENCES

[1] A. G. Jones (2002), Crystallization process systems. Oxford: Butterworth-Heinemann.

[2] A. D. Randolph, M. A. Larson (1988), Theory of particulate processes: Analysis and techniques of continuous crystallization (2nd edition). New York: Academic Press.

[3] H. J. M Kramer, P. J. Jasens (2003), Tools for Design and Control of Industrial Crystallizers – State of Art and Future Needs, Chem. Eng. Tech., 3, 247-255.

[4] J. W. Mullin (2001), Crystallization, 4th Edition, Oxford: Butterworth-Heinemann.

[5] J. Mydlarz, and A. G. Jones (1989), Crystallization and subsequent solid-liquid separation of potassium sulphate, Part II: Slurry filterability, Chem. Eng. Res. Des., 67, 294-300.

[6] M. Giulietti, M. M. Seckler, S. Derenzo, M. I. Ré and E. Cekinski (2001), Industrial crystallization and precipitation from solutions: state of the technique, Braz. J. Chem. Eng., 18 (4), 423-440.

[7] B. L. Aslund and A. C Rasmuson (1992), Semi batch reaction crystallization of benzoic acid, AIChE J. 38 (3), 328-342.

[8] X. M. Liu, D. Hatziavramidis, H. Arastoopour and A. S. Myerson (2006), CFD simulations for analysis and scale-up of anti-solvent crystallization. AIChE J., 52 (10), 3621-3625.

[9] D. E. Fitchett and J M Tarbell (1990), Effect of mixing on the precipitation of barium sulfate in an MSMPR reactor, AIChE, 36 (4), 511–52.

[10] C. V. Rane, E. Kalekudithi, J. B. Joshi and D. Ramkrishna (2014), Effect of impeller design and power consumption on crystal size distribution. AIChE J. 60 (10) 3596-2313.

[11] H. H Tung (2013) Industrial perspectives of pharmaceutical crystallization, Org. Process Res. Dev. 17, 445−454.

[12] C. V. Rane, A. A. Ganguli, E. Kalekudithi, R. B. Patil, J. B. Joshi and D. Ramkrishna (2014), CFD simulation and comparison of industrial crystallizers, Can. J. Chem. Eng. 92, 2138-2156.

[13] J. L Woolfrey (1978), The preperation of UO2 powder: effect of ammonium uranate properties, J. Nucl. Mater., 74, 123-131.

[14] C. K. Gupta (2001), Chemical Metallurgy: Principles and Practice, Wiley-VCH, Springer, Germany.

[15] S. Manna, S. Chowdhury, S.K. Satpati and S.B. Roy (2007), Prediction of firing time of magnesio thermic reduction (MTR) reaction and study of relative importance of the dependent parameters using artificial neural network, Indian Chem. Engg., 49 (3), 221-232.

[16] F. S. Patton, J.M. Googin and W.L. Griffith (1963), Enriched Uranium processing, Pegamon Press, London.

[17] G. Tridot (1950), Ann Chim, 12 (5), 358.

[18] W. T. Bourns and L. C. Watson (1958), Preparation of uranium dioxide for use in ceramic fuels - Part I: batch precipitation of ammonium diuranate Report AECL-757.

[19] A. M. Deane (1961), The infra-red spectra and structures of some hydrated uranium trioxides and ammonium diuranate, J. Inog. Nucl. Chem., 21, 238-252.

[20] A. Deptula (1962), A study of composition of ammonium uranates, Nukleonika, 7, 265-275.

[21] E. V. Garner (1962), X-Ray diffraction studies on compounds related to uranium trioxide dehydrate, J. Inog. Nucl. Chem., 21, 380-381.

[22] E. H. P. Cordfunke (1962), On the Uranates of Ammonium-I: The ternary system NH_3-UO_3-H_2O, J. Inog. Nucl. Chem., 24, 303-307.

[23] P. C. Debets and B. O. Loopstra (1963), On the Uranates of Ammonium-II x-ray investigation of the compounds in the system NH_3-UO_2-H_2O, J. Inog. Nucl. Chem., 25, 945-953.

[24] M. E. A. Hermans and T. Markestein (1963), Ammonium urinates and UO3-hydrates ammoniates, J. Inorg. Nucl. Chem., 25, 461-462.

[25] S. D. L. Roux and A. Van Tets (1983), The space group determination from a single crystal of a member of the ADU family on a reciprocal lattice explorer, J. Nucl. Mat., 119, 110-115.

[26] L. Chen-Yeh, Yeh Tu-Chai and P.R. Griffiths (1989), Study of ammonium urinate by X-ray diffraction and diffuse reflectance infrared spectrometry, J. Radioanal. Nucl. Chem., 131, 131-137.

[27] B. M. Narsimha, P. Balakrishna, R.B. Yadav and C. Ganguly (2001), Influence of temperature of precipitation on agglomeration and other powder characteristics of ammonium di-uranate, Powder Technol., 115, 167-183.

[28] M. S. Das, T. S. Krishnamoorthy P. V. Ravindran and N. Mahadevan, Precipitation of ammonium di uranates: a reinvestigation, unpublished internal report of BARC, DAE, India.

[29] J. Sutton, The hydrolysis of the uranyl ion: Part I (1949), J. Chem. Soc., 275-286.

[30] K. J. Notz, M. C. Mendel, C. W. Huntington, and T. J. Collopy (1960), On the structure and thermal decomposition of ammonium diuranate, U. S. Atomic. Energy commission, Rep., TID-6228.

[31] H. Brusset and C. R. Hebd (1967), Seanc. Acad. Sci. Paris C 265, 141, 1967.

[32] W. I. Stuart and T. I. Whateley (1969), Composition and structure of ammonium uranetes, J. Inog. Nucl. Chem., 31, 1639-1647.

[33] V. Urbanek, V. Sara and J. Moravec (1979), Study of formation and composition of ammonium uranates, J. Inorg. Nucl. Chem., 41, 537.

[34] M. Volmer (1939), Kinetic der Phasenbildung. Steinkopf, Leipsig.

[35] R. C. Hoyt (1978), Precipitation kinetics of a continuous precipitator, with application to the precipitation of ammonium polyuranate. Retrospective Theses and Dissertations. Paper 6459.

[36] A. S. Myerson (1993), Handbook of industrial crystallization, Butterworth-Heinemann, Boston.

[37] S. Vedantam and V. V. Ranade (2013), Cystallization: Key thermodynamic, kinetics and hydrodynamic aspects, Sadhna, 38 (6) 1287-1337.

[38] J. Cheng, C. Yang, Z. S. Mao and C. Zhao (2009), CFD Modeling of nucleation, growth, aggregation, and breakage in continuous precipitation of barium sulfate in a stirred tank, Ind. Eng. Chem. Res., 48, 6992–7003.

[39] H. Doi and. T. Ito (1964), Significance of physical state of starting precipitate in growth of uranium dioxide particles, J. Nucl. Mater., 11, 94-106.

[40] J. Janov, P.G. Alfredson and V.K. Vilkaitis (1972), The influence of precipitation conditions on the properties of ammonium diuranate and uranium dioxide powders, J. Nucl. Mat., 44, 161-174.

[41] T. J. Steeper and J. C. Zink (1974), Particle size distribution of ammonium diuranate precipitate, Proc. Okha. Acad.Sci., 54, 83-87.

[42] S. B. Roy, S. K. Satpati, A. M. Meghal and T. K Mukherjee (1995), A gas liquid ADU reaction in stirred tank and the effect of the presence of immiscible inert gas on the product solid Heat and Mass transfer Conference, Suratkal, Karnataka, 609-613.

[43] H. Wei and J. Garside (1997), Application of CFD modelling to precipitation systems, Trans IChemE, 75(A), 219-227.

[44] M. H. Al-Rashed and A. G. Jones (1999), CFD modelling of gas liquid reactive precipitation, Chemical Engineering Science, 54, 4779–4784.

[45] J. Garside, & H. Wei (1997), Pumped, stirred and maybe precipitated: Simulation of precipitation processes using CFD. Acta. Polytech. Scand., Chem. Technol. Metall. Ser., 244, 9-15.

[46] J. Baldyga, & W. Orciuch, (2001), Barium sulphate precipitation in a pipe—an experimental study and CFD modelling, Chemical Engineering Science, 56 (7), 2435–2444.

[47] D. L. Marchisio, A. A. Barresi and R. O. Fox (2001), Simulation of Turbulent Precipitation in a Semi-batch Taylor-Couette Reactor Using CFD, AIChE Journa, l47(3), 664-676.

[48] D. L. Marchisio, R. O. Fox, A. A. Barresi, M. Garbero and G. Baldi (2001), On the simulation of turbulent precipitation in a tubular reactor via computational fluid dynamics (CFD), Trans IChemE, 79 (A), 998-1004.

[49] D. L. Marchisio and A. A Barresi, (2003), CFD simulation of mixing and reaction: the relevance of the micro-mixing model, Chemical Engineering Science, 58, 3579 – 3587

[50] V. V. Ranade and J. B. Joshi, (1989), Flow generated by pitched bladed turbine Part I: Experimental, Chem. Eng. Commun., 81, 197-224.

[51] V. V. Ranade, J. B. Joshi and A. G. Marathe, (1989), Flow generated by pitched bladed turbine Part II: Mathematical Modelling and Comparison with Experimental Data. Chem. Eng. Commun., 81, 225-248,

[52] V. V. Ranade and J. B. Joshi, (1990), Flow generated by a disc turbine I: Experimental. Trans. Instn. Chem. Engrs. (U.K.).-A: Chem. Eng. Res. Des., 68, 19-33.

[53] V. V. Ranade and J. B. Joshi, (1990), Flow generated by a disc turbine II: Mathematical Model. Trans. Intsn. Chem. Engrs. (U.K.).-A: Chem. Eng. Res. Des., 68, 34-50.

[54] A. A. Kulkarni, J. B. Joshi, V. Ravikumar and B. D. Kulkarni, (2001), Application of multi-resolution analysis for simultaneous measurement of gas and liquid velocities and fractional gas hold-up in bubble column using LDA, Chem. Eng. Sci., 56, 5037-5048.

[55] T. Kumaresan and J. B. Joshi, (2006), Effect of impeller design on the flow pattern and mixing in stirred tanks, Chem. Eng. J., 115, 173-193.

[56] B. N. Murthy, R. S. Ghadge and J. B. Joshi (2007). CFD simulations of gas-liquid-solid stirred reactor: prediction of critical impeller speed for solid suspension. Chem. Eng. Sci., 62, 7184-7195.

[57] S. S. Deshpande, J. B. Joshi, V. R .Kumar and B. D. Kulkarni, (2008), Identification and characterization of flow structures in chemical process equipment using multi-resolution techniques. Chem. Eng. Sci., 63, 5330-5346.

[58] M. V. Tabib and J. B. Joshi (2008), Analysis of dominant flow structures and their flow dynamics in industrially relevant equipment using proper orthogonal decomposition. Chem. Eng. Sci., 63, 3695-3715.

[59] C. S. Mathpati, M. V. Tabib, S. S. Deshpande and J. B. Joshi, (2009), Dynamics of flow structures and transport phenomena-2: relationship with design objectives and design optimization. Ind. Eng. Chem. Res., 48, 8285–8311.

[60] J. B. Joshi, M. V. Tabib, S. S. Deshpande and C. S. Mathpati, (2009), Dynamics of flow structures and transport phenomena-1: experimental and numerical techniques

for identification and energy content of flow structures. Ind. Eng. Chem. Res., 48, 8244–8284.

[61] J. B. Joshi, N. K. Nere, C. V. Rane, B. N. Murthy, C. S. Mathpati, A. W. Patwardhan and V. V. Ranade, (2011), CFD simulation of stirred tanks: comparison of turbulence models. Part II: Radial flow impellers. Can. J. Chem. Eng., 89, 23-82.

[62] J. B. Joshi, N. K. Nere, C. V. Rane, B. N. Murthy, C. S. Mathpati, A. W. Patwardhan and V. V. Ranade, (2011), CFD simulation of stirred tanks: comparison of turbulence models. Part II: Axial flow impellers, multiple impellers and multiphase dispersions. Can. J. Chem. Eng., 89, 754-816.

[63] Z. Sha, S. Palosaari (2000), Mixing and crystallization in suspensions. Chemical Engineering Science, 55, 1797-1806.

[64] M. L. J. Leeuwen, O. S. L. Bruinsma and G. M. V. Rosmalen (1996), Influence of mixing on the product quality in precipitation. Chem. Eng. Sci. 51 (11): 2595-2600.

[65] D. Y Wong, Z. Jaworski and A. W. Nienow (2001), Effect of ion excess on particle size and morphology during barium sulphate precipitation: An experimental study, Chem. Eng. Sci. 56: 727–734.

[66] R. Pohorecki and J. Baldyga (1983), The use of a new model of micromixing for determination of crystal size in precipitation, Chem. Eng. Sci., 38, 79-83.

[67] G. Tosun (1988), An experimental study of the effect of mixing on the particle size distribution in $BaSO_4$ precipitation reaction. Proc. Europ. Conf. Mixing, Pavia, Italy, 161: 161-170.

[68] H. Wei, W. Zhou and J. Garside, (2001), Computational Fluid Dynamics Modelling of the Precipitation Process in a Semibatch Crystallizer, Ind. Eng. Chem. Res., 40, 5255-5261.

[69] Z. Jaworski and A. W. Nienow (2003), CFD modelling of continuous precipitation of barium sulphate in a stirred tank, Chemical Engineering Journal, 91, 167–174.

[70] W. Zheng, M. Zaisha, Y. Chao and S. Xiangqian (2006), Computational fluid dynamics approach to the effect of mixing and draft tube on the precipitation of barium sulfate in a continuous stirred tank, Chinese J. Chem. Eng., 14 (6) 713-722.

[71] M. M. Kamyabia , H. Hashemipourb and S. Kamyabib (2012), CFD Modeling of Barium Sulfate Nano Particles Crystallization in a Tank Reactor by Using Population Balance Equations, Proceedings of the 4th International Conference on Nanostructures (ICNS4) 12-14 March, Kish Island, I.R. Iran.

[72] J. M. Rousseaux, C. Vial, H. Muhr and E. Plasari, (2001), CFD simulation of precipitation in the sliding-surface mixing device, 56, 1677-1685.

[73] G. H. Price (1971), Self reduction in ammonium urinates, J. Inog. Nucl. Chem., 33, 4085-4092.

[74] C. D. Harrington and A. E. Euchle (1959), Uranium Production Technology, D. Van Nostrand Company Inc., Princeton.

[75] C. K. Gupta and H. Singh (2003), Uranium Resource Processing: Secondary Resources, Springer, Germany.

[76] Y.S Ladola, S. Chowdhury, S. Sharma and S.B. Roy (2008), Recovery of locked-up uranium in slag disc by co-melting in Magnesio-Thermic Reduction, Trans. Indian Inst. Met., 61 (2-3), 103-106.

[77] https://www.google.co.in.

[78] http://www.wikipedia.org.

[79] B. Tomazic, M. Samarzija and M. Branica (1969), Precipitation and hydrolysis of uranium (VI) in aqueous solutions-VI: investigation on the prcipittion of ammonium uranates, J. Inorg. Nucl. Chem., 31, 1771-1782.

[80] B. N. Murthy and J. B. Joshi (2008), Assessment of standard k–ε, RSM and LES turbulence models in a baffled stirred vessel agitated by various impeller designs, Chem. Eng. Sci., 63, 5468-5495.

[81] V. B Rewatkar, K. S. M. S. R Rao and J. B. Joshi (1990), Power consumption in mechanically agitated contactors using pitched bladed turbine impellers. Chem. Eng. Comm., 88, 69-90.

[82] Nguyen-Quy-Dao (1968), On the formation of Alkali Uranates in aqueous solutions. A General Review, Bull. Soc. Chim. Fr., 3542.

[83] Seleznev et al (1971), Russ. J. Inorg. Chem. (Engl. Transl.), 16 1174.

[84] International Atomic Energy Agency, Specific Considerations and Milestones for a Research Reactor Project, IAEA-NP-T-5.1, IAEA, Vienna, 2012.

[85] International Atomic Energy Agency, Strategic Planning for Research Reactors, IAEA-TECDOC-1212, IAEA, Vienna, 2001.

[86] International Atomic Energy Agency, Applications of Research Reactors, IAEA-NP-T-5.3, IAEA, Vienna, 2014.

[87] International Atomic Energy Agency, Commercial Products and Services of Research Reactors, IAEA-TECDOC-1715, IAEA, Vienna, 2013.

[88] A. M. Saliba-Silva, E. F. Urano de Carvalho, H. G. Riella and M. Durazzo (2011), Radioisotopes - Applications in Physical Sciences: Chapter 2, In Tech.

[89] International Atomic Energy Agency, The Applications of Research Reactors, IAEA-TECDOC-1234, IAEA, Vienna, 1999.

[90] N.P. Galkin, Technology of Uranium, Israel Program for Scientific Translations Ltd., Jerusalem, 1966.

[91] Calculated from ICSD using POWD-12++ 85 (1997),135

[92] P. Taylor, D. Wood and A. Duclos (1992), The early stages of U_3O_8, formation on unirradiated CANDU UO_2 fuel oxidized in air at 200-300 °C, J. Nucl. Mater., 189, 116-123.

[93] D. Smith (1979), Penn State University, University Park, Pennsylvania, USA, ICDD Grant-in-Aid,

[94] Calculated from ICSD using POWD-12++ 39, (1997), 75

[95] R. Fritsche, C. Sussieck-Fornefeld (1988), Min.-Petr. Inst., Univ. Heidelberg, Germany, ICDD Grant-in-Aid,

[96] Calculated from ICSD using POWD-12++ 101, (1997) 9333.